

# THEORY OF CLASSICAL SURFACE DIFFUSION

T. ALA-NISSLILA and S.C. YING\*

*University of Helsinki, Research Institute for Theoretical Physics,  
Siltavuorenpenneri 20 C, SF-00170, Helsinki, and*

*Department of Physics, Tampere University of Technology,  
P.O. Box 527, SF-33101, Tampere, Finland*

\**Department of Physics, Brown University, Box 1843, Providence, RI 02912*

## Abstract

We present a review of recent theoretical developments in classical surface diffusion. We start with a brief survey of theoretical and experimental works in surface diffusion to date, and point out some of the open problems in the field that have not received widespread attention. We then proceed to a detailed exposition of an analytic, microscope theory of classical diffusion of adatoms on surfaces. This is based on a Mori projection operator formalism in which the various dynamic correlation functions of the adatom are evaluated. The zero frequency limit of the velocity autocorrelation function yields the diffusion tensor. Subsequently, we use the microscopic theory to examine the qualitative, universal features of surface diffusion. These include the validity and emergence of the Arrhenius form of the activated diffusion at low temperatures, the random walk theory and the diffusion anisotropy on surfaces with different symmetries. We then discuss the surface diffusion on substrates with special properties. The first of these is a substrate with large adatom induced local distortions. This is motivated by the observed anomalous diffusion anisotropy of the H/W(110) system. We introduce a two-step lattice gas model for this problem and justify the model by a parallel description of the deformable lattice within the microscopic theory. Detailed Monte Carlo simulation studies are then presented for the two-step lattice gas model. Another special case is a substrate which undergoes an intrinsic structural transition. We show that the adatom diffusion coefficient would vanish anomalously as the transition is approached due to the coupling with critical fluctuations. We conclude with a summary of the results and a discussion on the directions for future research.

Contents

## Page

1.	Introduction	229
2.	Survey of Existing Theoretical and Experimental Studies of Surface Diffusion	231
A.	Theoretical studies of surface diffusion	231
B.	Experimental studies of surface diffusion	235
C.	Some open problems in surface diffusion studies	239
3.	Microscopic Theory of Classical Surface Diffusion	240
A.	Introduction	240
B.	Derivation of the diffusion tensor	241
4.	Universal Features of Surface Diffusion	250
A.	Low and high temperature limit	250
B.	Diffusion on lattices with different symmetries	252
C.	Second order friction expansion	263
5.	Diffusion on Lattices with Local Distortions	267
A.	Two-step lattice gas model of diffusion for $H$ and $O$ on $W(110)$	269
B.	Microscopic theory of diffusion on substrates with local distortions	273
C.	Monte Carlo simulation studies of the two-step lattice gas model	281

6.	Diffusion Anomaly Near Structural Phase Transitions	301
A.	Critical dynamics of the surface at the reconstruction	302
B.	Evaluation of the diffusion coefficient	304
7.	Summary and Discussion	310
	Acknowledgements	314
	References	314

### 1. Introduction

The central role of migration of atoms and molecules on solid surfaces in such physical processes as chemical reactions, or crystal growth can hardly be overemphasized. Since the pioneering experiments by Hamburger [1], Volmer and Estermann [2], Langmuir and Taylor [3], and later by Ahearn and Becker [4] exposed the importance of surface diffusion it has developed into one of the most actively studied fields of research. With the advent of modern high vacuum technology, experimental research on surface diffusion has reached a new level of sophistication. A variety of modern experimental tools are now available for direct studies of atomic scale diffusion on clean surfaces.

In light of the hundreds - perhaps thousands - of works published in the field of surface diffusion, it may then strike as surprising that there are still many important subjects which have not received much attention. For example, most experimental studies of single adatom diffusion have concentrated on the determination of the Arrhenius parameters (the prefactor and the activation barrier for diffusion) for a given system, while fewer attempts have been made to understand the microscopic dependence of these quantities on the form of the surface potential, or possible systematic deviations from the Arrhenius form [5]. Additionally, in the case where adatom interaction effects dominate leading to the appearance of ordered phases on the surface, there exists relatively few experiments where surface diffusion has been systematically studied as a function of coverage and temperature [6]. Partially, these gaps in the experimental work are due to the limitations of the experimental methods, as we will further discuss in chapter 2.

As regards the theoretical developments, although the macroscopic thermodynamics of diffusion is well understood [5] there have been relatively few works to study its microscopic origins.

Most of the progress in the latter until recently has come from Monte Carlo and molecular dynamics studies using simple interaction potentials, as first - principles calculations of surface properties have not usually been available. A large majority of the molecular dynamics studies have followed the experimental trend of concentrating on the quantitative determination of diffusion constants for various systems, either in the high or low temperature limit. While these works are certainly useful for understanding general trends in diffusion, there are still relatively few attempts to study several important microscopic aspects. These include deviations of diffusion from the usual low temperature activated Arrhenius behavior both in the high temperature and in the low temperature quantum limit, the anisotropy of the diffusion tensor, the role of multiple saddle points in the surface potential, the effects of local or global surface distortions, possible phase transitions on surfaces, and the influence of randomness in surface potential.

Our main purpose in this review article is to concentrate on recent important theoretical developments of surface diffusion. In particular, we will present results on two main subjects. The first concerns a microscopic, analytic theory of classical surface diffusion of single adatoms on a periodic substrate. Using this theory, we can study many of the open issues and obtain a more complete microscopic understanding. Instead of trying to obtain quantitative numbers for the diffusion coefficients for various systems, we will emphasize the study of *qualitative, universal features*. By this we mean properties which are largely independent of the details of the atomistic interactions, but are determined for example by the topology and symmetry of the surface potential. Critical phenomena on the surface and their influence on diffusion also belong to this category. This is our main subject, and in addition to reviewing our previous works [7-14] we will also present new, unpublished results. We note however that although our theoretical approach is completely general we will not deal with such issues as cluster diffusion, or exotic exchange diffusion mechanisms which have recently been studied theoretically [15,16].

The second part of the review is concerned with diffusion at finite coverages in strongly interacting systems. Currently, we know of no microscopic theory that can deal with this complicated many - body interaction problem, although work in this direction is in progress [17]. To illustrate the complicated nature of this problem, we present a comprehensive study of diffusion in a lattice gas model of a deformable lattice, using a combination of analytic Green's function approach and Monte Carlo simulation methods. Although originally postulated to describe diffusion in the  $H/W(110)$  adsorption system, this model elucidates many of the general features of interacting adsorption systems. We will show results for the diffusion tensor in the model as a function of coverage in the presence of finite adatom - adatom interactions

and spatially ordered phases, and discuss the results in terms of the thermodynamics of the model system. Although the quantitative nature of these results is limited by the assumptions underlying the model, the qualitative features due to strong interactions are expected to be relevant in real systems.

The organization of this review is as follows. In chapter 2, we present a brief survey of the existing theoretical and experimental works on surface diffusion. This will by no means be exhaustive since several excellent and comprehensive reviews already exist on the subject [5,6,18-20]. Our aim here is twofold. First, we want to introduce the fundamental concepts so that this article can be reasonably self-contained. Second, our goal is to provide a guide map to the many apparently unrelated approaches and techniques in the study of surface diffusion. These studies usually focus on a particular aspect or employ a particular approximation valid only in a certain physical regime. The nonexperts can find this wealth of literature rather confusing. We shall try to point out the common features and the connections between the various theoretical and experimental approaches in this chapter. This also sets the background for a better understanding of the role of the microscopic theory of surface diffusion which will be presented in detail in chapters 3 and 4. We will particularly emphasize the universal features which are not sensitive to the details of the model or various approximations in the theory. After this we shall present results for diffusion on substrates with large local distortions. In particular, we present results of Monte Carlo simulations for a novel two-step lattice gas model, which describes the diffusion of  $H$  and  $O$  on the  $W(110)$  surface. These results are also discussed from the point of view of the experimental data. In chapter 6 we present calculations based on the microscopic theory for diffusion of an adatom on a surface, which undergoes a structural phase transition. We demonstrate using  $W(100)$  as an example that the diffusion coefficient vanishes anomalously at a surface structural phase transition. Finally, in chapter 7 we summarize the material within this review and discuss briefly some special topics and directions for future theoretical and experimental work.

## 2. Survey of Existing Theoretical and Experimental Studies of Surface Diffusion

### A. Theoretical studies of surface diffusion

We shall start this chapter with a survey of the theoretical approaches to the study of surface diffusion. The earliest theoretical treatment of the surface diffusion problem is based on the transition state theory [21-25]. There are two basic ingredients. First, the adatom is assumed to make random jumps between adjacent sites. Second and more importantly, the jump rate is simply calculated in terms of the number of crossings of adatoms across a

somewhat arbitrary saddle surface dividing adjacent cells in the equilibrium state. This then converts the problem of calculating a dynamic quantity like diffusion constant into a much easier calculation of equilibrium quantities. Within the quasi - harmonic approximation, the problem can be further simplified leading to an analytic expression for the diffusion constant. This is the well known Vineyard expression for the diffusion constant [23]. In recent years, with the advent of more powerful computers, the full expression for the diffusion constant can be easily evaluated with for example Monte Carlo simulation techniques [26-28].

Although the transition state theory is very successful in providing a qualitative and even semi - quantitative description of the surface diffusion problem, the dynamical intricacies such as saddle surface recrossings and multiple jumps are all neglected in this approach. The most common theoretical approach avoiding these approximations is the molecular dynamics simulation technique [29-37]. The only limitation here is the finite size limited by numerical capabilities and the accuracy of the interaction potentials. However, brute force molecular dynamics simulation is only feasible at temperatures comparable to or higher than the diffusion barrier. At lower temperatures, jumps between neighbours are so rare that the computer time required to follow the diffusive motion of the adatom becomes prohibitively long. In recent years, a very elegant approach has been developed to solve this rare event problem [38-50]. This is based on the idea of expressing the true diffusion constant as the transition state theory result multiplied by a correction factor. This correction factor can be expressed in terms of the properties of the trajectory of the adatom near the saddle point crossing for only a short correlation time. Thus, molecular dynamics simulation techniques could be used at low temperatures to calculate this correction factor rather than to directly evaluate the total diffusion constant. The studies also demonstrate that the transition state theory is fairly accurate at low temperatures provided that the dividing surfaces between adjacent cells are chosen appropriately. In regard to this issue, there are also a series of studies in which the proper choice of a dividing surface to minimize recrossing events is analysed in terms of the geometry of the binding potential [51-55].

Except for the full molecular dynamics simulation studies, the theoretical approaches discussed above are mainly for the study of single adatom diffusion constants. The extension of these methods to finite coverages are at best limited to small sizes and/or simple interactions. At a finite coverage, the term diffusion constant itself is ambiguous. Namely, there are two different diffusion constants - the tracer or self diffusion constant  $D^t$  and the chemical or collective diffusion constant  $D^c$ . The tracer diffusion constant is defined through the long time behaviour of the mean square displacement of an adatom as

$$\begin{aligned} \mathbf{D}^t &= \frac{1}{N} \sum_{i=1}^N \int dt \langle \vec{v}_i(t) \cdot \vec{v}_i(0) \rangle \\ &= \lim_{t \rightarrow \infty} \frac{1}{Nt} \sum_{i=1}^N \langle [\vec{r}_i(t) - \vec{r}_i(0)]^2 \rangle, \end{aligned} \quad (2.1)$$

where  $\vec{v}_i(t)$  and  $\vec{r}_i(t)$  denote the velocity and position vectors of the  $i^{\text{th}}$  particle at a time  $t$ , and the brackets denote statistical averaging. The collective diffusion constant in turn is defined through the Fick's law for the relaxation of density fluctuations:

$$\frac{dn(\vec{r}, t)}{dt} = \nabla \cdot \mathbf{D}^c \cdot \nabla n(\vec{r}, t), \quad (2.2)$$

where  $n(\vec{r}, t)$  is the density of the adatoms. It can be shown that  $D^c$  can be expressed in terms of the center of mass velocity correlation functions as [56]

$$\mathbf{D}^c = \frac{1}{k_B T(\frac{dn}{d\mu}) L^d d} \int_0^\infty dt \langle \vec{V}(t) \cdot \vec{V}(0) \rangle, \quad (2.3)$$

where  $\vec{V} \equiv \sum_i \vec{v}_i$ ,  $\bar{n}$  is the average density,  $\mu$  the chemical potential, and  $d$  the spatial dimension. Only in the limit of noninteracting adatoms are the two quantities  $D^t$  and  $D^c$  equal for finite coverages. We shall see below that different experiments measure one or the other of these diffusion constants and care must be exercised in comparing the corresponding theoretical result with experimental data.

There is a whole array of interesting physical phenomena related to diffusion which only manifest themselves at finite coverages. These are for example the correlation of diffusion constant with the order in the adlayer, critical slowing down of diffusion near a phase transition boundary and the differences between tracer and collective diffusion. In the literature, these questions are often studied with a lattice gas model. The basis of the lattice gas model is again the idea that at low temperatures, the motion of an adatom is limited to random jumps between adjacent sites. Also, most of the time the adatoms would be localized around the minima of the binding potential. Thus the adatom configurations can be approximated by a set of occupation numbers for each lattice. The dynamical information is buried in the elementary jump rate of an adatom from one site to another. The stochastic transition from one configuration to another is then amenable to standard Monte Carlo simulation studies. The difficulty with this model is that within the constraint of the system being able to reach a canonical ensemble equilibrium, the jump probability from one configuration to another is not uniquely determined and there are many plausible choices. Also, the elemental jump rate

itself should contain temperature and coverage dependence which is usually neglected. This is just another way of saying that there exists no simple relation between the stochastic dynamics implied in the lattice gas model and the real dynamics as employed in the molecular dynamics studies. Nonetheless, the lattice gas model is useful in studying the qualitative features of diffusion such as anisotropy and critical slowing down.

Another drawback in the lattice gas model is that the role of the substrate in the model is totally static. It provides only an array of adsorption sites for the adatoms; the geometry of which being determined by the clean surface. In recent years, it has been found repeatedly that the role of the substrate is often more active [57]. It can undergo a reconstruction to a different phase under the influence of the adsorption of atoms or molecules. Even in the absence of adsorbate induced reconstructions, there can still be strong local distortions around an adatom which can be viewed as a precursor of a reconstruction transition. Since diffusion (at least at low and medium temperatures) consists of jumps between neighbouring sites, we expect that the diffusion should be very sensitive to these local distortions. We have shown in recent studies that this is indeed the case [7,10,13,14]. Under suitable conditions, the lattice gas model could be generalized to allow for the presence of lattice distortion. This will be the topic of discussion in chapter 5 of this article.

As indicated in the above discussion, except in the case of full numerical simulations, the starting point of the theoretical analysis is usually phrased in terms of the jumps of the adatom between neighbouring sites. This language, while appropriate for low temperatures, is not as useful for temperatures higher than the diffusion barrier. At high enough temperatures, the periodic potential of the substrate becomes irrelevant and the diffusion behaviour should reduce to that of a simple Brownian particle in two dimensions. Thus, we should expect a smooth crossover from the Arrhenius activated diffusion to that of simple Brownian motion. An entirely different approach without a bias *a priori* to the high or low temperature regimes is the Langevin equation and the related Fokker - Planck equation approach [58,59]. In the more phenomenological studies based on this approach, the friction or memory functions in these equations are simply regarded as parameters. However, the kinetic equations can actually be derived from the Mori projection operator formalism. As a result, the friction can be expressed in terms of the vibrational correlation functions of the substrate and the adatom - substrate interaction potential. This then provides a starting point for a microscopic theory of surface diffusion. Zeyher and Kleppmann [60], and Wahnström [61] have studied the case of surface diffusion along one easy direction using this approach. Recently, we have developed a microscopic theory of surface diffusion using this approach for the full semi - infinite three

dimensional substrate [8,9,62]. Instead of solving the kinetic equation directly, we solve the set of coupled equations for various time dependent correlation functions. In a series of recent articles [8-12], we have explored the universal properties of surface diffusion with this theory. This will be the main body of discussion in chapters 3 and 4 of this article.

In most of the existing works, the adatom - substrate interaction is treated as a parametric input. However, with the recent rapid advances in first principles total energy calculations, the actual adatom - substrate potential and the diffusion paths have been calculated for some adsorption systems [63-68]. Combined with the the various theoretical approaches to incorporate the dynamics as described above, this holds great promise for a comprehensive quantitative study of surface diffusion. These total energy calculations also revealed that in many adsorption systems, more exotic mechanisms such as correlated dimer diffusion or exchange with the substrate atoms can take precedence over the simple picture of an adatom hopping over the saddle point barrier [15,16,69-72]. Whether these are isolated incidences or of a more general occurence remains to be studied. In this review, we shall restrict ourselves only to the conventional hopping mechanisms.

## B. Experimental studies of surface diffusion

The very first experiments where the importance of surface diffusion was realised were based on indirect observations of mass transport along surfaces [1,3]. Although an ingenious experiment by Ahearn and Becker [4] using the surface of a tungsten crystal as a part of an electron microscope demonstrated the importance of the surface orientation for diffusion, it was not until the advent of the field emission microscope [73] and the field ion microscope [74] that the modern atomistic view of diffusion started developing. The historical developments, together with the first applications of the field emission and microscope methods are nicely reviewed by Erlich and Stolt [19].

The development of the modern high vacuum technology over the last three decades has lead to a proliferation of new techniques to study surface diffusion *in situ* vacuum conditions. Besides direct adatom imaging, most of the modern spectroscopic analysis methods can be used assuming that a strong enough signal can be obtained to detect mass transport. Thus, current experimental methods can be divided in two broad categories: direct imaging methods, where the actual real - space motion of diffusing atoms, clusters or a density profile are imaged on the surface and spectroscopic, somewhat more indirect methods where emission or scattering signals related to the internal structure of adatoms or molecules are monitored as a function of time. Classification can also be made between methods measuring diffusion under equilibrium, or nonequilibrium conditions [5]. Another useful categorization is to distinguish between methods

suited best for measuring the tracer diffusion coefficient  $D^t$  (usually of single particles or small clusters), and those measuring the collective diffusion coefficient  $D^c$  at finite coverages. From the point of view of the fundamental difference between the tracer and collective diffusion tensors which will be extensively discussed in chapter 5, this is the categorization which we will use, although somewhat haphazardly. Due to the availability of recent comprehensive reviews on the various methods [5,6,18-20,73-86] this section will be rather brief.

(i) Studies of tracer diffusion. The field ion microscopy technique (FIM) [5,19,74,76-78,80,82, 84, 86-90] has been one of the most useful and commonly used tools to study the diffusion of single adatoms or small clusters on the surface. In modern FIM studies, a highly magnified image of the surface and the adatoms is created by an inert imaging gas under a high electric field at a metal tip. During the imaging stage, the temperature of the substrate is lowered so that no diffusion occurs. After each such imaging, the field is removed and the sample is heated to the desired temperature, where surface diffusion takes place. From a series of successive images, the tracer diffusion coefficient of the adatoms can be determined according to Eq. (2.1), by measuring the mean square displacement of the adatom. However, it must be noted that a proper diffusion constant can only be extracted from Eq. (2.1) in the long time limit where the mean square displacement is linearly proportional to time. In practice the motion of the adatom is often followed over only a few lattice sites. This limits the accuracy of  $D^t$  that can be measured. FIM is also limited mainly to the study of metallic substrates and adatoms which are not desorbed by the strong electric field. Recent reviews summarizing the current technical state of the method can be found in [5,86]. FIM has been particularly useful for studies of the Arrhenius parameters, and anisotropy of the diffusion tensor. Real space figures of diffusion can also yield valuable information about physically distinct diffusion mechanisms on the surface.

The scanning transmission electron microscopy (STEM) offers a method complementary to FIM to obtain information about single adatom diffusion. Using a tightly focused electron beam (with a diameter of a few Ångströms), elastic cross sections of electrons scattered from single adatoms can be measured. By subtracting the background due to the substrate, a series of micrographs can be obtained which can be analysed using Eq. (2.1). The method can be used to image much larger surface areas than the FIM, up to several hundred Ångströms in linear size. However, the resolution is somewhat limited, and only adatoms relatively heavy with respect to the substrate can be resolved. Only few STEM measurements of single adatom diffusion exist up to date [77,91]. Related methods to measure collective diffusion will be discussed in Sec. (ii).

The relatively recent advent of the scanning tunneling microscopy (STM) [92-94] offers an alternative way to image single adatoms and clusters on surfaces. The unparalleled resolution offered by the tunneling current between the surface and the STM tip can be used to resolve finest atomistic details on the surface, thus allowing the study of single adatom diffusion under a variety of conditions (the effects of steps, kinks, impurities etc.). In principle then, the STM images can be directly analysed using Eq. (2.1). Recently, more sophisticated versions of the STM technique have become available. Surface areas as large as in the STEM method can be imaged, and thus also the effects of finite concentrations can be studied. The tracer diffusion coefficient of *Si* on *Si*(001) for low coverages was studied by STM [95]. The results were analyzed in terms of a simple rate equation model based on the diffusion and creation of monomers on the surface as a function of the deposition rate [95]. Obviously, since STM data yields quantitative information about the formation and diffusion of island and clusters, more sophisticated theoretical models could be constructed for the analysis of experimental data and obtaining diffusion coefficients. Work in this direction has just begun.

The three methods mentioned above have been the most widely used in the study of single adatom diffusion. There are other ways of directly observing the motion of adatoms on surfaces, such as the radioactive tracer method which has been commonly used to study volume diffusion in solids. However, only a few experiments on surfaces exist [6]. Another way to extract  $D^t$  is to use some of the methods discussed below to measure the collective diffusion coefficient  $D^c$  at small values of the coverage, and to extrapolate to the limit of zero coverage, where  $D^t$  and  $D^c$  become identical. For systems where interactions are not very strong,  $D^c$  is only weakly coverage dependent, as we will further discuss in chapter 5.

(ii) Collective diffusion. Historically, the first observations of surface diffusion were based on macroscopic mass transport [2]. Techniques for this purpose were later developed, and used extensively to measure surface self - diffusion on various metal surfaces [18,20,96,97]. Mass transport across surfaces is macroscopically driven by a gradient in the chemical potential. To determine  $D^c$ , the diffusion equation (2.2) can then be solved either analytically or numerically in various geometries for a given initial condition of the density. The chemical potential gradient can be introduced on the surface by e.g. sinusoidal grooving [98], or creating arrays of particles [99]. The time decay of these defects can then be monitored by e.g. an interference microscope, or laser diffraction techniques [20]. Another popular technique consists of following the blunting of the tip of a field emission microscope [100] (cf. Sec. (i)). Often the effects of evaporation and volume diffusion must also be included in the analysis. Traditionally, the method has been used to determine the Arrhenius parameters over a wide range of temperatures. Although

the approach is clearly macroscopic in nature, it has been used to study the effects of surface anisotropy as well [20,101]. It is best suited for cases, where the coverage dependence of  $D^c$  is not of primary interest.

Closely related to the previous method are the more microscopic measurements of concentration gradients on surfaces, which allow the determination of the coverage dependence of  $D^c$ . A straightforward method of determining  $D^c(\theta)$  is based on the Boltzmann - Matano analysis of a spreading of a concentration profile  $\theta(x, t)$ . Its time dependent width can be related to the diffusion equation, from which [5]

$$D^c(\theta) = \frac{1}{2t} \left( \frac{d\theta}{dx} \right)^{-1}_{|\theta} \int_{\theta(x=0, t=0)}^{\theta} x d\theta, \quad (2.4)$$

where the position of the line  $x = 0$  is determined from the condition  $\int_{\theta(x=0, t=0)}^{\theta} x d\theta = 0$ . There are several techniques for both creating the required initial concentration profile and monitoring its spread as a function of time. Particularly useful for the latter are methods based on local work function changes and various spectroscopic methods such as the scanning Auger microscopy [102,103], STEM of Sec. (i), and the scanning electron microscope. The spreading of a radioactive isotope can also be monitored [6]. However, the method is rather sensitive to the presence of impurities and defects (steps) on the surface, as well as systematic errors arising from large density gradients and nonequilibrium effects. In a more sophisticated version of the method, called the method of the base, the coverage dependence of  $D^c$  can be determined more accurately by creating a small excess density profile on top of an underlying, constant density layer [6]. Thus, the system can be kept very close to equilibrium and its coverage precisely controlled.

The field emission microscopy (FEM) technique [5,6,73,75,76,81,105-108], where an electron current from the surface under a high electric field is monitored in time, has been extensively used to measure  $D^c$ . A particularly useful application of the technique capable of measuring the coverage dependence of diffusion is based on monitoring the decay of an emission current autocorrelation function in time through a probehole (the fluctuation method) [5]. The characteristic time constant of this decay  $\tau = r^2/D^c$  where  $r$  is the radius of the probehole, can be determined by fitting to the experimental decay curves yielding  $D^c$  for a given, fixed coverage. The technique can also be used to measure anisotropy of diffusion by using a rectangular probehole, in which case the tensor components of  $D^c$  can be obtained separately [104-108]. The method is, however, limited to systems which can withstand high electric fields without desorption. The coupling of the auxiliary field to the dipole moment of the adsorbates can also lead to systematic errors in the coverage dependence of  $D^c$  [5]. In practice, measurable

coverages seem to vary between  $0.1 \lesssim \theta \lesssim 0.9$ .

A relatively recent technique, the laser induced thermal desorption (LITD) method [83,109-118] has been shown to give results comparable to those obtained with the fluctuation method. A fast, focused laser pulse is used to desorb adatoms from a macroscopic area on the surface. Subsequent laser pulses are used to monitor the refilling of the area as a function of time. The time dependent refilling signal  $S(t)$  can be related to the average diffusion coefficient  $D^c$  by

$$S(t)/S(\infty) = 1 - 2 \int_0^\infty \frac{J_1^2(r/r_0)}{r/r_0} e^{-(D^c t/r_0^2)(r/r_0)^2} d(r/r_0), \quad (2.5)$$

where  $r_0$  is the radius of the desorbed area, and  $J_1$  is a first - order Bessel function. Using Eq. (2.5), the normalized refilling signal can be fitted to obtain  $D^c$ , which in Eq. (2.5) is assumed to be coverage independent. However, it has been shown that in the presence of substantial adatom interactions, nonequilibrium conditions created by the desorption can lead to systematic errors in  $D^c$  [119-121]. Thus, the method is best applicable to systems where the fluctuation method cannot be used, and where the coverage dependence of  $D^c$  is not strong. Since temperature can be easily varied, LITD has been used to determine Arrhenius parameters as well. Finally, it should be mentioned here that another possible source of error in extracting  $D^c$  from most of the experimental methods discussed above is that Fick's law (2.2) is only valid in the hydrodynamic limit of small density gradients, while the experimental data is an integrated result which contains contributions from density fluctuations of all length scales.

The techniques covered above are principally responsible for most of the current existing measurements of  $D^c$ . Rather recently, there have been several suggestions to use other spectroscopic methods which have been sufficiently refined for diffusion measurements. These include  $He$  scattering to measure self - diffusion in metals [122-124], the Mössbauer effect [125], time - resolved infrared spectroscopy [126], and nuclear spin relaxation of spin polarized adatoms [127]. An interesting new technique combines laser - induced grating of adsorbed molecules, with optical second - harmonic generation to follow the smearing of the grating [128,129]. This seems to be a particularly clean technique for diffusion anisotropy studies of adsorbed molecules on the surface, albeit with the caveats mentioned earlier.

### C. Some open problems in surface diffusion studies

We would like to end this chapter by pointing out some aspects of surface diffusion studies which we feel are still somewhat unresolved. This is partly due to limitations of the experimental techniques, and partly due to the lack of theoretical developments:

- (a) From a purely quantitative point of view, there are still large variations in the measured

Arrhenius parameters of some systems which have been measured using different methods [5]. Especially in the older literature of mass transport studies, the surface cleanliness and the influence of defects were often not considered [18].

- (b) There are relatively few systems, where the coverage dependence of  $D^c$  has been measured and correlated with the phase changes at low temperatures [5,6,108,130-136]. The influence of phase transitions of either the substrate or the adsorbed overlayer on diffusion, has only been considered in qualitative terms.
- (c) Although anisotropy of diffusion has been recognized on many surfaces [4,5,20,93,101,105-107,129,137-145], there are very few cases where it has been studied systematically as a function of temperature *and* coverage [5,105,107,140,145]. This quantity is particularly interesting because anisotropy of diffusion can be very sensitive to local changes in the surface potential [7,10,13,14,17].
- (d) Systematic effects of randomness on the surface have only been studied in some special cases [83,111,114-116,146]. The effects of well defined randomness to e.g. the Arrhenius form have not been measured to our knowledge.
- (e) We know of no studies of the coverage dependence of tracer diffusion, which is an interesting problem in itself. Tracer diffusion bears significance to e.g. cluster growth problems on surfaces [95,147]. Its measurement would be of considerable theoretical interest, too.

A main part of the theoretical approaches discussed in the following chapters will be focussed on these and related issues.

### 3. Microscopic Theory of Classical Surface Diffusion

#### A. Introduction

The classical diffusive motion of a particle in an external potential which is either random or periodic constitutes an important problem central to many different areas of physics [147,148]. In the study of surface kinetics, the motion of an adatom is quite often treated as strictly two dimensional. This restriction has some shortcomings. First and foremost, by eliminating the vertical motion of the adatom, we lose the most readily observable normal vibrational mode of the adatom. Moreover, at a quantitative level, it has been shown that the coupling of the parallel motion to the vertical motion has also important consequence on the rate of diffusion [149,150]. Technically, the difficulty of including the vertical motion arises from the fact that for a chemisorbed atom, the vertical motion is bounded and oscillatory in nature, while the motion parallel to the surface is extended.

We will present in this chapter a microscopic theory of surface diffusion which explicitly includes the vertical motion [8,9]. To achieve this, a localized basis set is introduced for describing the spatial dependence of the adatom in the normal direction, as contrasted with the plane wave basis used for the parallel extended motion. For calculation of the diffusion tensor, the inclusion of vertical motion results eventually in a renormalized friction and an effective adiabatic potential. Besides yielding a more quantitative theory for surface diffusion, the present formalism facilitates future studies of the vibrational relaxation of an adatom.

### B. Derivation of the diffusion tensor

(i) Basic Hamiltonian and variables. We start with a completely general Hamiltonian describing the adatom and substrate as

$$H = \frac{P^2}{2M} + V[\vec{R}, \{\vec{R}_\ell\}] + H_s, \quad (3.1)$$

where

$$H_s = \sum_\ell \frac{P_\ell^2}{2m} + W[\{\vec{R}_\ell\}]. \quad (3.2)$$

The first two terms in  $H$  describe the kinetic and potential energy of the adatom and its interaction with the substrate. The second part of the Hamiltonian  $H_s$  includes all the kinetic and potential energy of the substrate. For a classical adatom, the kinetic energy  $P^2/(2M)$  factors out in a trivial manner and we can define a reduced Hamiltonian

$$H_r = H_s + V[\vec{R}, \{\vec{R}_\ell\}]. \quad (3.3)$$

Next, we introduce a projection operator  $\mathcal{P}_b$ . When operated on an arbitrary variable  $A$ ,  $\mathcal{P}_b$  corresponds to taking a partial thermal average over the background degrees of freedom, i.e.

$$\mathcal{P}_b A = Z_r^{-1} \Pi_\ell \int d\vec{P}_\ell d\vec{R}_\ell e^{-\beta H_r} A, \quad (3.4)$$

Here

$$Z_r = \Pi_\ell \int d\vec{P}_\ell d\vec{R}_\ell e^{-\beta H_r} \quad (3.5)$$

denotes a configuration integral over the background. It is also useful to introduce an adiabatic potential  $V_A(\vec{R})$  defined in the following way:

$$e^{-\beta V_A(\vec{R})} \equiv \mathcal{P}_b e^{-\beta V[\vec{R}, \{\vec{R}_t\}]}. \quad (3.6)$$

This adiabatic potential represents a potential experienced by the diffusing particle at point  $\vec{R}$  averaged over the background vibrational degrees of freedom. It will play a central role in determining the properties of diffusion. Under normal conditions in the study of surface diffusion, the motion of the adatom perpendicular to the surface involves only small amplitude oscillations. Denoting the coordinate vector parallel to the surface as  $\vec{r}$  and the normal coordinate as  $z$ , we can expand the potential  $V_A(\vec{r}, z)$  around the local minimum  $z_0(\vec{r})$  as

$$V_A(\vec{r}, z) \approx V_1(\vec{r}) + c[1 + V_2(\vec{r})] [z - z_0(\vec{r})]^2. \quad (3.7)$$

Here  $V_1(\vec{r})$  and  $V_2(\vec{r})$  are periodic functions of  $\vec{r}$  with the latter defined such that it contains only non-zero Fourier components. It is also convenient to change the variable form  $z$  to  $u$  s.t.

$$u \equiv (\beta c)^{1/2} [z - z_0(\vec{r})]. \quad (3.8)$$

In what follows, we will make the simplifying assumption that we can neglect the dependence of  $z_0$  on  $\vec{r}$ . This allows us to treat  $u$  as an independent variable. Physically this means that the vertical motion is considered as a "harmonic oscillator", with a periodic "spring constant"  $2c[1 + V_2(\vec{r})]$ .

Next we introduce an orthogonal set of slow variables  $\{\mathbf{A}_n\}$  and their corresponding projection operators  $\{\mathcal{P}_n\}$  of the diffusing particle:

$$\begin{aligned} \mathbf{A}_0 &= \{e^{i\vec{G}\cdot\vec{r}} \psi_j(u)\} \\ \mathbf{A}_1 &= \left\{ \frac{\vec{P}}{M} e^{i\vec{G}\cdot\vec{r}} \psi_j(u) \right\} \\ &\dots \\ \mathbf{A}_n &= (1 - \mathcal{P}_{n-1} - \mathcal{P}_{n-2}) \mathcal{P}_b \dot{\mathbf{A}}_{n-1}. \end{aligned} \quad (3.9)$$

Here, the  $\vec{G}$ 's stand for the set of two dimensional reciprocal lattice vectors appropriate for the substrate, and

$$\psi_j(u) = \frac{1}{\sqrt{2^j \pi^{1/2} j!}} H_j(u) \quad (3.10)$$

are eigenfunctions proportional to the  $j^{th}$  order Hermite polynomials which have been normalized such that

$$\int_{-\infty}^{+\infty} du \psi_j(u) \psi_{j'}(u) e^{-u^2} = \delta_{jj'}. \quad (3.11)$$

The choice of the slow variables, which is crucial for the development of the theory, is motivated by the nature of the diffusion problem. The plane waves in Eq. (3.9) form a suitable basis for extended motion, while in the spirit of the small oscillations in the  $z$  direction, harmonic oscillator eigenfunctions are utilized. We also note that in our definition, each basic variable  $\mathbf{A}_n$  has actually an infinite (but countable) number of components corresponding to different reciprocal lattice wavevectors, Cartesian coordinates of the momentum vector, and the order of the functions  $\psi_j$ . In Eq. (3.9), the projection operators  $\mathcal{P}_n$  are defined as

$$\mathcal{P}_n \mathbf{A} = \mathbf{A} \chi_{nn}^{-1}(\mathbf{A}_n, \mathbf{A}), \quad (3.12)$$

with

$$\chi_{nn} = (\mathbf{A}_n, \mathbf{A}_n), \quad (3.13)$$

where the scalar product  $(A, B)$  is defined as the thermal average of  $A^*B$ . It is easy to verify from these definitions that the  $\mathbf{A}$ 's are orthogonal to each other. With these definitions of the basic variables and the projection operators we can now apply the standard Mori formalism [58,62,151] to obtain a formal equation for the Laplace transform of the correlation functions  $\phi_{nn'}(\omega)$  defined as

$$\phi_{nn'}(\omega) = \int_0^\infty e^{i\omega t} \phi_{nn'}(t) dt. \quad (3.14)$$

These correlation functions contain all the physically relevant information about the system. The equation for the whole set of  $\phi(\omega)$ 's is given by [62]

$$[-i\omega\chi^{-1} + \mathbf{b} + \Sigma(\omega)]\phi(\omega) = \mathbf{1}, \quad (3.15)$$

with

$$\mathbf{b} = i\chi^{-1}(\mathbf{A}, L\mathbf{A})\chi^{-1}, \quad (3.16)$$

and the memory function  $\Sigma(\omega)$  given by

$$\Sigma(\omega) = \chi^{-1}(QL\mathbf{A}, \frac{i}{\omega - QLQ} QL\mathbf{A})\chi^{-1}. \quad (3.17)$$

In this equation,  $Q$  is the projection operator into the space orthogonal to that spanned by the basic variables  $\{\mathbf{A}_n\}$ ,

$$Q = 1 - \sum_{i=0}^{\infty} \mathcal{P}_i, \quad (3.18)$$

and  $L$  is the Liouville operator:

$$iL\mathbf{A} = \frac{d\mathbf{A}}{dt}. \quad (3.19)$$

The set of equations in (3.15) is equivalent to the Kramers equation [62]. However, since we start from a lattice dynamic Hamiltonian, we have an additional advantage in the fact that instead of a phenomenological damping constant, we have a *microscopic* memory function  $\Sigma(\omega)$  which contains the damping effects. As we shall see in the next section, the memory function can be related to the vibrational properties of the background. Together with the adiabatic potential (cf. Eq. (3.6)) it will play a crucial role in determining the properties of diffusion.

(ii) Inverse friction expansion. Starting from the general equation (3.15) for the correlation functions  $\phi_{nn'}(\omega)$ , we can now develop a continued fraction expansion for  $\phi_{11}(\omega)$  which is directly related to the diffusion constant. As we shall see below, this expansion is actually an expansion in inverse powers of the friction. The leading term corresponding to the high friction limit has a very simple form. Let us define

$$\mathbf{a}_i(\omega) \equiv -i\omega\chi_{ii}^{-1} + \Sigma_{ii}(\omega). \quad (3.20)$$

Then from Eq. (3.15) we obtain the set of equations

$$\begin{aligned} \mathbf{a}_0\phi_{01}(\omega) + \mathbf{b}_{01}\phi_{11}(\omega) &= 0 \\ \mathbf{b}_{10}\phi_{01}(\omega) + \mathbf{a}_1\phi_{11}(\omega) + \mathbf{b}_{12}\phi_{21}(\omega) &= 1 \\ &\vdots \\ \mathbf{b}_{n,n-1}\phi_{n-1,1}(\omega) + \mathbf{a}_n\phi_{n1}(\omega) + \mathbf{b}_{n,n+1}\phi_{n+1,1}(\omega) &= 0 \quad \text{for } n > 1. \end{aligned} \quad (3.21)$$

Now we introduce the functions  $\mathbf{B}_n(\omega)$  defined as

$$\phi_{n1}(\omega) = \mathbf{B}_{n-1}(\omega)\phi_{n-1,1}(\omega). \quad (3.22)$$

Then we have from Eq. (3.20)

$$\phi_{11}(\omega) = [\mathbf{a}_1 - \mathbf{b}_{10}\mathbf{a}_0^{-1}\mathbf{b}_{01} + \mathbf{b}_{12}\mathbf{B}_1(\omega)]^{-1}, \quad (3.23)$$

and for  $n > 1$

$$\mathbf{B}_{n-1}(\omega) = -[\mathbf{a}_n + \mathbf{b}_{n,n+1}\mathbf{B}_n(\omega)]^{-1}\mathbf{b}_{n,n-1}. \quad (3.24)$$

Equations (3.23) and (3.24) together constitute a continued fraction expansion for the correlation function  $\phi_{11}(\omega)$ . Note that the diffusion tensor, which is the zero frequency limit of the Laplace transform of the velocity autocorrelation function [58], is given in terms of  $\phi_{11}(\omega)$  by the expression

$$\begin{aligned} D_{\alpha\beta} &= \int_0^\infty \langle V_\alpha(t)V_\beta(0) \rangle dt \\ &= \lim_{\omega \rightarrow 0} \phi_{11}^{\alpha\beta}(\vec{G} = 0, j = 0; \vec{G}' = 0, j' = 0; \omega). \end{aligned} \quad (3.25)$$

In the limit  $\omega \rightarrow 0$ , the  $\mathbf{a}$ 's are proportional to the friction memory function  $\Sigma_{ii}(\omega)$ . Therefore, the continued fraction expansion (3.23) and (3.24) is equivalent to an inverse friction expansion. The expansion parameter is the inverse of the friction measured in units of the substrate Debye frequency  $\eta/\omega_D$ . In the high friction limit s.t.  $\eta/\omega_D \gg 1$ , we can drop all the  $\mathbf{B}_n(\omega)$ 's in the continued fraction expansion for  $n \geq 1$ , the result for  $\phi_{11}(\omega)$  is then the simple expression

$$\phi_{11}(\omega) = [\mathbf{a}_1(\omega) - \mathbf{b}_{10}\mathbf{a}_0^{-1}(\omega)\mathbf{b}_{01}]^{-1}. \quad (3.26)$$

Equation (3.26) is a formal solution in the high friction limit, so it is equivalent to a solution of the corresponding Smoluchowski equation [62]. The important feature of the present method is that we have also a microscopic expression for the frictional force. Equation (3.26) can be simplified further. First, we note that

$$\chi_{11} = \frac{k_B T}{M} \chi_{00} \delta_{\alpha\beta}, \quad (3.27)$$

and hence

$$\mathbf{a}_1(\omega) = -i\omega \frac{M}{k_B T} \delta_{\alpha\beta} \chi_{00}^{-1} + \Sigma_{11}(\omega). \quad (3.28)$$

It can then be shown that the matrix elements of  $\mathbf{F}_1(\omega) \equiv \mathbf{b}_{10}\mathbf{a}_0^{-1}(\omega)\mathbf{b}_{01}$  appearing in (3.26) are given by [9]

$$\begin{aligned}
\mathbf{F}_1^{\alpha\beta}(s, s'; \omega) &= -\frac{i}{\omega} G_\alpha \chi_{00}^{-1}(\vec{G}, \vec{G}'; j, j') G'_\beta \\
\mathbf{F}_1^{zz}(s, s'; \omega) &= -\frac{2ic}{\omega k_B T} \sqrt{(j+1)(j'+1)} \chi_{00}^{-1}(\vec{G}, \vec{G}'^{-1}; j+1, j'+1) \\
\mathbf{F}_1^{\alpha z}(s, s'; \omega) &= \frac{\sqrt{2(j'+1)}}{\omega} \sqrt{\frac{c}{k_B T}} G_\alpha \chi_{00}^{-1}(\vec{G}, \vec{G}'; j, j'+1) \\
\mathbf{F}_1^{z\alpha}(s, s'; \omega) &= \frac{\sqrt{2(j+1)}}{\omega} \sqrt{\frac{c}{k_B T}} G'_\alpha \chi_{00}^{-1}(\vec{G}, \vec{G}'; j+1, j'),
\end{aligned} \tag{3.29}$$

for  $\alpha, \beta = x, y$ . Here  $s \equiv (\mathbf{G}, j)$ , and we have listed the indices in  $\chi_{00}^{-1}$  in detail. In terms of  $\mathbf{F}_1$ , we finally have the general result for the frequency dependent velocity - velocity correlation function:

$$\phi_{11}(\omega) = [-i\omega \frac{M}{k_B T} \delta_{\alpha\beta} \chi_{00}^{-1} + \Sigma_{11}(\omega) + \mathbf{F}_1(\omega)]^{-1}. \tag{3.30}$$

This is the general expression from which the diffusion tensor can be calculated, once the density and the memory function are known. It constitutes one of the central results of this chapter. It should be noted that the right hand side of Eq. (3.30) involves the inverse of an infinite matrix in terms of the reciprocal lattice vectors and the indices of the Hermite polynomials.

(iii) Density and the memory function. The two fundamental matrices needed in the evaluation of  $\phi_{11}(\omega)$  through Eq. (3.20) are  $\chi_{00}^{-1}$  and  $\Sigma_{11}(\omega)$ . We shall show here how they are related to the density of the adatom and the substrate vibrational properties. First, using the definition of  $\chi_{00}$  and the adiabatic potential  $V_A(\vec{R})$  in Eq. (3.6) we can write explicitly

$$\chi_{00}(s, s') = \int d\vec{r} du n(\vec{r}, u) \psi_j(u) \psi_{j'}(u) e^{-i(\vec{G} - \vec{G}') \cdot \vec{r}}. \tag{3.31}$$

Here

$$n(\vec{r}, u) = Z^{-1} e^{-\beta V_A(\vec{r}, u)}, \tag{3.32}$$

with

$$Z = \int d\vec{r} du e^{-\beta V_A} \tag{3.33}$$

denotes the average density of the adatom. However, since

$$V_A(\vec{r}, u) = V_1(\vec{r}) + k_B T [1 + V_2(\vec{r})] u^2, \tag{3.34}$$

the density function  $n(\vec{r}, u)$  can be simplified to

$$n(\vec{r}, u) = \tilde{n}(\vec{r}, u)e^{-u^2}, \quad (3.35)$$

with

$$\tilde{n}(\vec{r}, u) = Z^{-1}e^{-\beta[V_1(\vec{r}) + V_2(\vec{r})\beta^{-1}u^2]} \quad (3.36)$$

being the reduced density. Note that the boundary condition that the motion is bounded in the  $z$ -direction imposes the restriction  $V_2(\vec{r}) < 1$ . Substitution of (3.35) into (3.31) results in the following expression for  $\chi_{00}$ :

$$\chi_{00}(s, s') = \int d\vec{r} du \tilde{n}(\vec{r}, u)\psi_j(u)\psi_{j'}(u)e^{-u^2}e^{-i(\vec{G}-\vec{G}')\cdot\vec{r}}. \quad (3.36)$$

From Eq. (3.36), we can easily accomplish the inversion of the matrix  $\chi_{00}$  to obtain

$$\chi_{00}^{-1}(s, s') = \frac{1}{A_0^2} \int d\vec{r} du \tilde{n}^{-1}(\vec{r}, u)\psi_j(u)\psi_{j'}(u)e^{-u^2}e^{-i(\vec{G}-\vec{G}')\cdot\vec{r}}. \quad (3.37)$$

In Eq. (3.37), the integration of  $d\vec{r}$  is over the unit cell with an area  $A_0$ .

The memory function contains the details of the coupling of the adatom motion to the background vibrations. Here we examine the most important component - the (1,1) element of the memory function  $\Sigma$  in detail. From Eq. (3.17) we have

$$\Sigma_{11}(\omega) = \frac{k_B T}{M} \chi_{11}^{-1} \gamma_1(\omega) \chi_{11}^{-1} \quad (3.38)$$

with

$$\gamma_1(\omega) = \frac{1}{M k_B T} \int_0^\infty dt e^{i\omega t} (Q L \vec{P} \mathbf{A}_0, e^{-i Q L Q t} Q L \vec{P} \mathbf{A}_0). \quad (3.39)$$

It is easy to see that to lowest order in the displacement of the substrate atoms we have

$$Q L \vec{P} \mathbf{A}_0 = -(1 - \mathcal{P}_b) \frac{\partial V}{\partial \vec{R}} e^{i \vec{G} \cdot \vec{r}} \psi_j(u). \quad (3.40)$$

The  $\vec{G} = 0$ ,  $j = 0$  component of Eq. (3.40) corresponds simply to the frictional force on the atom due to the vibrational motion of the substrate. The projection operator  $Q$  serves to separate out the regular force on the adatom due to the interaction with the substrate at the equilibrium position  $\{\vec{R}_j^0\}$ .

There is one limiting case when  $\gamma_1$  can be simplified considerably. This is when the time scale of the diffusive motion is much longer than the time scale for the vibrational motion of the background. Under this circumstance, the time dependence of the coordinates of the diffusing particle can be neglected in the memory function and replaced by its initial value. This is the initial value approximation [61]. Furthermore, we decouple  $\gamma_1$  into the product of averages involving the adatom and the substrate atoms separately. For the case where the diffusion and the substrate time scales are comparable, the initial value approximation is no longer valid. In this case the time dependent correlation function in Eq. (3.39) can be factorized into the product of a substrate displacement correlation function and an adatom correlation function, involving the correlation of the position coordinate of the adatom at one time to another. This adatom correlation function can be expressed in terms of  $\chi_{00}(t)$  which in turn depends on  $\chi_{11}(t)$  through the set of equations (3.21) [17]. The whole set of equations can then be solved self - consistently. This is the so - called mode - model coupling approximation [61]. In this review, we will concentrate on results obtained within the initial value approximation only.

To simplify the memory function further, we now consider the case of a pairwise interaction potential, and utilize the harmonic approximation for the background vibrational motion. In this case the adiabatic potential  $V_A(\vec{R})$  is given by the expression

$$V_A(\vec{R}) = \sum_{\ell} v^{\text{eff}}(\vec{R} - \vec{R}_{\ell}), \quad (3.41)$$

where  $v^{\text{eff}}$  is the thermally averaged pair interaction of the adatom with the substrate atom at position  $\vec{R}_{\ell}$ . The expression for  $\gamma_1$  can then be simplified to

$$\gamma_1^{\alpha\beta}(\omega) = \int d\vec{r} du \tilde{n}(\vec{r}, u) \psi_j(u) \psi_{j'}(u) \eta^{\alpha\beta}(\vec{r}, u; \omega) e^{-u^2} e^{-i(\vec{G} - \vec{G}') \cdot \vec{r}}, \quad (3.42)$$

where the *friction tensor* is given by

$$\eta^{\alpha\beta}(\vec{r}, u; \omega) = \frac{1}{Mk_B T} \sum_{\ell\ell';\gamma\delta} C_{\ell\ell'}^{\gamma\delta}(\omega) v_{\text{eff}}^{\alpha\gamma}(\vec{R} - \vec{R}_{\ell}^0) v_{\text{eff}}^{\beta\delta}(\vec{R} - \vec{R}_{\ell'}^0). \quad (3.43)$$

In Eq. (3.43),

$$C_{\ell\ell'}^{\gamma\delta}(\omega) = \int_0^\infty dt e^{i\omega t} (u_{\ell\gamma}, e^{-iQLQt} u_{\ell'\delta}) \quad (3.44)$$

and  $\vec{R} = (\vec{r}, z)$ , where  $z \equiv (\beta c)^{-1/2} u + z_0(\vec{r})$ . The variable  $u_{\ell\alpha}$  denotes a spatial  $\alpha$  component of the lattice displacement at site  $\ell$ . The time dependence of the substrate correlation function in Eq. (3.43) is still governed by the complicated Liouville operator  $QLQ$ . In the weak coupling

approximation, we can neglect the influence of the diffusing particle on the vibrational motion of the background. This amounts to replacing the operator  $QLQ$  by the simpler operator  $L$  describing the dynamics of the substrate alone. Substitution of (3.39) into Eq. (3.38) and using (3.27) and (3.37) finally yields an expression for  $\Sigma_{11}$  as

$$\begin{aligned}\Sigma_{11}^{\alpha\beta}(s, s'; \omega) &= \frac{M}{A_0^2 k_B T} \int d\vec{r} du \tilde{n}^{-1}(\vec{r}, u) \eta^{\alpha\beta}(\vec{r}, u; \omega) \psi_j(u) \psi_{j'}(u) e^{-u^2} e^{-i(\vec{G} - \vec{G}') \cdot \vec{r}} \\ &= \frac{M}{A_0^2 k_B T} \int d\vec{r} du \tilde{\eta}^{\alpha\beta}(\vec{r}, u; \omega) \psi_j(u) \psi_{j'}(u) e^{-u^2} e^{-i(\vec{G} - \vec{G}') \cdot \vec{r}}.\end{aligned}\quad (3.45)$$

The modified friction tensor  $\tilde{\eta}$  is given by

$$\tilde{\eta}^{\alpha\beta}(\vec{r}, u; \omega) \equiv \tilde{n}^{-1}(\vec{r}, u) \eta^{\alpha\beta}(\vec{r}, u; \omega). \quad (3.46)$$

(iv) Analytic solution for special symmetries. To solve for the diffusion tensor in the most general case, one has to use Eq. (3.30) and invert the matrix on the right hand side numerically for a given finite set of reciprocal lattice vectors and Hermite polynomials, and verify convergence. However, for the special case of lattices with square or simple rectangular symmetry with adiabatic potentials which are separable with respect to the  $x$  and  $y$  coordinates, it is possible to achieve the inversion analytically in a closed form. Denoting the set of  $\vec{G}$ -vectors for these lattices as

$$\{\vec{G}_{nm}\} = \left\{ \left( \frac{2\pi n}{a_x}, \frac{2\pi m}{a_y} \right) \right\}, \quad (3.47)$$

where  $a_x$  and  $a_y$  are the lattice constants, it follows immediately that the diagonal elements of the diffusion tensor are given by

$$\begin{aligned}D_{zz} &= [\Sigma_{11}^{xx}(G_y, G'_y; j, j'; \omega = 0)]^{-1} |_{G_y = G'_y = 0; j = j' = 0} \\ D_{yy} &= [\Sigma_{11}^{yy}(G_z, G'_z; j, j'; \omega = 0)]^{-1} |_{G_z = G'_z = 0; j = j' = 0} \\ D_{zz} &= 0\end{aligned}\quad (3.48)$$

In Eq. (3.48),  $G_y, G'_y$  and  $G_z, G'_z$  denote the set of reciprocal vectors with no  $x$  or  $y$  components, respectively. Using the simplified initial value form of the memory function, its inverse can easily be found and Eq. (3.48) leads to the following result:

$$D_{\alpha\alpha} = \frac{a_\alpha^2 k_B T}{M} Z^{-1} \int dx_\beta \int_{-\infty}^{+\infty} du \frac{e^{-u^2}}{\sqrt{\pi}} \left[ \int dx_\alpha e^{V_1(\vec{r})/k_B T} e^{V_2(\vec{r})u^2} \eta^{\alpha\alpha}(\vec{r}, u; \omega = 0) \right]^{-1}, \quad (3.49)$$

where  $\alpha$  and  $\beta$  refer either to the  $x$  or  $y$  direction, and  $x_\alpha, x_\beta$  denote  $x, y$  or  $y, x$ . Integrals of  $x$  and  $y$  in Eq. (3.49) are over the unit cell with an area  $A_0 = a_x a_y$ . For the square lattice case,  $D$  is fully isotropic and the order of the spatial integration variables in (3.49) does not matter. In the limit where the coupling constant  $c \rightarrow \infty$ , and  $V_2 \rightarrow 0$ ,  $e^{-u^2}/\sqrt{\pi}$  is proportional to  $\delta[z - z_0(\vec{r})]$ . The formula (3.49) then reduces to a form, which involves only extended motion in two dimensions [62]:

$$D_{\alpha\alpha} = \frac{a_\alpha^2 k_B T}{M} Z^{-1} \int dx_\beta \left[ \int dx_\alpha e^{V_1(\vec{r})/k_B T} \eta^{\alpha\alpha}(\vec{r}; \omega = 0) \right]^{-1}. \quad (3.50)$$

These two equations together with Eq. (3.30), and the definitions of the adiabatic potential and the friction tensor, constitute the central results of the microscopic theory. We note that the diffusion constant  $D_{zz}$  always vanishes, as motion of the adatom in the vertical direction is bounded. Comparing Eq. (3.49) with Eq. (3.50) we can see that the effect of the vertical motion is basically to renormalize the adiabatic potential. This will be examined quantitatively in the next chapter.

#### 4. Universal Features of Surface Diffusion

The microscopic theory presented in the previous chapter allows us for the first time to study of the properties of surface diffusion systematically. In this chapter, we will first examine the qualitative features of surface diffusion in the high friction limit. These include a completely general examination of the high and low temperature limits of the theory and the solution of the diffusion tensor for different lattice symmetries with a particular emphasis on the diffusion anisotropy. Thus, we can develop a coherent and unified picture of the qualitative, universal properties of surface diffusion and examine issues such as the validity of the Arrhenius form and the random walk theories. In the last part of this chapter, we examine the next order correction to the result obtained in the high friction limit (cf. Chap. 3) and confirm that most of the qualitative features persist to this order in the theory.

##### A. Low and high temperature limit

Before proceeding with specific model calculations, let us examine the predictions of the microscopic theory in general. In particular, we can simplify the analytic expression for  $D$  in the limit of extremely low or high temperatures. For simplicity, we shall here set  $\eta(\vec{r}) = \text{const.}$  and neglect the vertical motion. In the limit where  $\beta\Delta \rightarrow \infty$ , we can calculate the leading terms for the integrals in Eq. (3.50) as follows. The configuration integral  $Z$  is clearly dominated by the minimum value of the adibatic potential  $V_A(x_m, y_m)$  at the point  $(x_m, y_m)$ . In the

numerator, the inner integral over e.g. the  $x$  direction picks up the *absolute maximum* value of  $V_A(x_0, y)$  at some  $x_0$ , while the second integral over the  $y$  direction is dominated by the *absolute minimum* value of  $V_A(x_0, y'_m)$  at some  $y'_m$ . Thus, we can write the general expression as

$$D_{xx} = D_0 e^{-\beta[V_A(x_0, y'_m) - V_A(x_m, y_m)]}, \quad (4.1)$$

and correspondingly for  $D_{yy}$ . In the limit of low temperatures, the difference of the potentials in Eq. (4.1) precisely becomes the difference between the classical saddle point and the minimum of the adiabatic potential given by

$$\Delta \equiv V_s - V_m, \quad (4.2)$$

in the spatial direction of diffusion. Thus, Eq. (4.1) is exactly the celebrated Arrhenius form of activated diffusion [152], which is recovered by our microscopic theory. To our knowledge, this form has never before been analytically derived from a microscopic theory for surface diffusion in two dimensions.

In the extreme high temperature limit, the exponential factors in the integrals can be neglected, and  $D$  becomes

$$D_{\alpha\alpha} = \frac{k_B T}{M \bar{\eta}^{\alpha\alpha}}, \quad (4.3)$$

with  $\alpha, \beta$  denoting  $x$  and  $y$  coordinates. Eq. (4.3) coincides with the well known Einstein - Stokes formula for a particle executing Brownian motion in a viscous fluid, with a viscosity coefficient  $\bar{\eta}^{\alpha\alpha}$  [58]. This result can also be derived analytically from the general matrix formula of Eq. (3.30) [17].

These limits of the diffusion theory give us a universal scheme of the properties of surface diffusion. At sufficiently low temperatures, the commonly accepted Arrhenius form of activated diffusion is recovered, and the particle trajectories are determined by those sections of the potential surface connecting adjacent minima via the saddle points. In the opposite limit, the modulation of the adiabatic potential is lost, and the particle will diffuse isotropically in a fluid - like manner. However, the crossover regime between these two limits and the manner in which they are approached is obviously a highly nontrivial problem. This is especially true for geometries other than the square or simple rectangular lattices, for which Eq. (3.50) does not hold, and for which e.g. multiple saddle points in the adiabatic potential can exist.

### B. Diffusion on lattices with different symmetries

In this section we shall apply the microscopic theory to study the properties of diffusion in a variety of two dimensional lattices. To this end, we will consider model systems and compute the diffusion tensor

$$\mathbf{D} = \begin{pmatrix} D_{xx} & D_{xy} \\ D_{yx} & D_{yy} \end{pmatrix} \quad (4.4)$$

as a function of temperature. In all cases, both the adiabatic potential  $V_A(\vec{R})$  and the friction tensor  $\eta^{\alpha\beta}(\vec{R}; \omega = 0)$  are chosen to be simple functions which nevertheless correctly obey the underlying symmetry of the lattice. On a square lattice, our simple analytic formula (3.49) allows us first to determine the effect of the bounded vertical oscillations on diffusion. In addition, we shall address such fundamental questions as the validity and emergence of the Arrhenius form of activated diffusion and the random walk limit of diffusion, and the role of multiple, physically distinct saddle points in determining diffusion anisotropies.

(i) The square lattice. For a square lattice with a separable potential, the analytic formula Eq. (3.49) reduces to an isotropic form. We can also expand any periodic adiabatic potential as a Fourier series in terms of the reciprocal lattice vectors. In particular, to first study the effect of the vertical motion to diffusion, we will consider the following simple forms for the potentials  $V_1$  and  $V_2$ :

$$\begin{aligned} V_1(\vec{r}) &= V_0(\cos \vec{G}_{10} \cdot \vec{r} + \cos \vec{G}_{01} \cdot \vec{r}) \\ V_2(\vec{r}) &= V'_0(\cos \vec{G}_{10} \cdot \vec{r} + \cos \vec{G}_{01} \cdot \vec{r}). \end{aligned} \quad (4.5)$$

By varying the ratio  $V'_0/V_0$  we can change the strength of the coupling. For the special case where  $V'_0 \equiv 0$ , we get an exact result as

$$D = \frac{k_B T}{M \eta} [I_0(\beta V_0)]^{-2} \quad (4.6)$$

assuming a constant, isotropic friction tensor. Eq. (4.6), in which  $I_0$  denotes the hyperbolic Bessel function of order zero, is formally identical to the corresponding one dimensional solution [153]. This indicates that for this special case, diffusion can be thought as a quasi - one dimensional process in the  $x$  and  $y$  directions of the lattice. In Fig. 1 (b) we show this solution for  $V_0 = 1/2$ , which is displayed in Fig. 1 (a). It is easy to verify analytically, that Eq. (4.6) gives the high temperature Brownian and low temperature Arrhenius limits, as expected from the general formula.

For  $V'_0 > 0$ , we have to integrate Eq. (3.49) numerically. In Fig. 1 (b) we further display results for two cases, for which  $V'_0/V_0$  is  $1/2$  and  $9/10$ . When the ratio approaches unity, the

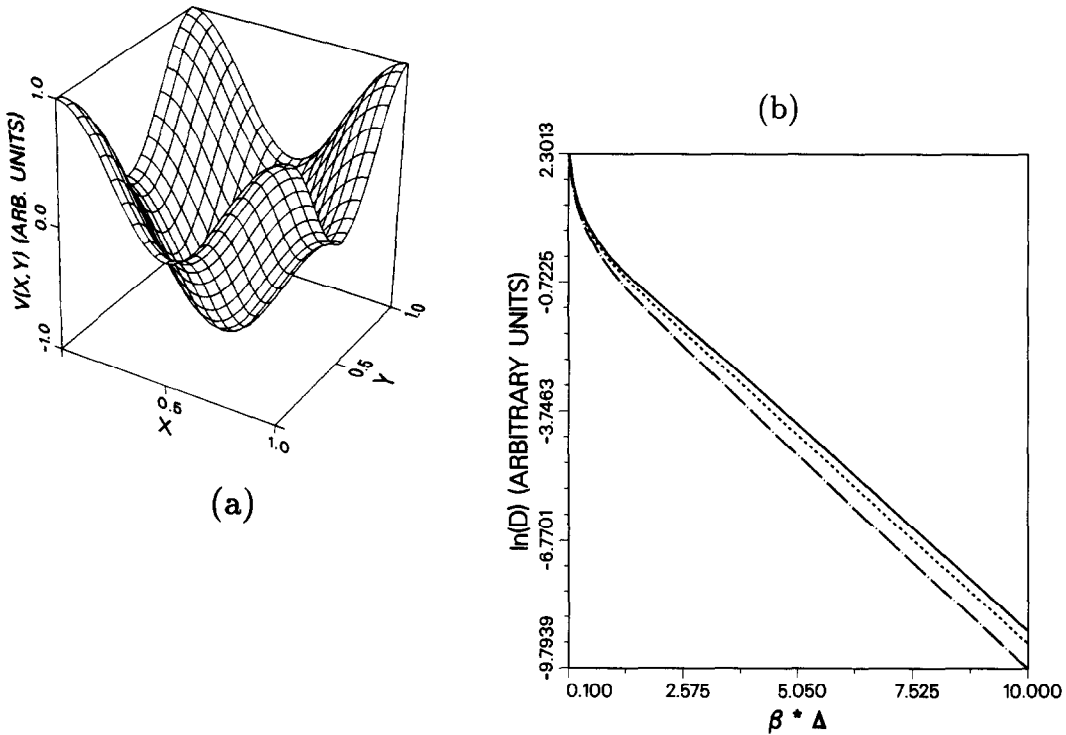


Fig. 1. (a) The simple cosine potential  $V_1(\vec{r})$  of Eq. (4.5) in the square lattice unit cell, with  $V_0 = 1/2$ . (b) Effect of the coupling of the vertical motion to diffusion on a square lattice [9]. Upper solid line indicates the exact solution given by Eq. (4.6) without vertical motion, while the two other curves are for  $V'_0/V_0 = 1/2$  (dashed line) and  $9/10$  (dash - dotted line).

effect of the vertical oscillations become quantitatively rather large. First, the friction in the Brownian form of uniform diffusion is renormalized by  $V_2$ . Also, at intermediate temperatures a finite  $V_2$  changes the effective diffusion barrier. In the low temperature limit, the barrier will be determined by  $V_1$  alone; however, the prefactor  $D_0$  decreases with increasing  $V'_0$ , leading to reduced diffusion rates. For example, at  $\beta\Delta = 10$ ,  $D$  for  $V'_0 = 0$  is about a factor 2.4 larger than

for  $V'_0/V_0 = 9/10$ . Thus, we can conclude that bounded vertical motion can cause substantial quantitative changes in  $D$ . On the other hand, the *universal* low and high temperature limits exhibited by the theory remain qualitatively unchanged.

(ii) The centered rectangular lattice. For a lattice for which the set of lattice vectors  $\{\vec{R}_\ell^0\}$  forms a centered rectangular lattice, the analytic solution (3.49) is no longer valid. To solve for  $\mathbf{D}$ , we have to calculate the the matrix elements of  $\chi_{00}^{-1}$ ,  $\Sigma_{11}$  and  $\mathbf{F}_1$ , and find the inverse of the right hand side of Eq. (3.30). As we have seen in the previous section, the universal properties of diffusion are unaltered by the oscillatory vertical motion. Thus, in this and in the following sections we will set  $V_2 \equiv 0$  which will not change the qualitative features of our results. Consequently, we consider the case for which the matrix index  $s$  contains only reciprocal lattice vectors, i.e.  $s = (\vec{G}, j = 0)$ , and the convergence of the results is determined by the number  $N$  of the  $\vec{G}$  vectors kept. As temperature decreases, the corrugation in the density increases, and the value of  $N$  required for convergence is correspondingly larger. Typically,  $N$  must be of the order of 300 - 400 for the lowest temperature results presented below.

To incorporate temperature dependent substrate effects into the calculation of surface diffusion, we have to examine the temperature dependence of the friction tensor  $\eta$ . From the continuum theory of lattice vibrations we can see that the factor  $\beta C_{\text{eff}}^{\gamma^6}$  in the friction tensor (3.43) is independent of temperature [154]. Within this approximation, the main temperature dependence left then comes from the Debye - Waller correction factor in the effective potential  $v_{\text{eff}}(\vec{R} - \vec{R}_\ell^0)$  [61]. Within the harmonic approximation, this factor can be written as [155]

$$d_w = e^{-w}, \quad (4.7)$$

where

$$w(\vec{G}_i) = \frac{3h^2 T^2}{8\pi^2 M k_B \theta_D^3} |\vec{G}_i|^2 \int_0^{\theta_D/T} dx \frac{x e^x}{e^x - 1}, \quad (4.8)$$

for each reciprocal lattice vector  $\vec{G}_i$ , using standard Debye theory. Here  $\theta_D$  is the Debye temperature of a given substrate. In the spirit of our model calculations, we will simply use expression (4.8) and multiply each Fourier component of the adiabatic potential by  $d_w(\vec{G})$  and the friction tensor  $\eta(\vec{G}, \vec{G}')$  by a factor  $d_w(\vec{G})d_w(\vec{G}')$ .

In Fig. 2 we show the general geometry pertaining to the centered rectangular lattice. The simplest periodic, effective potential can be written down as

$$V_1(\vec{r}) = V_0(\cos \vec{G}_1 \cdot \vec{r} + \cos \vec{G}_2 \cdot \vec{r}), \quad (4.9)$$

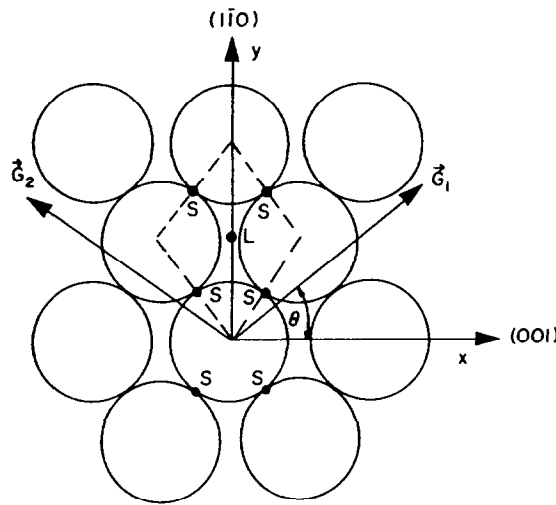


Fig. 2. Geometry of the rhomboidal lattice used in diffusion calculations [9]. For the case of a  $W(110)$  lattice with centered rectangular symmetry,  $\cot \theta = \sqrt{2}$ . The adiabatic potentials in Chap. 4 are chosen such that the long bridge sites  $L$  correspond to potential minimum, while classical saddle points are located at short bridge sites  $S$ .  $\mathbf{G}_1$  and  $\mathbf{G}_2$  denote the two basic reciprocal lattice vectors of Eq. (4.10).

with

$$\tilde{\mathbf{G}}_1 = (\cos \theta, \sin \theta) \mathbf{G}_0, \quad \tilde{\mathbf{G}}_2 = (-\cos \theta, \sin \theta) \mathbf{G}_0, \quad (4.10)$$

and

$$\mathbf{G}_0 = \frac{\pi}{a \cos \theta \sin \theta}, \quad (4.11)$$

where  $a$  is the separation between nearest neighbor atoms. The choice of axes in Fig. 2 corresponds to the principal axes of diffusion, in which  $\mathbf{D}$  is diagonal. The adiabatic potential possesses identical saddle points located at the short bridge sites  $S$  between atoms, while the minima are at the long bridge sites  $L$ . This geometry is believed to describe the diffusion of oxygen adatoms on  $W(110)$  surface, which has been studied both experimentally and theoretically [7-9, 105, 106, 156]. For this surface,  $\cot \theta = \sqrt{2}$ .

In Fig. 3 (b) we show results of our numerical calculations for a simple choice of the friction tensor, namely  $\eta^{xx} = \eta^{yy} = 1$ ,  $\eta^{xy} = \eta^{yx} = 0$ . Throughout this section, we measure energy

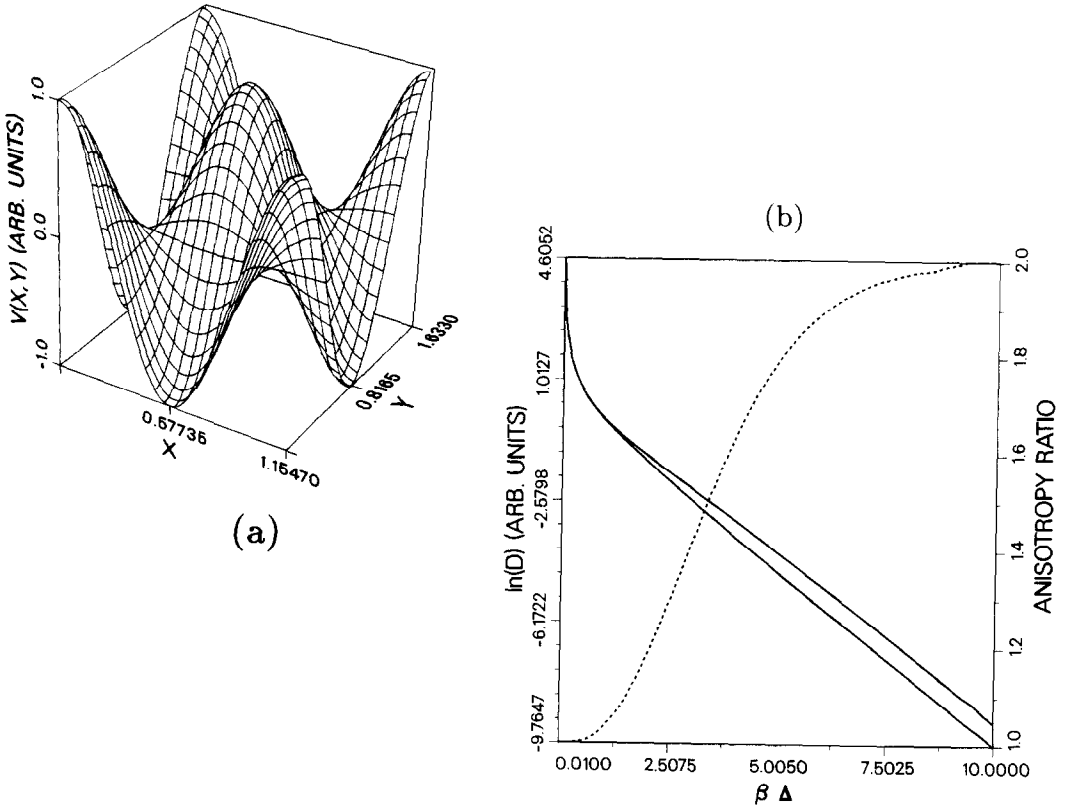


Fig. 3. (a) The simple cosine potential of Eq. (4.9) for the centered rectangular lattice, with  $V_0 = 1/2$ . (b)  $D_{zz}$  (lower solid curve) and  $D_{yy}$  (upper solid curve) vs.  $\beta\Delta$  for the centered rectangular lattice of Fig. 2, using the potential in (a). Dashed line denotes the anisotropy ratio  $D_{yy}/D_{zz}$ , which tends to the universal value  $\cot^2 \theta = 2$ .

in units of  $\Delta$ , and length in units of the lattice constant  $a$ . This implies a frequency scale of  $\sqrt{\Delta/(Ma^2)}$ . All values for the friction are then expressed in this unit. To include the Debye - Waller factors, we have used (4.8) and set  $\theta_D = 240$  K and  $\Delta = 1$  eV. This choice, in which the Debye temperature corresponds to the known value for the  $W(100)$  surface [157] and for which the barrier is very large, produces relatively large Debye - Waller correction factors. Even with these parameters the effect of this correction is rather small for  $\beta\Delta > 5$ , compared to our calculations with  $d_w \equiv 1$ .

In the high temperature limit, the solution depicted in Fig. 3 (b) correctly captures the isotropic limit of a Brownian particle. At low temperatures, both  $D_{yy}$  and  $D_{zz}$  cross over to an Arrhenius form at about  $\beta\Delta \sim 5$ , which correctly includes the energy barrier  $\Delta$  as given by the difference between the saddle point and minimum of the effective potential. In addition, at and below temperatures corresponding to  $\beta\Delta \sim 10$  the anisotropy ratio of diffusion  $D_{yy}/D_{zz}$  tends towards a universal limit

$$\frac{D_{yy}}{D_{zz}} = \cot^2 \theta, \quad (4.12)$$

which for the  $W(110)$  surface is two. This is *precisely* the value obtained using simple random walk theory, in which atoms execute random jumps across the long bridge sites  $L$  [7,105]. Namely, assuming that the diffusing particles hop between minima  $L$  via the saddle point barriers  $S$ , and using the random walk formula

$$D_{\alpha\alpha} = \frac{1}{4} \nu (\Delta r_\alpha)^2, \quad (4.13)$$

where  $\nu$  is the hopping rate and  $\Delta r_\alpha$  the distance of the hops in the  $x$  or  $y$  directions, we can immediately write

$$\frac{D_{yy}}{D_{zz}} = \frac{(\Delta y)^2}{(\Delta x)^2} = \frac{(a \cos \theta)^2}{(a \sin \theta)^2} = \cot^2 \theta. \quad (4.14)$$

An anisotropy ratio of two has also been experimentally measured for the  $O/W(110)$  system [105]. However, as our calculations demonstrate, the anisotropy ratio is very sensitive to temperature corrections of the diffusion prefactors *in addition to* the barrier, and thus the geometric limit generally appears at temperatures much lower than the beginning of the activated regime.

Another model potential, which we have used in our numerical calculations is a temperature dependent form given by

$$V_A(\vec{r}) = \frac{1}{\beta} \ln \left\{ \sum_i [e^{-\beta\alpha_x(x-R_{i,x}^0)^2} + e^{-\beta\alpha_y(y-R_{i,y}^0)^2}] \right\}. \quad (4.15)$$

In Figs. 4 (a) - (b) we show this potential at two different temperatures, with  $\alpha_x = 12$ ,  $\alpha_y = 4$ . Fig. 4 (c) shows calculations of  $\mathbf{D}$  for this potential using the same Debye - Waller factors as above and a friction tensor  $\eta^{xx} = \eta^{yy} = 1$ ,  $\eta^{xy} = \eta^{yx} = 0$ . Again, this result recovers both the correct Arrhenius form, with an asymptotically temperature independent energy barrier  $\Delta = 1$ , and the universal ratio (4.12) at the limit of low temperatures. For this potential the anisotropy ratio approaches its low temperature limit very fast due to a strong temperature

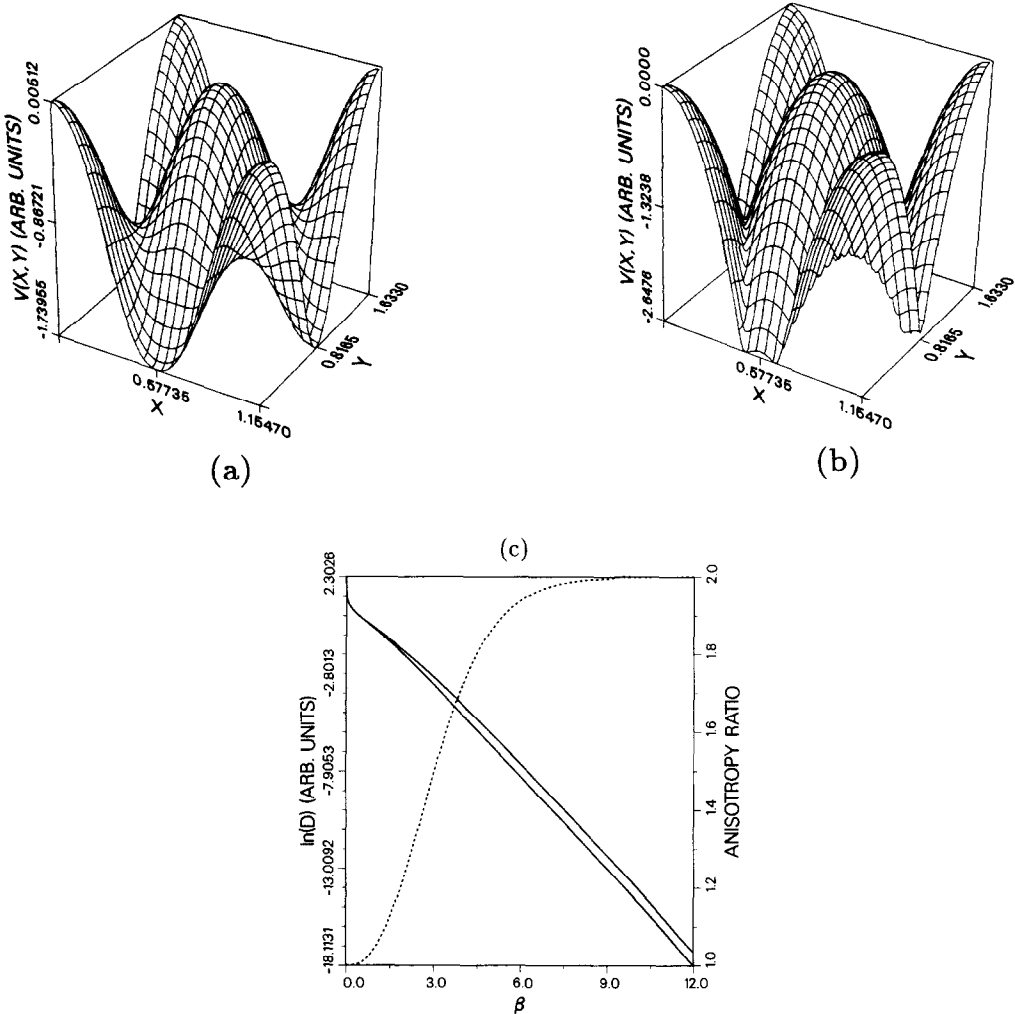


Fig. 4. Temperature dependent model potential of Eq. (4.15) at  $\beta = 1$  (a) and  $\beta = 8$  (b), for  $\alpha_x = 12$ ,  $\alpha_y = 4$ . At low temperatures, a narrow ridge develops connecting the minima. (c) Results for  $D_{zz}$  (lower solid curve) and  $D_{yy}$  (upper solid curve) vs.  $\beta\Delta$  for the potential in (a) - (b). Dashed line is the anisotropy ratio  $D_{yy}/D_{zz}$ , which now approaches  $\cot^2 \theta = 2$  rather rapidly (from Ref. [9]).

dependence of the curvature around the saddle point, see Fig. 4 (b). In Fig. 5 (c) we further show results for  $\mathbf{D}$  using  $\alpha_x = 6$ ,  $\alpha_y = 3$  in Eq. (4.15), as depicted in Figs. 5 (a) and (b). Additional calculations varying the adiabatic potentials and including spatial dependence in the friction tensor always reproduce the universal low temperature behavior [17]. However,

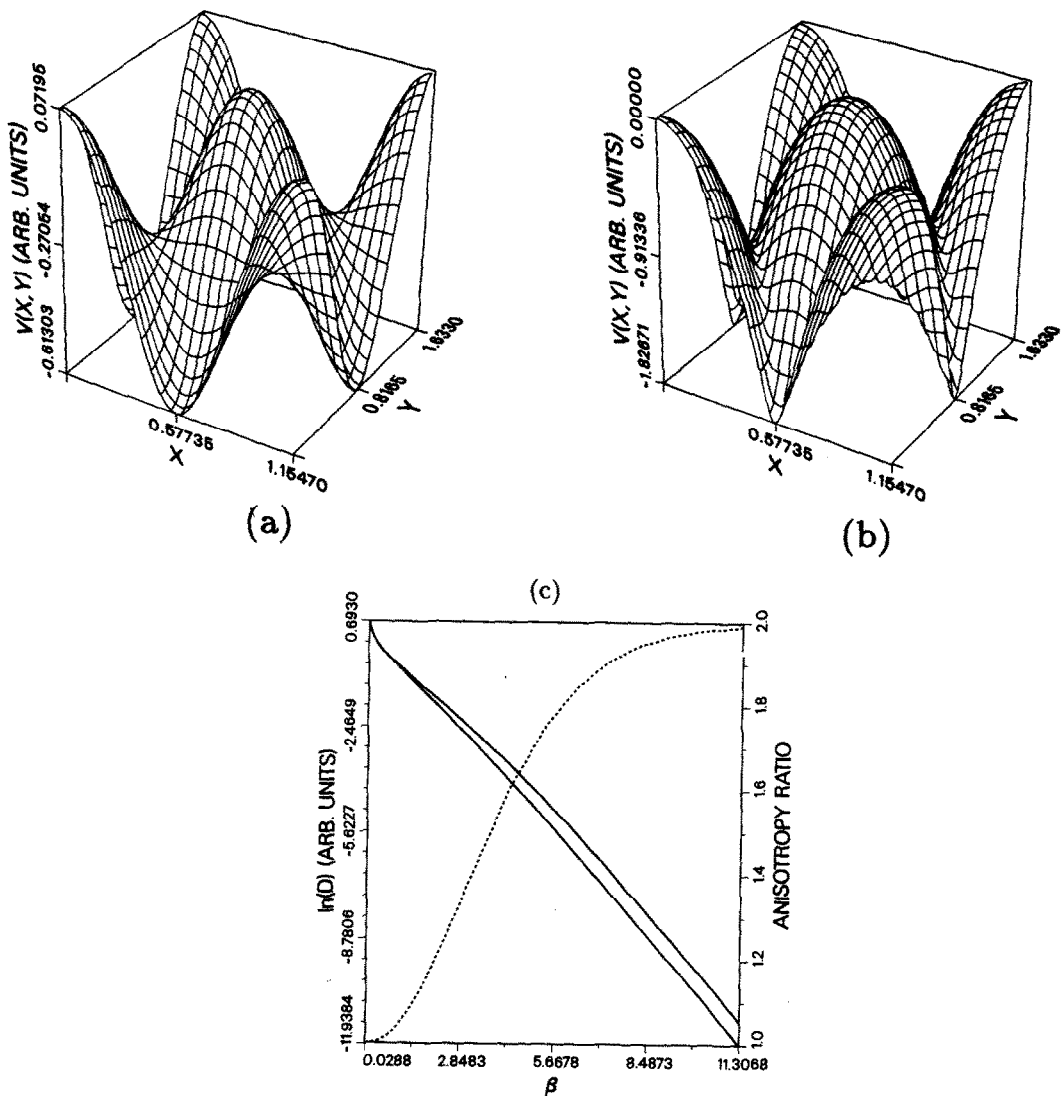
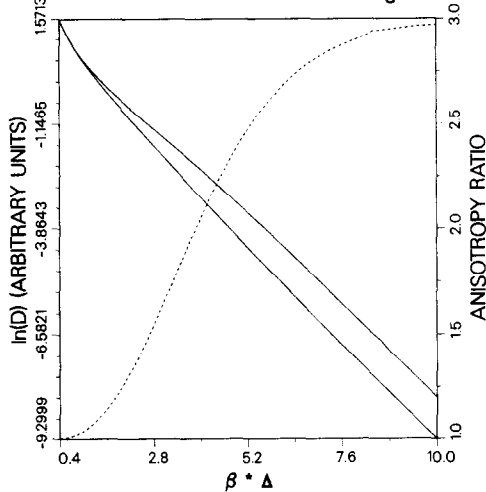


Fig. 5. Model potential of Eq. (4.15) at  $\beta = 1$  (a) and  $\beta = 8$  (b), for  $\alpha_x = 6$ ,  $\alpha_y = 3$ . (c) Results for  $D_{zz}$  (lower solid curve) and  $D_{yy}$  (upper solid curve) vs.  $\beta\Delta$  for the potential in (a) - (b). Dashed line is the anisotropy ratio  $D_{yy}/D_{zz}$ .

we note that at intermediate temperatures the detailed form of  $\mathbf{D}$  together with the diffusion anisotropy are model dependent, which can clearly be seen from our results in this chapter.



**Fig. 6.**  $D_{zz}$  (lower solid curve) and  $D_{yy}$  (upper solid curve) vs.  $\beta\Delta$  for the rhomboidal lattice of Fig. 2, with  $\cot\theta = \sqrt{3}$  [9]. Dashed line denotes the anisotropy ratio  $D_{yy}/D_{zz}$ , which tends to the universal value  $\cot^2\theta = 3$  for this case.

To verify the universal nature of the geometric result (4.12), we have done additional calculations using the geometry of Fig. 2, with  $\theta = 30^\circ$ . This corresponds to a slightly different rhomboidal lattice. We have again performed numerical calculations using a simple cosine potential. In Fig. 6 we show results for  $\mathbf{D}$  using the friction tensor  $\eta^{xz} = \eta^{yy} = 1/2$ ,  $\eta^{xy} = \eta^{yz} = 0$ . The Debye - Waller correction was the same as for the centered rectangular lattice. The results are also very similar, except that now the ratio  $D_{yy}/D_{zz}$  tends to  $\cot^2\theta = 3$  for this geometry.

(iii) The simple rectangular lattice. The simplest case in which the possibility of physically different saddle points arises naturally, is the simple rectangular lattice. Using our analytic formula Eq. (3.50) and the potential

$$V_1(\vec{r}) = V_A \cos \vec{G}_{10} \cdot \vec{r} + V_B \cos \vec{G}_{01} \cdot \vec{r}, \quad (4.16)$$

where a choice of  $V_A \neq V_B$  generates two distinct saddle points along the  $x$  and  $y$  axes, we obtain a generalization of the square lattice solution (4.6) as

$$\begin{aligned} D_{zz} &= \frac{k_B T}{M\eta^{zz}} [I_0(\beta V_A)]^{-2} \\ D_{yy} &= \frac{k_B T}{M\eta^{yy}} [I_0(\beta V_B)]^{-2}. \end{aligned} \quad (4.17)$$

The diffusion tensor now consists of two quasi - one - dimensional terms, which describe motion in the  $x$  and  $y$  directions separately. These solutions together with the adiabatic potential are

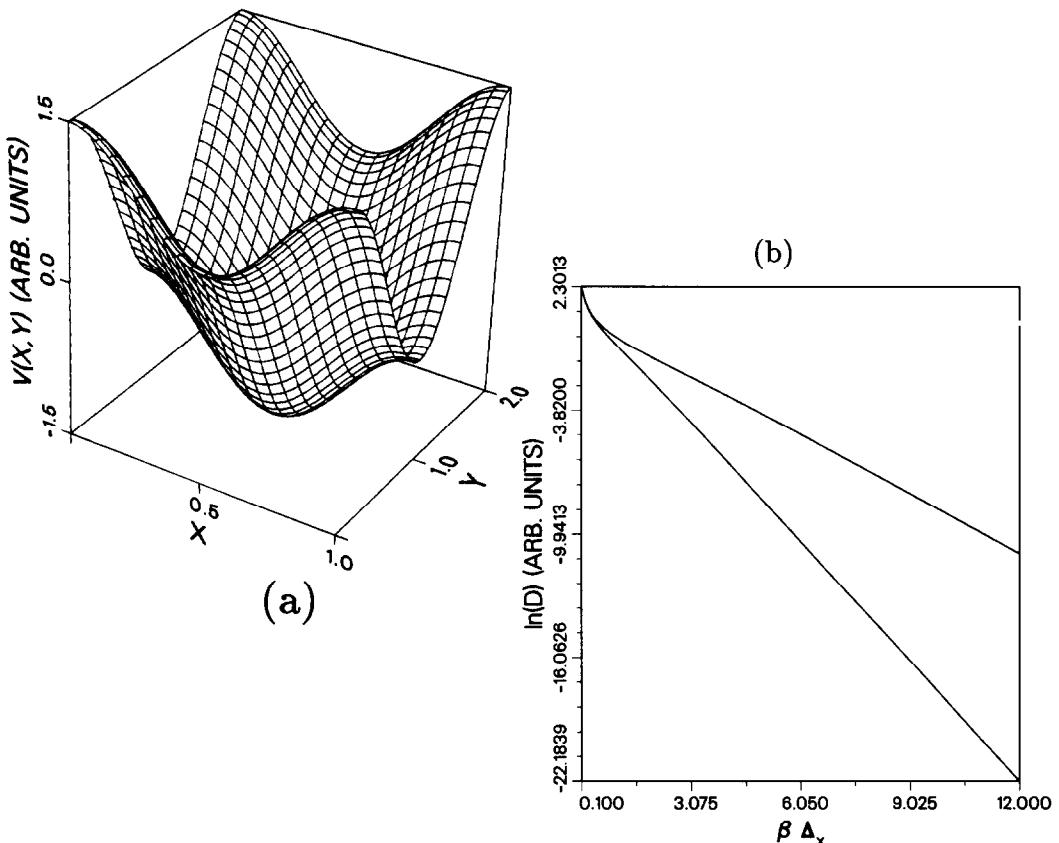


Fig. 7. (a) Cosine potential of Eq. (4.16) for a simple rectangular lattice, with  $V_A = 1/2$  and  $V_B = 1$ . The barriers are  $\Delta_z = 1$  and  $\Delta_y = 2$ . (b) Analytic solution of Eq. (4.17) for  $D_{zz}$  (upper curve) and  $D_{yy}$  (lower curve) vs.  $\beta\Delta_z$ , for the simple rectangular lattice.

shown in Figs. 7 (a) and (b). Both of these solutions start from their respective Brownian forms  $D_{\alpha\alpha} = k_B T / (M\eta^{\alpha\alpha})$  at high temperatures, and cross over to the Arrhenius form at low temperatures. However, the ratio  $D_{yy}/D_{zz}$  will go to zero exponentially fast for  $V_B > V_A$ , i.e. the saddle point with the lower energy barrier will dominate diffusion at low temperatures.

There exists a recent experimental study of a surface with simple rectangular symmetry, and two distinct energy barriers [107]. This involves self - diffusion of tungsten on a clean  $W(211)$  surface. In Fig. 8 (a) we show the experimentally measured components of the diffusion tensor. To illustrate the applicability of the microscopic theory presented here, we have done model

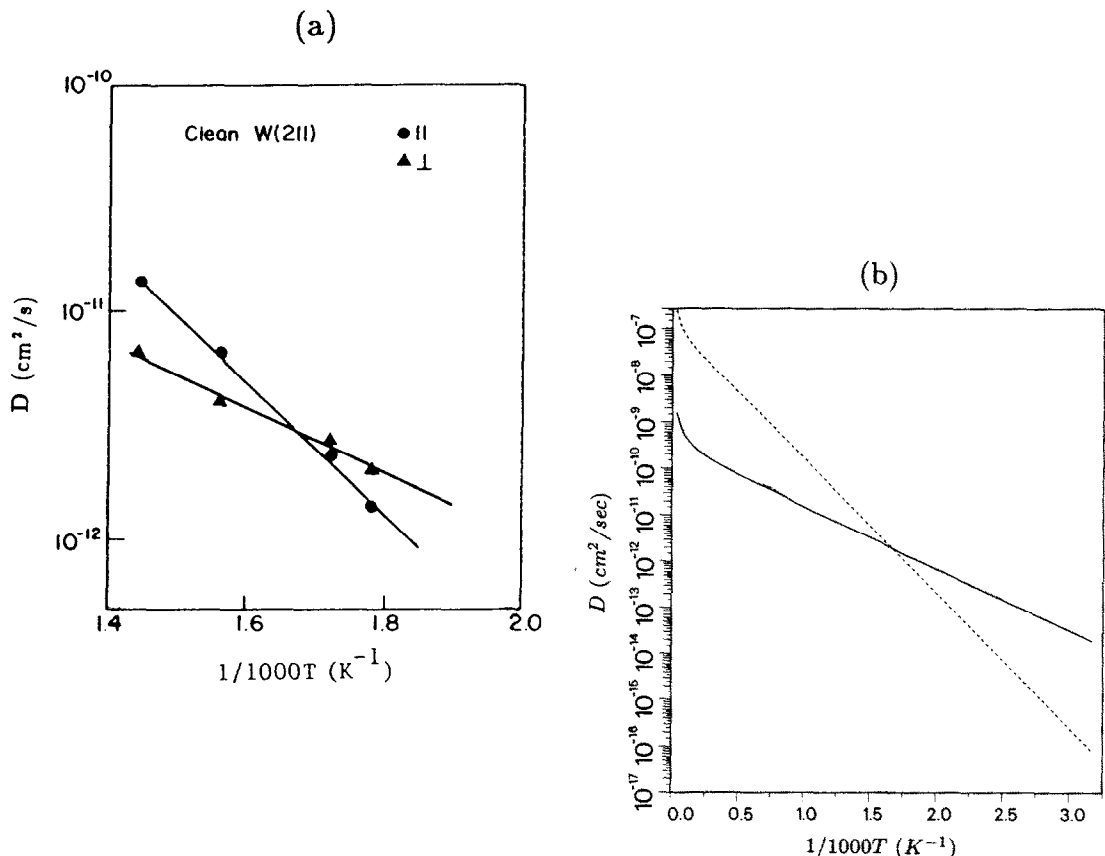


Fig. 8. (a) Experimental results of Tringides and Gomer [107] for self diffusion on the  $W(211)$  surface along two orthogonal directions. (b) Results of model calculations of  $W$  diffusion based on a simple rectangular lattice, as described in the text.  $D_{zz}$  (solid line) corresponds to the direction with the smaller barrier  $\Delta_z = 3125 \text{ K}$  [9].

calculations for this system. Using model potential of the form (4.16), we can incorporate the two different energy barriers seen in the experiments into the calculations. To obtain a quantitative fit, we have set the energy barriers  $\Delta_x = 1$ ,  $\Delta_y = 2.13$  (in normalized units in which  $\Delta_z = 3125 \text{ K}$ ), and used a constant anisotropic friction tensor with  $\eta^{xx}/\eta^{yy} = 0.0064$ ,  $\eta^{xy} = \eta^{yx} = 0$ . Setting the absolute values of  $\eta^{xx}$  and  $\eta^{yy}$  will then determine  $D$  in real units corresponding to the experiments. Additionally, the Debye - Waller parameters were set to correspond to  $\theta_D = 240 \text{ K}$ , and the corresponding energy barriers for each spatial

direction. In Fig. 8 (b) we display the results of these model calculations, which match with the experimentally observed curves very well. However, at higher temperatures we expect the simplified model used here not to be quantitatively correct [142].

### C. Second order friction expansion

As we have demonstrated in sections A and B, the diffusion of single adatoms on surfaces where the friction tensor undergoes no sudden changes displays universality both in the high and low temperature limits. In the high temperature limit, the diffusion tensor becomes spatially isotropic and approaches the Stokes - Einstein form of Eq. (4.3). For  $\beta\Delta \rightarrow 0$ ,  $\mathbf{D}$  is mainly determined by the geometry on the underlying lattice and the topology of the classical saddle points of the adiabatic potential as already qualitatively predicted by simple random walk theory.

However, all the theoretical results obtained this far are for the high friction limit, where  $\eta \gg 1$ . In real surface diffusion experiments there's no reason *a priori* why this should be true. In fact, there are such large variations of  $D$  in the experimental data that the friction can easily vary several orders in magnitude. For example, in the case of  $O/W(110)$  at 600 K, Chen and Gomer [158] have measured the Arrhenius activation energy to be 14 kcal/mol, while the prefactor  $D_0 \approx 2 \cdot 10^{-11} \text{ m}^2/\text{sec}$ . This corresponds to  $\eta/\omega_D \approx 150$ , which is in the high friction limit ( $\omega_D$  is the Debye frequency). However, for the same system at 1100 K, Butz and Wagner [130] measured  $\Delta = 27 \text{ kcal/mol}$  and  $D_0 = 3.8 \cdot 10^{-5} \text{ m}^2/\text{sec}$ , which corresponds to  $\eta/\omega_D \approx 8 \cdot 10^{-5}$ . For this case then, our results of the high friction limit can no longer be directly applied.

Despite the large variations in  $D$ , the activated Arrhenius form of diffusion is almost universally observed in the low temperature limit [5,152]. This is not too surprising in the sense that when  $\beta\Delta \gg 1$  the dominant energy scale determining  $D$  should certainly correspond to  $\Delta$  since diffusion always takes place through the lowest energy barrier in this limit. Unfortunately, to prove this from our microscopic theory without using the limit of high friction is exceedingly difficult at the moment. This is due to technical complications arising from the continued fraction expansion, which becomes rather involved when higher order terms in friction are taken into account. This is why we shall below only consider the expansion to second order in friction, and demonstrate that although  $\mathbf{D}$  and in particular, the diffusion anisotropy will be affected by higher order terms, the universal limits of diffusion remain unchanged.

In Sec. 3.B where we developed a general continued fraction expansion for the correlation functions  $\phi_{nn'}(\omega)$  of Eq. (3.14) the high friction limit corresponded to setting  $\mathbf{B}_n(\omega) = 0$  for  $n \geq 1$  in Eq. (3.21). This is equivalent to including only the first (1,1) element of the total

memory function  $\Sigma$ . To include the second order term within the continued fraction expansion, we must then set  $\mathbf{B}_n(\omega) = 0$  for  $n \geq 2$ , which gives

$$\mathbf{B}_1(\omega) = -\mathbf{a}_2^{-1}(\omega)\mathbf{b}_{21}. \quad (4.18)$$

This leads to a general expression for  $\phi_{11}(\omega)$  as

$$\phi_{11}(\omega) = [\mathbf{a}_1(\omega) - \mathbf{b}_{10}\mathbf{a}_0^{-1}(\omega)\mathbf{b}_{01} - \mathbf{b}_{12}\mathbf{a}_2^{-1}(\omega)\mathbf{b}_{21}]^{-1}. \quad (4.19)$$

The matrix  $\mathbf{a}_2(\omega)$  is given by

$$\mathbf{a}_2(\omega) \equiv -i\omega\chi_{22}^{-1} + \Sigma_{22}(\omega), \quad (4.20)$$

where the new (2,2) element of the memory function can be written as

$$\Sigma_{22}(\omega) = \chi_{22}^{-1}\gamma_2(\omega)\chi_{22}^{-1}, \quad (4.21)$$

with

$$\gamma_2(\omega) = \int_0^\infty dt e^{i\omega t}(Q L \mathbf{A}_2, e^{-iQ L Q t} Q L \mathbf{A}_2). \quad (4.22)$$

The  $\mathbf{b}$ 's are defined by

$$\mathbf{b}_{nm} = i\chi_{nn}^{-1}(\mathbf{A}_n, L\mathbf{A}_m)\chi_{mm}^{-1}. \quad (4.23)$$

The additional slow variable  $\mathbf{A}_2$ , which must now be explicitly included is given by

$$\mathbf{A}_2 = \{(\frac{P_\alpha P_\beta}{M^2} - \frac{k_B T}{M}\delta_{\alpha\beta})e^{i\bar{G}\cdot\vec{r}}\psi_j(u)\}. \quad (4.24)$$

It must be noted that both matrices  $\chi_{22}$  and  $\gamma_2(\omega)$  now depend on two pairs of spatial indices  $(\lambda, \lambda')$  in addition to  $s$  and  $s'$  (cf. Sec. 3.B), where  $\lambda$  and  $\lambda'$  are used here to denote the six possible inequivalent combinations  $xx, yy, zz, xy, xz$ , and  $yz$ .

To proceed further, we must simplify the (2,2) element of the memory function. First, we can easily show that

$$[\chi_{22}^{\lambda\lambda'}(s, s')]^{-1} = c_\lambda\chi_{00}^{-1}(s, s')\delta_{\lambda\lambda'}, \quad (4.25)$$

where

$$c_\lambda \equiv \begin{cases} \frac{1}{2} \left( \frac{M}{k_B T} \right)^2 & \text{for } xx, yy, zz; \\ \left( \frac{M}{k_B T} \right)^2 & \text{for } xy, xz, yz, \end{cases} \quad (4.26)$$

and  $\chi_{00}^{-1}$  is given by Eq. (3.37). We shall again employ the initial value approximation, and the harmonic approximation for the background vibrations. This leads to an expression for  $\gamma_2(\omega)$  in terms of the components of the friction tensor  $\eta^{\alpha\beta}(\vec{R}; \omega)$  of Eq. (3.43), in a manner very similar to the (1,1) element of the memory function. Making the additional simplifying assumption that the friction tensor is spatially diagonal, we obtain

$$\Sigma_{22}^{\lambda\lambda'}(s, s'; \omega) = \frac{2}{A_0^2} \left( \frac{k_B T}{M} \right)^2 c_\lambda^2 \int d\vec{r} du \tilde{n}^{-1}(\vec{r}, u) \eta^\lambda(\vec{r}, u; \omega) \psi_j(u) \psi_{j'}(u) \times e^{-u^2} e^{-i(\vec{G} - \vec{G}') \cdot \vec{r}} \delta_{\lambda\lambda'}, \quad (4.27)$$

where

$$\eta^\lambda(\vec{r}, u; \omega) \equiv 2[\eta^{\alpha\alpha}(\vec{r}, u; \omega) + \eta^{\beta\beta}(\vec{r}, u; \omega)], \text{ for } \lambda = (\alpha\beta). \quad (4.28)$$

The Eqs. (4.25) and (4.28) are both diagonal in terms of the spatial index pairs  $\lambda, \lambda'$ , which allows a considerable simplification of the matrix product in Eq. (4.19), and inversion of  $\mathbf{a}_2$ .

Next we must calculate the matrices  $\mathbf{b}_{12}$  and  $\mathbf{b}_{21}$ . The results are:

$$\mathbf{b}_{12}^{\alpha\lambda}(s, s') = \frac{M}{k_B T} [i \sum_\gamma G'_\gamma \chi_{00}^{-1}(s, s') \delta_{\lambda, \gamma\alpha} - \sqrt{\frac{c}{k_B T}} \sqrt{2(j' + 1)} \chi_{00}^{-1}(s; \vec{G}', j' + 1) \delta_{\lambda, z\alpha}], \quad (4.29)$$

and

$$\mathbf{b}_{21}^{\lambda\alpha}(s, s') = \frac{M}{k_B T} [i \sum_\gamma G_\gamma \chi_{00}^{-1}(s, s') \delta_{\lambda, \alpha\gamma} + \sqrt{\frac{c}{k_B T}} \sqrt{2(j + 1)} \chi_{00}^{-1}(\vec{G}, j + 1; s') \delta_{\lambda, \alpha z}], \quad (4.30)$$

where we have again listed the indices in detail. Using these equations with Eqs. (4.20), (4.21) and (4.25) it is possible to work out the matrix elements of

$$\mathbf{F}_2(\omega) = \mathbf{b}_{12} \mathbf{a}_2^{-1}(\omega) \mathbf{b}_{21}, \quad (4.31)$$

which are infinite in terms of two spatial indices  $\alpha\beta$  and  $(s, s')$ . The complete result for the frequency dependent velocity - velocity correlation function then becomes

$$\phi_{11}(\omega) = [-i\omega \frac{M}{k_B T} \delta_{\alpha\beta} \chi_{00}^{-1} + \Sigma_{11}(\omega) + \mathbf{F}_1(\omega) + \mathbf{F}_2(\omega)]^{-1}. \quad (4.32)$$

Since  $\mathbf{F}_2$  is proportional to  $\mathbf{a}_2^{-1}$ , which in turn contains the friction tensor, the new term in Eq. (4.32) is of the order of  $\mathcal{O}(\eta^{-1})$  in the limit  $\omega \rightarrow 0$ , as compared with the high friction limit where  $\Sigma \sim \mathcal{O}(\eta)$ .

Eq. (4.32) is the general expression from which the diffusion tensor can be calculated, once  $\mathbf{F}_2$  is known. However, in the most general case the expression for its matrix elements becomes rather complicated, and will be presented elsewhere [17]. Instead, to study the effect of the additional term to diffusion, we shall hereon neglect the vertical motion, which will only renormalize the value of  $D$  (cf. Sec. B.(i)). If we furthermore assume that the friction tensor is simply an isotropic constant, it can be shown that all the spatial elements of the memory function  $\Sigma_{22}$  become proportional to the isotropic elements of  $\Sigma_{11}$  which can be inverted analytically [17]. Thus, we can derive relatively simple expressions for the matrix elements in terms of the density  $n(\vec{r})$  and the adiabatic potential. Unfortunately, even in this special case there seems to be no analogue of an analytic closed form expression for  $D$ , which was found in the high friction limit. Thus, one always has to calculate all the matrix elements of  $\phi_{11}$  and invert Eq. (4.32) numerically.

(i) Results for the square lattice. We shall first examine the case of the square lattice, where  $D$  is isotropic. To study the effect of the additional term, we have chosen  $\eta$  to be a simple isotropic constant whose magnitude varies, and used the adiabatic cosine potential of Eq. (4.5), with  $V_2 \equiv 0$ . In Fig. 9 (a) we display results for  $\eta^{xx} = \eta^{yy} = 10$ , while in Fig. 9 (b)  $\eta^{xx} = \eta^{yy} = 1$ , both compared with the corresponding high friction limits. For the first case, the friction is large enough that there is only a small quantitative change in  $D$  as a function of temperature. In the other case, there is a quantitatively large difference between the results obtained in the high friction limit, and with the additional term included. However, as can be clearly seen from both figures, the *universal limits* of  $D$  at high and low temperatures remain qualitatively unchanged. In particular, for  $\beta\Delta \rightarrow \infty$  the Arrhenius form is again recovered. Additional calculations for other values of the friction recover analogous results.

(ii) Results for the centered rectangular lattice. For the centered rectangular lattice of Sec. B.(ii), we used the cosine potential of Eq. (4.9). In Figs. 10 (a) and (b) we show results for  $\eta^{xx} = \eta^{yy} = 10$ , and  $\eta^{xx} = \eta^{yy} = 1$ , both again compared to the corresponding high friction limits. In the first case the additional term is again very small compared with the high friction limit, but for smaller friction quantitative differences become large. In particular, although the high and low temperature limits remain qualitatively unchanged, the *diffusion anisotropy* behaves in a markedly different manner from that in the high friction limit at inter-

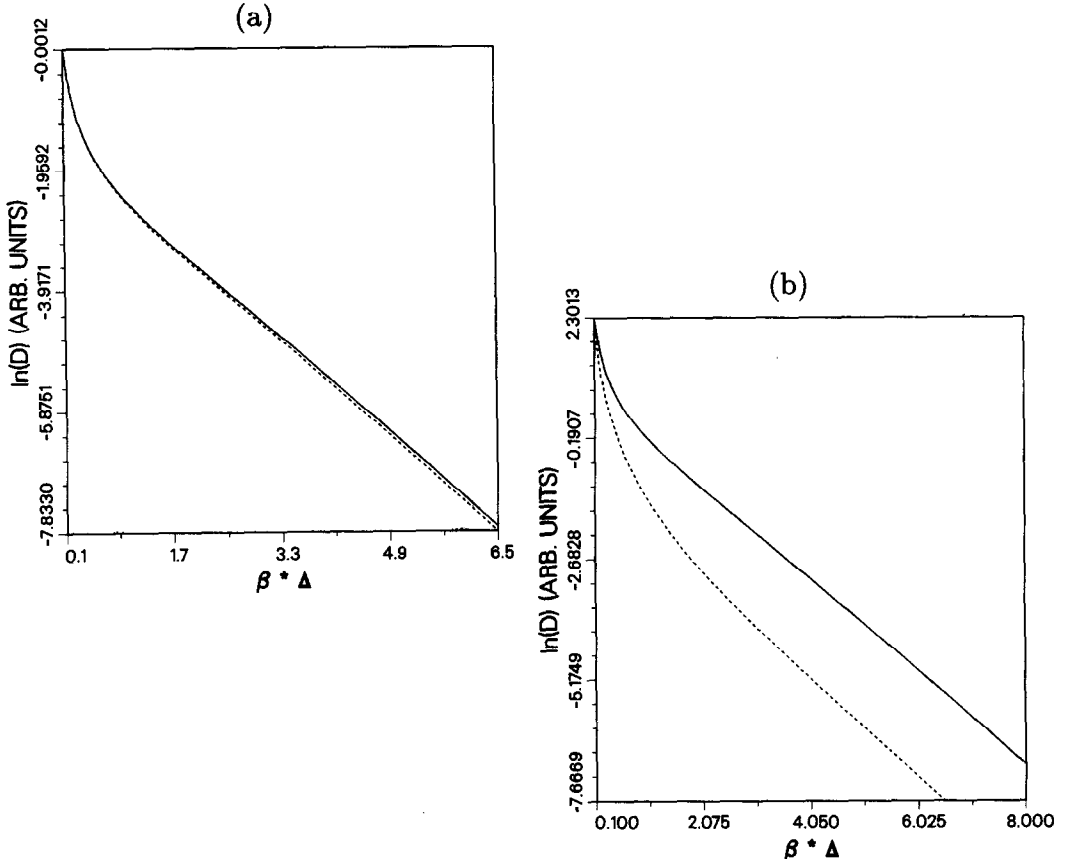


Fig. 9. Comparison between the analytic square lattice result of Eq. (4.6) in the high friction limit (solid line) with  $V_0 = 1/2$ , and results obtained with the next order friction term included (dashed line). (a) the friction  $\eta = 10$ , and (b)  $\eta = 1$ .

mediate temperatures, in that the geometric random walk limit  $D_{yy}/D_{zz} = 2$  sets in at much lower temperatures. Our further calculations varying the friction gave similar results.

### 5. Diffusion on Lattices with Local Distortions

In this chapter, we consider the diffusion on substrates with large local distortions induced by adatoms on the surface [7,10,13,14,17]. Since diffusion is strongly influenced by the form of the adibatic potential in the local environment, we expect local distortions to have a strong influence on the diffusion coefficients. We shall indeed see below that the diffusion anisotropy

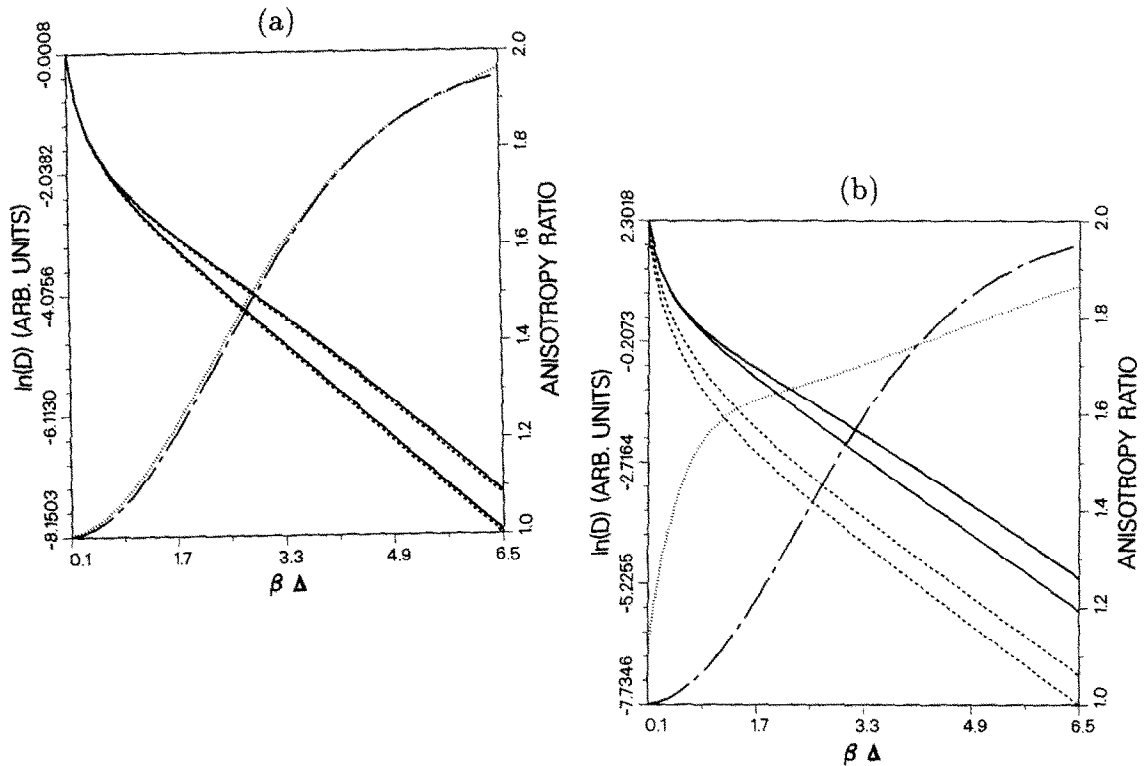


Fig. 10. Comparison between  $D$  obtained for the cosine potential of Eq. (4.9) (with  $V_0 = 1/2$ ) in the high friction limit ( $D_{yy}$ , upper solid line;  $D_{zz}$ , lower solid line;  $D_{yy}/D_{zz}$ , chain - dashed line), and the next order friction term included ( $D_{yy}$ , upper dashed line;  $D_{zz}$ , lower dashed line;  $D_{yy}/D_{zz}$ , dotted line). (a)  $\eta^{xz} = \eta^{yy} = 10$ ,  $\eta^{xy} = \eta^{yz} = 0$ ; (b)  $\eta^{xz} = \eta^{yy} = 1$ ,  $\eta^{xy} = \eta^{yz} = 0$ .

in particular can be qualitatively different from that on a rigid substrate. Our work here is motivated by the observed diffusion anisotropies of  $H$  and  $O$  adatoms on the  $W(110)$  surface [105,159]. In section A, we present a novel two - step lattice gas model appropriate for the study of diffusion of these adatoms on the tungsten surface. This model is a generalization of the standard lattice gas model. It allows an extra internal barrier within the unit cell of the  $W(110)$  surface, which is created by a local distortion. In section B, we examine local lattice distortions from the point of view of the microscopic theory discussed in chapters 3 and 4. Our

calculations also provide a justification for the two - step lattice gas model of section A in the low temperature regime. Finally, we present extensive Monte Carlo simulation studies together with some analytic results for the two - step model at finite coverages, and discuss the results in light of the experimental works on *H* and *O* diffusion on *W*(110).

### A. Two - step lattice gas model of diffusion for *H* and *O* on *W*(110)

Recently, the diffusion tensor associated with collective diffusion of hydrogen and oxygen adatoms on *W*(110) surface was studied by the field emission fluctuation method [105,159]. An intriguing aspect of the results obtained is the marked difference of the diffusion anisotropy of the two atomic species. Along the two principal symmetry directions of the surface, namely  $(\bar{1}\bar{1}0)$  and  $(001)$ , it was found that  $D_{(\bar{1}\bar{1}0)}^c/D_{(001)}^c \approx 2$  for *O*, whereas for *H* adatoms this ratio was considerably closer to unity. In both cases, the ratio was found not to be very strongly coverage - dependent.

The observed anisotropy for oxygen can be easily understood within the standard lattice - gas model as resulting from purely geometrical considerations of the underlying *W*(110) lattice which forms a centered rectangular lattice, as discussed in Sec. 4.B.(ii). Namely, referring to Fig. 2 both *O* and *H* are believed to chemisorb on *W*(110) at the long bridge sites. The lowest energy barriers for crossing from one adsorption site to another are located symmetrically at the short bridge sites. This topology is supported by total energy calculations [160], as well as experimental measurements of local vibrational modes [161]. Within the conventional lattice - gas model [162,163], an adatom performs a random walk on the lattice. This atomic motion consists of uncorrelated diffusion jumps from one adsorption site to another via the lowest energy barrier connecting the unit cells, i.e. the jumps are along  $(\bar{1}\bar{1}1)$  directions in the plane. Denoting the  $(001)$  and  $(\bar{1}\bar{1}0)$  directions by  $x$  and  $y$ , respectively, we can immediately obtain the zero - coverage limit random walk result of Eq. (4.14), where  $D_{yy}/D_{xx} = y_0^2/x_0^2 = 2$ , and  $2x_0 = 2a \sin \theta$  and  $2y_0 = 2a \cos \theta$  are the dimensions of the centered rectangular unit cell along  $x$  and  $y$  axes. By symmetry, the off - diagonal elements of the diffusion tensor  $D_{xy} = D_{yx} = 0$ . From the calculations done with our microscopic theory, we know that this anisotropy with the corresponding diffusion paths is always approached in the limit  $\beta\Delta \rightarrow \infty$  for this geometry. Additionally, it has been established [164,165] that for a non - interacting system (including the case of no multiple occupancy of sites), the collective or chemical diffusion constant is strictly independent of coverage, and equal to the zero - coverage random walk result. Thus, for a weakly interacting adsorbate system Eq. (4.14) should hold to a good degree of accuracy. This is believed to be the situation for *O* on *W*(110), although the *O* - *O* interactions may play a role in determining the details of the anisotropy at lower temperatures.

Clearly, the experimental results indicate that this simple model fails to describe the diffusion of  $H$ . An important clue to the differences between  $O$  and  $H$  chemisorption are effects observed at higher coverages. It has been found that at coverages  $\theta \gtrsim 0.5$ , hydrogen induces a global substrate reconstruction which involves a shift of the top layer of the substrate relative to the bulk [166]. No such reconstruction is observed for oxygen. This has lead to the speculation that a symmetry - breaking associated with the reconstruction is the origin for the reduced ratio of  $D_{yy}/D_{zz}$  for  $H$  [105]. However, this effect can clearly at best account for the observed behaviour at  $\theta \gtrsim 0.5$ , where the reconstructed phase sets in.

To explain the experimental findings, we have recently proposed [7] a simple generalization of the usual lattice - gas model for diffusion which accounts quantitatively for the diffusion anisotropy of  $H$  and  $O$  adatoms. It also relates the low coverage behaviour of hydrogen to the high coverage  $H$  - induced reconstruction in a natural way. The key ingredient in the model is to recognize that at low coverages of  $H$ , even when the *global* substrate reconstruction does not yet occur, there can be a substantial degree of *local* distortion around each chemisorbed hydrogen atom, which changes diffusion behaviour in a fundamental way as we shall elucidate below.

First, we describe briefly the proposed driving mechanism of Ref. [166] for the  $H$  - induced reconstruction. It has been established that the binding potential well in the 'hourglass' region of the long bridge sites for  $H/W(110)$  is very flat [160]. A surface reconstruction of a top layer shift along the  $(1\bar{1}0)$  direction would lower the symmetry of the well resulting in an increased binding energy. Because of the large cost of the elastic energy associated with the lateral shift of the entire top layer, this reconstruction is only energetically feasible when the coverage exceeds a critical value [166]. However, a single hydrogen atom can still induce a local substrate distortion with the four immediate neighbouring  $W$  atoms displaced along  $(1\bar{1}0)$ . The resultant gain in binding energy can overcome the elastic energy of the distortion if the amplitude of the distortion decays rapidly to zero away from the adatom site as illustrated in Fig. 11 (a). This is analogous to the classic Jahn - Teller symmetry lowering effects in a molecule. The resultant potential well now develops a double well structure within the 'hourglass' adsorption site. When the adatom sits on one side of this double well, it is accompanied by a local shift of  $W$  atoms along the  $(1\bar{1}0)$  direction. The direction of these displacements is reversed when  $H$  occupies the other site within the 'hourglass'. For low coverages, the local distortions around each  $H$  adatom do not overlap, and there are no correlations between them. As a result, there is no long range order or global surface reconstruction. As the coverage increases, these local distortions start to overlap and the system can lower its elastic energy by correlating all the

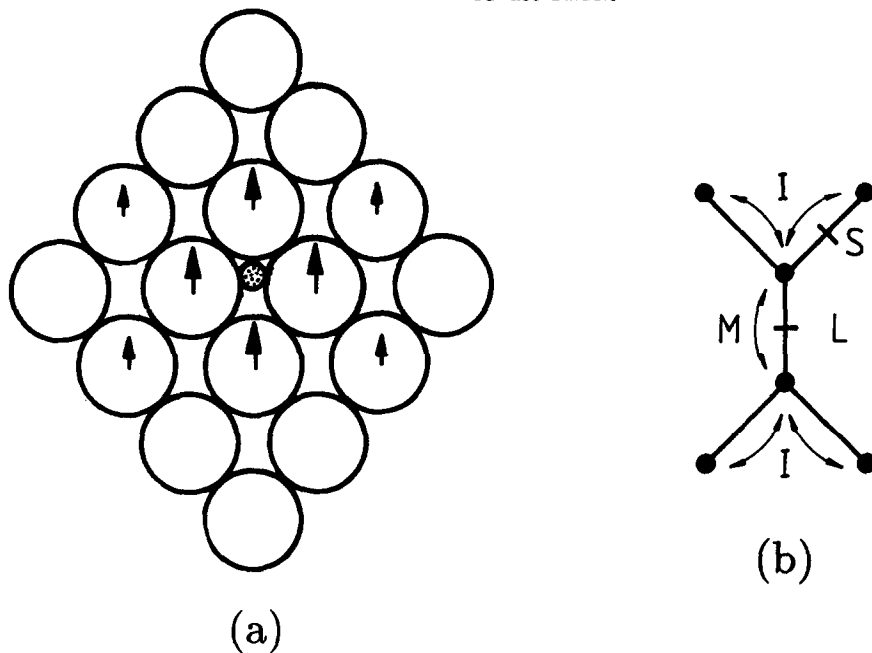


Fig. 11. (a) A schematic picture of the local distortion field  $\tilde{u}(\vec{r})$  induced by an adsorbed  $H$  atom on the  $W(110)$  surface, which is depicted in Fig. 2 [7]. The initially flat hourglass site develops an additional saddle point with an energy barrier  $\Delta_i$ , which controls the intracell jumps in the two - step model. (b) The two - step lattice gas model with intracell and intercell rates  $M$  and  $I$  shown schematically.  $L$  and  $S$  correspond to the orginal surface geometry of Fig. 2 [13].

local distortions, with all  $H$  atoms now adsorbed on the same side of the double well potential. This corresponds to a reconstructed phase with a global shift of the top layer relative to the bulk. In fact, this picture is just one particular example of the currently accepted picture of structural phase transitions [167]. Since  $O$  does not induce any observable reconstruction on  $W(110)$ , we conclude that the local substrate distortion for  $O/W(110)$  is negligible or at least much smaller than that for  $H/W(110)$ .

An important feature of the model is that even without direct adatom interactions, double occupation of an adsorption site is not favorable. This happens because of the opposing substrate distortions of two adatoms within the same cell that leads to a large local increase in the energy. Since the time scale for the adatom motion is much longer than a typical time scale for the substrate response, the effect just described can be approximately modeled by splitting the original single adsorption site into *two* symmetric sites. When this is done, an energy barrier

$\Delta_i$  exists for the motion from one subsite to another. Moreover, a simultaneous occupation of the two subsites is then forbidden, i.e. the hardcore repulsion applies within each *cell*. In the context of a simple random walk theory, the diffusive motion of the adatoms can then be analysed in terms of two fundamental jumps on a static lattice. The first is an *intracell* jump across the barrier  $\Delta_i$  with a rate  $M$  (see Fig. 11 (b)) originating from the local distortion. The second is an *intercell* jump with a rate  $I$  across the barrier  $\Delta_e$  due to the usual periodic arrangement of the substrate atoms. The competition between these two processes can be parametrized by a *branching ratio*  $r \equiv M/I$ , which is the ratio of the intracell to intercell diffusion rates. In realistic adsorption systems, additional direct or indirect interactions exist between adatoms on different adsorption sites, as evidenced by the appearance of many distinct ordered phases of the adlayer [168]. However, even without these interactions, the presence of both intracell and intercell jumps as well as the exclusion of double occupancy within a cell already lead to a very complicated coverage dependence and cause strong correlation effects to appear for both tracer and collective diffusion in the model. Having said this, a note of caution must also be added : the assumption of a static substrate renders the model physically applicable for  $H/W(110)$  only in the regime where no global reconstruction of the substrate occurs, i.e. for coverages  $\theta \lesssim 0.5$ .

It is easy to see that this new two - step lattice gas model contains the right ingredients for the explanation of the observed differences in the diffusion anisotropies of  $H$  and  $O$  adatoms. In the zero coverage limit of  $\theta \rightarrow 0$ , the diffusion tensor can be obtained exactly by enumerating all the possible two - jump processes in the model which bring the adatom back into an equivalent site. The result is [7]:

$$D_{zz} = x_0^2 \nu \frac{1}{2+r} \quad (5.1)$$

$$D_{yy} = y_0^2 \nu \frac{r}{(2+r)^2} \quad (5.2)$$

or

$$\frac{D_{yy}}{D_{zz}} = \frac{y_0^2}{x_0^2} \frac{r}{2+r} \quad (5.3)$$

Here  $\nu$  denotes the overall jump frequency, and  $r = M/I$  is the branching ratio. By symmetry, the off - diagonal terms are again zero. The conventional lattice gas model corresponds to the case of no local distortion and an infinite branching ratio, in which case Eq. (5.3) gives  $D_{yy}/D_{zz} = 2$ , just as in the results of Sec. 4.B.(ii). This should correspond to the diffusion of

*O.* However, for the large local distortion as expected for  $H$ , the branching ratio is finite and  $D_{yy}/D_{zz}$  is always less than two, as seen in the experiments.

Before proceeding with more detailed calculations within the two - step model presented above we shall examine its validity from the point of view of the microscopic theory of Chap. 3.

### B. Microscopic theory of diffusion on substrates with local distortions

In this section, we consider the adatom induced local distortions from a microscopic point of view [10]. This allows us to examine the validity of the two - step lattice gas model and the *full temperature dependence* of the branching ratio  $r$  on a general theoretical basis. We find that it is indeed possible to describe diffusion in this case simply as consisting of two separate jumps over the saddle points as described in the previous section, except at low temperatures. The main prediction Eq. (5.3) of the two - step model for the diffusion anisotropy still holds qualitatively. Namely, the local distortion lowers the anisotropy compared to the undistorted case. However, in the general case the detailed behavior of the anisotropy is sensitive to the entire adiabatic surface potential and not just the intracell and intercell barrier heights  $\Delta_i$  and  $\Delta_e$ .

In the following, we will set  $\eta_{zx} = \eta_{yy} = 1$ ,  $\eta_{zy} = \eta_{yx} = 0$ , which will not affect the qualitative features of our results (cf. Sec. 4.B.). We note that the theory is valid *at all temperatures* within the high friction approximation, and *no assumptions* about thermal activation or individual diffusion jumps are made. To model a distorted centered rectangular lattice, we first write the total clean surface potential as

$$V_0(\vec{r}) = \sum_{\ell} v(\vec{r} - \vec{R}_{\ell}) e^{-\gamma z_{\ell}^2} + \sum_{\ell} v(\vec{r} - \vec{R}_{\ell} + \vec{\delta}) e^{-\gamma(z_{\ell} + d)^2}. \quad (5.4)$$

The first term in Eq. (5.4) describes the sum of pair potentials from the surface layer, while the second is the contribution from an underlying layer of atoms at depth  $d$ . For the centered rectangular case, the second layer is displaced horizontally by  $\vec{\delta}$ , which causes the the second layer atoms to lie directly beneath the clean surface adsorption sites. In Eq. (5.4),  $\gamma$  and  $z_0$  are constants. In the presence of an  $H$  adatom, a local distortion in the first layer of surface atoms occurs. For short range  $H - W$  interactions, we can approximate the local distortion by a uniform displacement  $\vec{u}(\vec{r})$  of the first layer since the displacement of the  $W$  atoms beyond the range of interaction has no effect on the adsorption potential. The displacement  $\vec{u}(\vec{r})$ , however, is a strong function of the position of the adatom. By symmetry, it should vanish when the  $H$  adatom is at the center of the hourglass region. The displacement also has to be periodic, being

an odd function of the  $y$  and an even function of the  $x$  coordinates of the adatom measured from the center of the hourglass. The general form of the distorted surface potential is

$$V(\vec{r}) = \sum_{\ell} v(\vec{r} - \vec{R}_{\ell} - \vec{u}) e^{-\gamma z_0^2} + \sum_{\ell} v(\vec{r} - \vec{R}_{\ell} + \vec{\delta}) e^{-\gamma(z_0+d)^2}. \quad (5.5)$$

In the limit  $u \rightarrow 0$ , this becomes

$$V(\vec{r}) = V_0(\vec{r}) + \sum_{\ell} \nabla v(\vec{r} - \vec{R}_{\ell}) \cdot \vec{u} e^{-\gamma z_0^2}. \quad (5.6)$$

By choosing an appropriate  $\vec{u}(\vec{r})$ , one can then obtain the corresponding distorted adiabatic potential  $V_A$ . However, perhaps the easiest way to construct a desired potential is to modify the Fourier components of  $V(\vec{G})$  for various reciprocal lattice vectors while respecting the symmetry constraints imposed by  $\vec{u}(\vec{r})$ .

In Fig. 3 of Sec. 4.B.(ii) we have shown results of calculations for an atom on an undistorted surface (i.e.  $\vec{u} \equiv 0$ ), with an adiabatic potential  $V_0(\vec{r}) = (1/2)(\cos \vec{G}_1 \cdot \vec{r} + \cos \vec{G}_2 \cdot \vec{r})$ . This corresponds to  $\Delta_e = 1$  and  $\Delta_i \equiv 0$ . In the high temperature limit the theory correctly recovers the case of diffusion in a viscous, uniform medium for which  $\mathbf{D}$  is isotropic. Also, both the Arrhenius form  $D_{zz} \sim D_{yy} \sim e^{-\beta \Delta_e}$  and the geometric random walk limit  $D_{yy}/D_{zz} = 2$  emerge in the low temperature limit. The barrier  $\Delta_e$  corresponds precisely to the energy difference between the saddle point and the minimum of  $V_0(\vec{r})$ . In the presence of a small displacement  $\vec{u}(\vec{r})$ , an additional barrier  $\Delta_i < \Delta_e$  is introduced in the middle of the original hourglass potential well. In Figs. 12 (b), 13 (b) and 14 (b) we show results of calculations of  $\mathbf{D}$  for a potential of the form:

$$V_A(\vec{r}) = V_0(\vec{r}) - V_1 (\sin \vec{G}_1 \cdot \vec{r} + \sin \vec{G}_2 \cdot \vec{r})^2. \quad (5.7)$$

Obviously,  $V_1$  is proportional to the magnitude of the displacement of  $W$  atoms involved in the local distortion. We have chosen  $V_1 = (2 + \sqrt{3})/8$  in Fig. 12 (a), and  $V_1 = (10 + 3\sqrt{11})/8$  in Fig. 13 (a). This leads to the barrier values  $\Delta_i = 1$ ,  $\Delta_e = 2$ , and  $\Delta_i = 9$ ,  $\Delta_e = 10$ , respectively. The diffusion tensor  $\mathbf{D}$  is controlled by the larger external barrier  $\Delta_e$ , which appears in the effective Arrhenius form  $D_{zz} \sim D_{yy} \sim e^{-\beta \Delta_e}$  at low temperatures. The geometric ratio  $D_{yy}/D_{zz} = 2$  is obtained in the limit  $\beta \Delta \rightarrow \infty$ , as predicted by the random walk theory with  $r \rightarrow \infty$ . At intermediate temperatures the anisotropy ratio is considerably *smaller* than in the undistorted case. In Fig. 14 (b) we display results for an extreme case of potential of Fig. 14 (a) with  $V_1 = (100 + 3\sqrt{1111})/8$ , where the barriers are almost equal, with  $\Delta_i = 99$  and  $\Delta_e = 100$ .

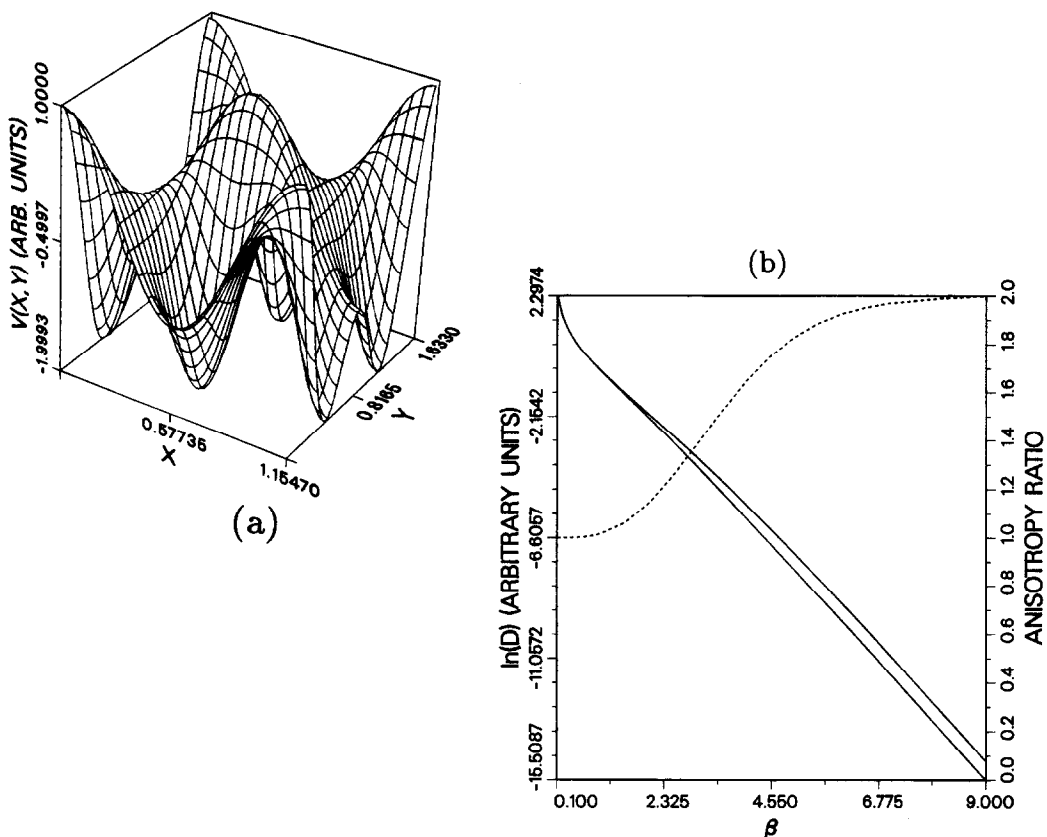


Fig. 12. (a) Adiabatic potential for a model of a distorted  $W(110)$  surface, with  $\Delta_e = 2$ ,  $\Delta_i = 1$ . The unit cell shown has an  $W$  atom at each corner, and one in the middle. As a consequence of the local distortion, there are two minima within each hourglass adsorption site. (b)  $D_{yy}$  (upper curve) and  $D_{zz}$  (lower curve) vs. inverse temperature  $\beta$  for the potential surface in (a). The anisotropy ratio  $D_{yy}/D_{zz}$  (dashed line) approaches its universal limit of two for  $\beta\Delta \rightarrow \infty$  in a manner similar to the undistorted surface. We note that  $\beta^{-1}$  and  $\Delta$  are scaled to a common energy unit in this and all the other figures of this section.

Although  $D$  varies about 36 orders in magnitude, the anisotropy ratio remains very close to one and is not approaching its limiting value of 2 at the temperatures shown here. However, the Arrhenius form is nevertheless obeyed to a rather good degree of accuracy.

In the opposite case of a strong reconstruction where  $\Delta_i > \Delta_e$ , we expect the diffusion in

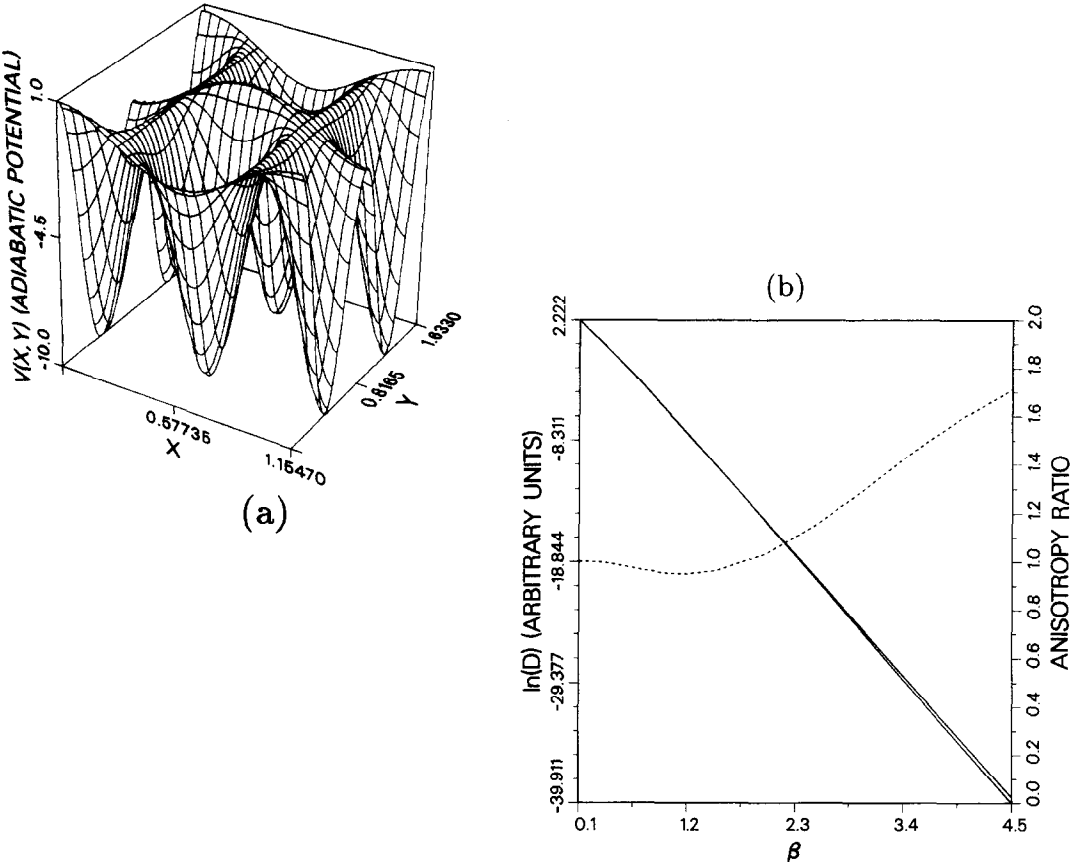


Fig. 13. (a) Adiabatic potential of Eq. (5.7) with  $\Delta_e = 10$  and  $\Delta_i = 9$ . (b)  $D_{yy}$  (upper curve) and  $D_{zz}$  (lower curve) vs. inverse temperature  $\beta$  for the potential surface in (a). The anisotropy ratio  $D_{yy}/D_{zz}$  (dashed line) approaches its universal limit much slower than in Fig. 12 [10].

the  $y$ -direction to be suppressed by the larger internal barrier. In Fig. 15 we show results for a potential of the form

$$V_A(\vec{r}) = V_0(\vec{r}) - V_1 (\sin \vec{G}_1 \cdot \vec{r} + \sin \vec{G}_2 \cdot \vec{r})^2 + V_2 (\cos \vec{G}_+ \cdot \vec{r} + \cos \vec{G}_- \cdot \vec{r}), \quad (5.8)$$

for which we have chosen  $V_1 = 5$ ,  $V_2 = 1/2$ , leading to  $\Delta_i = 20.01$ ,  $\Delta_e = 19.85$ . In Eq. (5.9),  $\vec{G}_+ \equiv \vec{G}_1 + \vec{G}_2$  and  $\vec{G}_- \equiv \vec{G}_1 - \vec{G}_2$ .  $D_{zz}$  and  $D_{yy}$  now follow distinct effective Arrhenius forms  $D_{zz} \sim e^{-\beta \Delta_e}$  and  $D_{yy} \sim e^{-\beta \Delta_i}$ , which causes the ratio  $D_{yy}/D_{zz}$  to vanish in

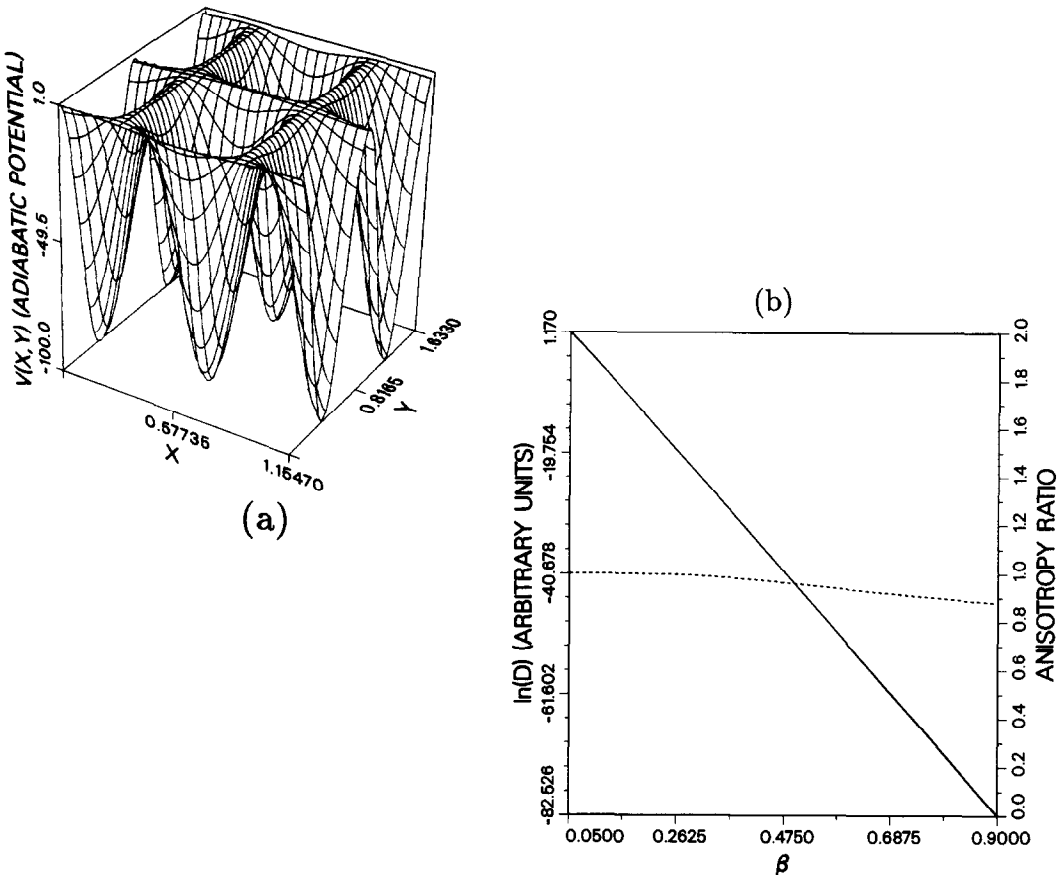


Fig. 14. (a) Adiabatic potential of Eq. (5.7) with  $\Delta_e = 100$  and  $\Delta_i = 99$ . (b)  $D_{yy}$  (lower curve) and  $D_{zz}$  (upper curve) vs.  $\beta$ .  $D_{yy}/D_{zz}$  (dashed line) approaches its asymptotic limit of two only well below the temperature range shown here [10].

the low temperature limit. Other calculations with similar potentials and larger ratios of  $\Delta_i/\Delta_e$  showed a more rapid approach of the anisotropy ratio towards zero.

An interesting special case arises if  $\Delta_i = \Delta_e$ . Referring to the two - step model, we then expect the ratio  $D_{yy}/D_{zz}$  to approach a nontrivial fixed value as  $\beta\Delta \rightarrow \infty$ , which for  $r = 1$  equals  $2/3$ . In Figs. 16 (b), 17 (b) and 18 (b) we show results of calculations for potentials of the type (5.8), chosen such that  $\Delta_i/\Delta_e = 1$  and varying the absolute magnitudes of the barriers. In all cases, the low temperature behavior follows an Arrhenius form  $D_{zz} \sim D_{yy} \sim e^{-\beta\Delta_e}$ , with an anisotropy ratio  $D_{yy}/D_{zz}$  attaining a potential dependent fixed value in the limit  $\beta\Delta \rightarrow \infty$ .

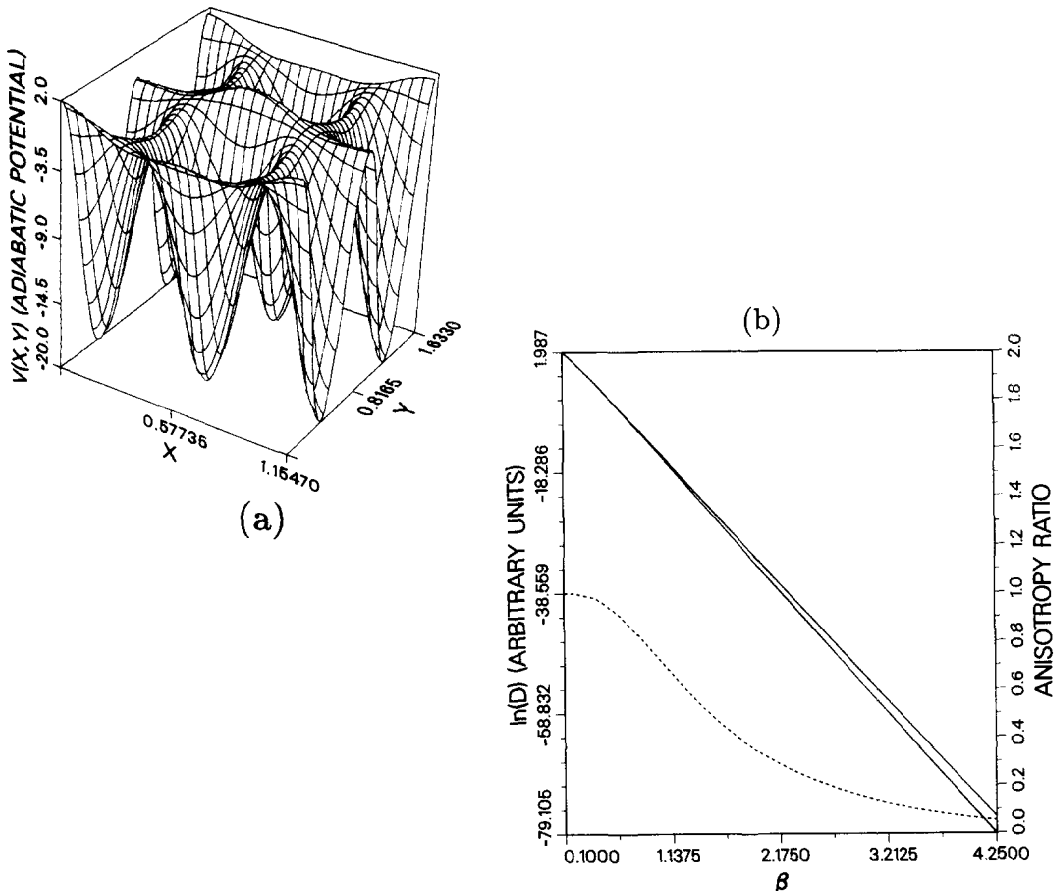


Fig. 15. (a) Adiabatic potential of Eq. (5.8) with  $\Delta_e = 19.85$ ,  $\Delta_i = 20.01$ . (b)  $D_{yy}$  (lower curve) and  $D_{zz}$  (upper curve) vs.  $\beta$  for the potential surface in (a). The larger internal barrier suppresses  $D_{yy}$  in the Arrhenius regime so that  $D_{yy}/D_{zz}$  (dashed line) approaches zero as its asymptotic limit [10].

Interestingly enough, for potentials of the type described here these values are rather close to the prediction of the two - step model with a branching ratio  $r = 1$ .

To summarize, our microscopic theoretical calculations of models of the  $W(110)$  surface with local distortions support the use of the phenomenological two - step model for qualitative purposes. In all the cases studied involving different ratios of the two barriers  $\Delta_i/\Delta_e$  the zero temperature limit for the diffusion anisotropy factor is always correctly predicted by the two - step model. At finite temperatures, the actual diffusion path is far more complicated than the

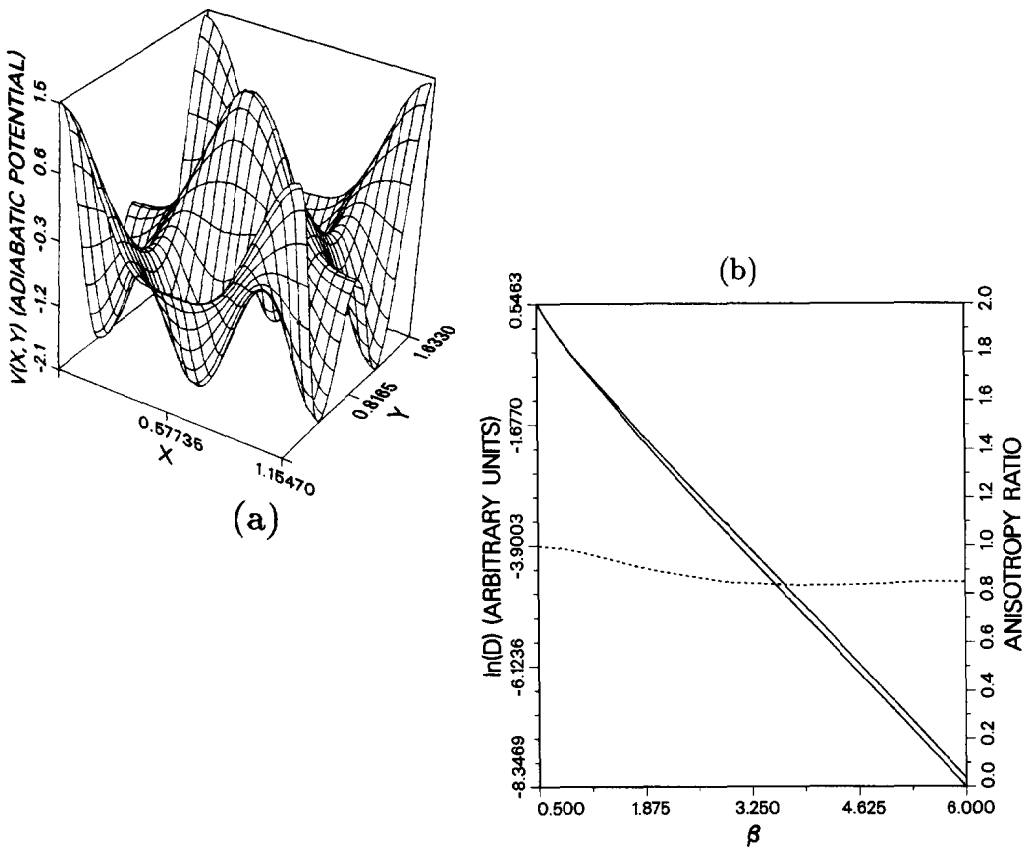


Fig. 16. (a) Adiabatic potential with equal barriers  $\Delta_e = \Delta_i = 1.60$ . (b)  $D_{yy}$  (lower curve) and  $D_{zz}$  (upper curve) vs.  $\beta$  for the potential surface in (a). In the limit  $\beta\Delta \rightarrow \infty$  the ratio  $D_{yy}/D_{zz}$  (dashed line) approaches a nontrivial fixed value of  $\simeq 0.85$ .

naive picture of the two - step model which then is not quantitatively correct. Nevertheless, the diffusion anisotropy is well described by the simple two - step model with an effective temperature dependent branching ratio  $r$ . Assuming a simple Arrhenius form in the low temperature regime, we can write

$$r = \frac{a_0}{b_0} e^{-\beta(\Delta_i - \Delta_e)} \quad (5.9)$$

where the prefactors  $a_0$  and  $b_0$  for internal and external rates, respectively, are usually different. Experimentally, the diffusion anisotropy ratio  $D_{yy}/D_{zz}$  for the  $H/W(110)$  system was observed

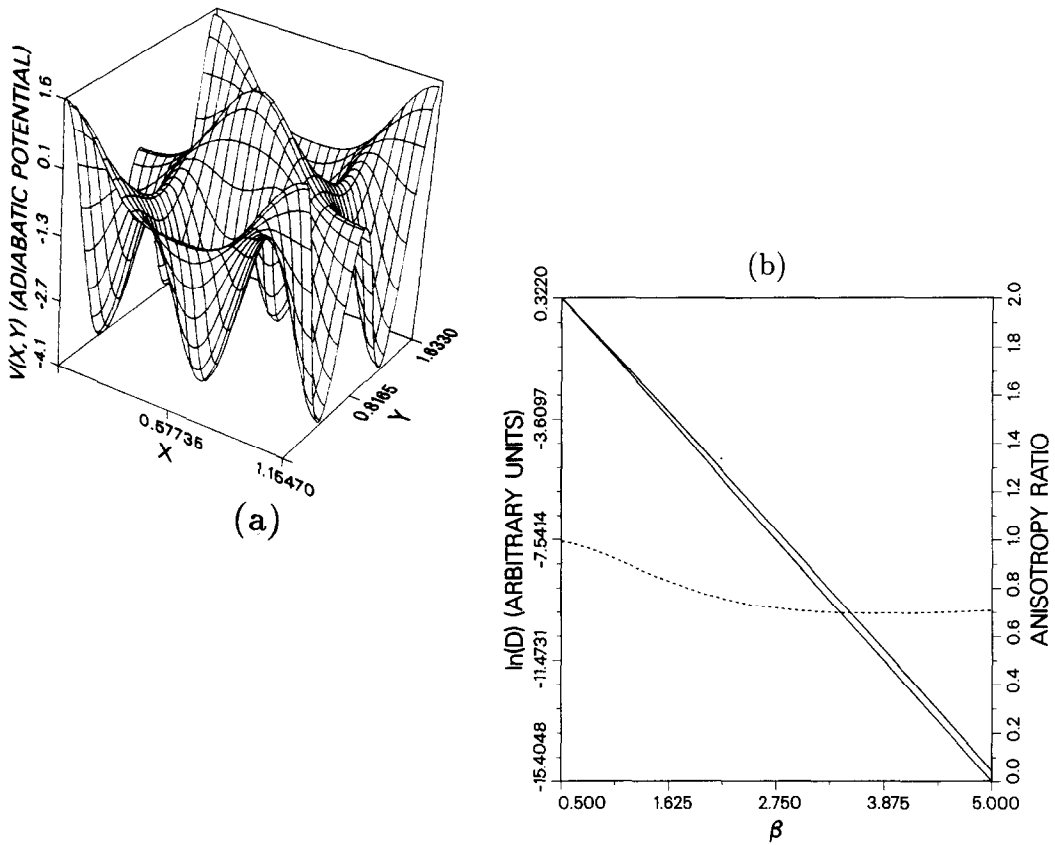


Fig. 17. (a) Adiabatic potential with equal barriers  $\Delta_e = \Delta_i = 2.06$ . (b)  $D_{yy}$  (lower curve) and  $D_{zz}$  (upper curve) vs.  $\beta$ . In the limit  $\beta\Delta \rightarrow \infty$  the ratio  $D_{yy}/D_{zz} \approx 0.7$  (dashed line).

to be approximately 1.2 [105]. Moreover, both  $D_{yy}$  and  $D_{zz}$  were found to obey Arrhenius behavior with the same activation energy of about 5 kcal. According to our theory, this would indicate that for the diffusion of  $H$  the barriers on  $W(110)$  surface have values such that  $\Delta_i < \Delta_e$ . We can estimate that the branching ratio  $r \approx 3$  at room temperature. Referring back to Eq. (5.9), this would correspond to the case  $\Delta_i = 9$ ,  $\Delta_e = 10$  discussed above if we assume that  $a_0 \approx b_0$ . Finally, we like to point out that because of the sensitivity of diffusion anisotropy to local surface distortions, experimental measurements of this ratio can be used as an effective tool in probing local changes in the adsorbate environment.

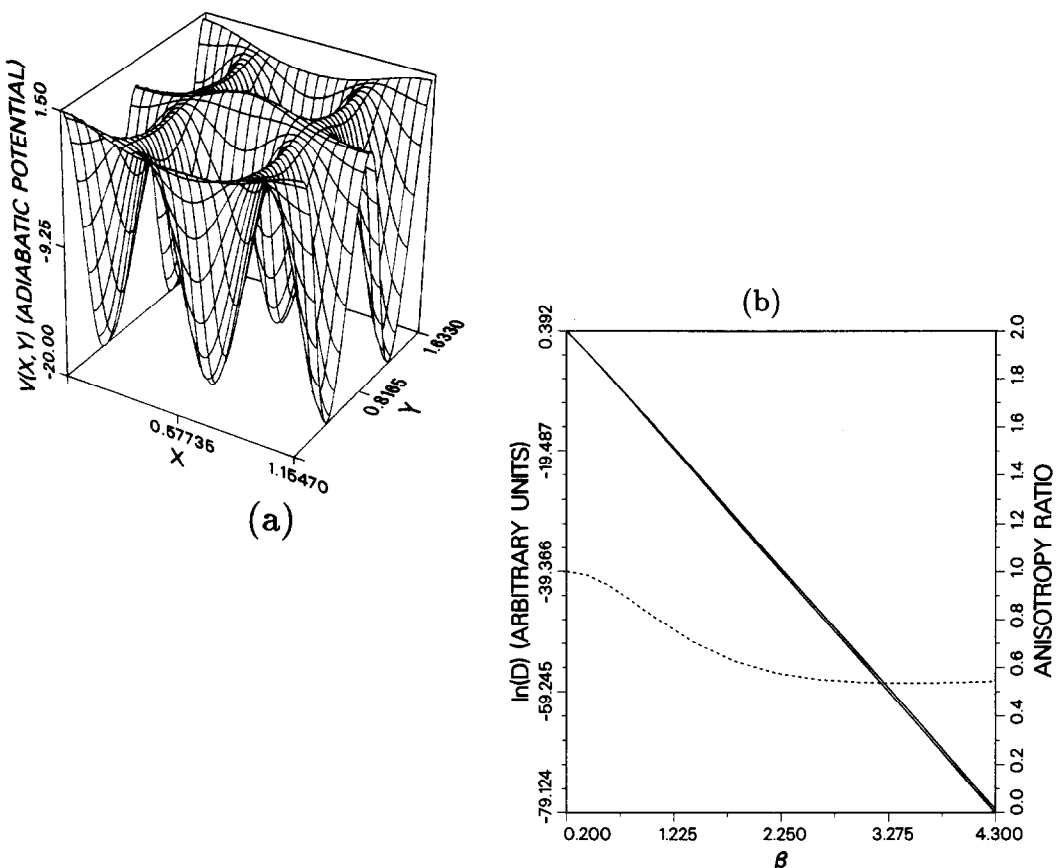


Fig. 18. (a) An adiabatic potential with equal, steep barriers  $\Delta_e = \Delta_i = 19.51$ . (b)  $D_{yy}$  (lower curve) and  $D_{zz}$  (upper curve) vs.  $\beta$ . In the limit  $\beta\Delta \rightarrow \infty$ ,  $D_{yy}/D_{zz} \approx 0.54$  (dashed line).

### C. Monte Carlo simulation studies of the two - step lattice gas model

In the last two sections, we have examined the effect of a local substrate distortion on adatom diffusion from both the phenomenological two - step lattice gas model and the microscopic theory points of view (cf. chapters 3 and 4). We found that at low temperatures the two - step lattice gas model provides a basically correct description of diffusion. The advantage of the model is that it easily allows an incorporation of realistic adatom interactions which should become important at low temperatures for finite coverages. A microscopic calculation of these effects is at present beyond the scope of the theory described in Chap. 3.

(i) Case of hardcore interactions only. To begin with, we present results of extensive Monte Carlo random walk simulations of *collective and tracer diffusion as a function of coverage* for several values of the branching ratio  $r$  [13,14]. We assume no direct adatom - adatom interactions except for the in cell exclusion within each hourglass. To obtain the elements of the collective diffusion tensor  $D_{yy}^c$  and  $D_{xx}^c$ , we have computed the density fluctuation autocorrelation function [7,116]

$$S(\vec{r}, \vec{r}', t) = \langle \delta n(\vec{r}, t) \delta n(\vec{r}', 0) \rangle, \quad (5.10)$$

where the spontaneous density fluctuations are given by  $\delta n(\vec{r}, t) = n(\vec{r}, t) - \langle n(\vec{r}, t) \rangle$ . In the hydrodynamic regime, the Fourier transform of this correlation function decays as

$$S(\vec{k}, t) = S(\vec{k}, 0) e^{-\vec{k} \cdot \mathbf{D}^c \cdot \vec{k} t}. \quad (5.11)$$

This allows us to extract the elements of  $\mathbf{D}^c$  by choosing  $\vec{k}$  along the  $x$  and  $y$  axes. In our simulations, we have first computed the sine and cosine transforms of the density fluctuations separately, and then added the corresponding correlation functions together to reduce noise. For the case of tracer diffusion, we have used the definition of Eq. (2.1):

$$D_{\alpha\alpha}^t = \frac{1}{N} \lim_{t \rightarrow \infty} \frac{1}{t} \sum_{i=1}^N \langle |r_\alpha^i(0) - r_\alpha^i(t)|^2 \rangle, \quad \alpha = x, y \quad (5.12)$$

where  $N$  is the number of particles,  $r_\alpha^i(t)$  denotes the spatial component of the position vector of the  $i^{\text{th}}$  particle, and  $\langle \rangle$  denotes configuration averaging. In the random walk algorithm for tracer diffusion, each particle is tagged and the displacements are averaged over all particles. To study finite size behavior, we have used systems of sizes  $30 \times 30$ ,  $60 \times 60$  and  $100 \times 100$ , with fully periodic boundary conditions. Most of the results presented here are for  $60 \times 60$  lattices.

Before discussing the results of simulations, we will briefly review analytic results obtained for the two - step lattice gas model using and extension of the Green's function method of Tahir - Kheli and Elliott [169]. In particular, for reference it is useful to introduce the mean field solution as obtained from the calculations of Ala - Nissila *et al.* [13,14]. In their method, the coverage dependent diffusion coefficients are calculated from the poles of the two - body *collective* Green's function  $G_{gg'}^c(t) = -2\pi i \Theta(t) \langle n_g(t) n_{g'}(t) \rangle$ , or the corresponding *tracer* Green's function  $G_{gg'}^t(t) = -2\pi i \Theta(t) \langle p_g(t) p_{g'}(t) \rangle$  (for details of notation and definitions, see original Refs. [13] and [14]). In the mean field approximation, the fluctuations of the occupation numbers on each site are neglected, and analytic forms for the diffusion coefficients for the two - step model of Fig. 11 (b) can be obtained as

$$D_{zz}^c = Ix_0^2, \quad (5.13)$$

and

$$D_{yy}^c = \frac{IM}{M + 2vI} y_0^2, \quad (5.14)$$

and for the tracer diffusion coefficients:

$$D_{zz}^t = vIx_0^2, \quad (5.15)$$

and

$$D_{yy}^t = \frac{vIM}{(M + 2vI)} y_0^2. \quad (5.16)$$

Here,  $v = 1 - \theta$  is the vacancy factor which contains the nontrivial coverage dependence of diffusion. First, we note that even in the mean field limit, the  $y$  component of the collective diffusion tensor has nontrivial coverage dependence. In the limit  $r \rightarrow \infty$ , it becomes constant as required by the rigorous results [164,165]. Both  $D_{zz}^t$  and  $D_{yy}^t$  differ from their collective counterparts by an additional multiplicative factor  $v$ . Interestingly enough, this latter result applies for the conventional lattice cases as well, where collective diffusion is constant for all coverages  $\theta < 1$  and is given simply by  $D_0^c = D^c(\theta = 0)$  [164,165].

The mean field solutions are useful in the sense that even though they are incorrect on a quantitative level, they contain the essence of the coverage dependence of diffusion for  $r$  not too small. For both collective and tracer diffusion, the anisotropy ratio becomes

$$\frac{D_{yy}^c}{D_{zz}^c} = \frac{D_{yy}^t}{D_{zz}^t} = \frac{r}{r + 2v} \left( \frac{y_0}{x_0} \right)^2. \quad (5.17)$$

In the limit  $r \rightarrow \infty$ , the mean field anisotropy ratio (5.17) reduces to the correct geometric limit which for the  $W(110)$  surface is  $(y_0/x_0)^2 = 2$ . For values of  $r$  of unity or larger, it provides a reasonably good description of the collective diffusion case, as will be shown below. However, for smaller values of the branching ratio, the interparticle correlations play a significant role. at high coverages. Nevertheless, Eq. (5.17) is always guaranteed to be correct at  $\theta = 0$  and  $\theta = 1$ , since blocking of intercell jumps corresponds to  $r \rightarrow \infty$  for  $\theta \rightarrow 1$ , and thus  $D_{yy}/D_{zz} \rightarrow 2$ . In the figures presented below, we shall also include some of the results obtained by Ala - Nissila *et al.* [13,14] using an improved version of the Green's function theory beyond the mean field

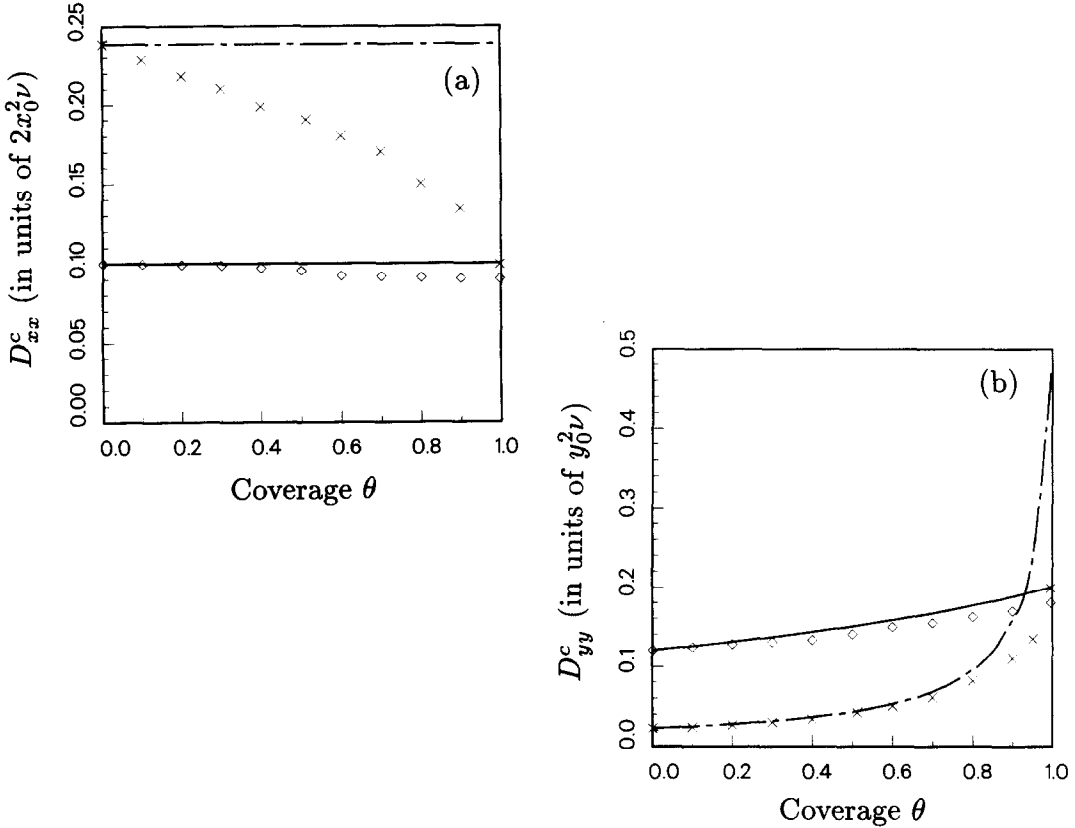


**Fig. 19.** Figure showing the results of simulations for the model of collective diffusion on the  $W(110)$  surface, where  $2x_0^2 = y_0^2$ . The magnitude of the overall rate coefficient  $\nu$  is arbitrary. (a)  $D_{zz}^c$  vs. coverage for branching ratios  $r = 3$  (diamonds) and  $r = 1/10$  (crosses). For comparison, the mean field results are also shown (solid line for  $r = 3$ , chain - dashed line for  $r = 1/10$ ). (b)  $D_{yy}^c$  for  $r = 3$  (diamonds for Monte Carlo and solid line for mean field data), and  $r = 1/10$  (crosses for Monte Carlo and dash - chained line for mean field data). The error bars for Monte Carlo results are smaller than the sizes of the points. From Ref. [13].

approximation. It is customary to write the diffusion coefficients thus obtained in terms of collective or tracer *correlation factors* defined by

$$D_{\alpha\beta} \equiv D_{\alpha\beta}^{\text{MF}} f_{\alpha\beta}, \quad (5.18)$$

where  $D^{\text{MF}}$  is the mean field result, and all quantities in Eq. (5.18) refer to collective or tracer

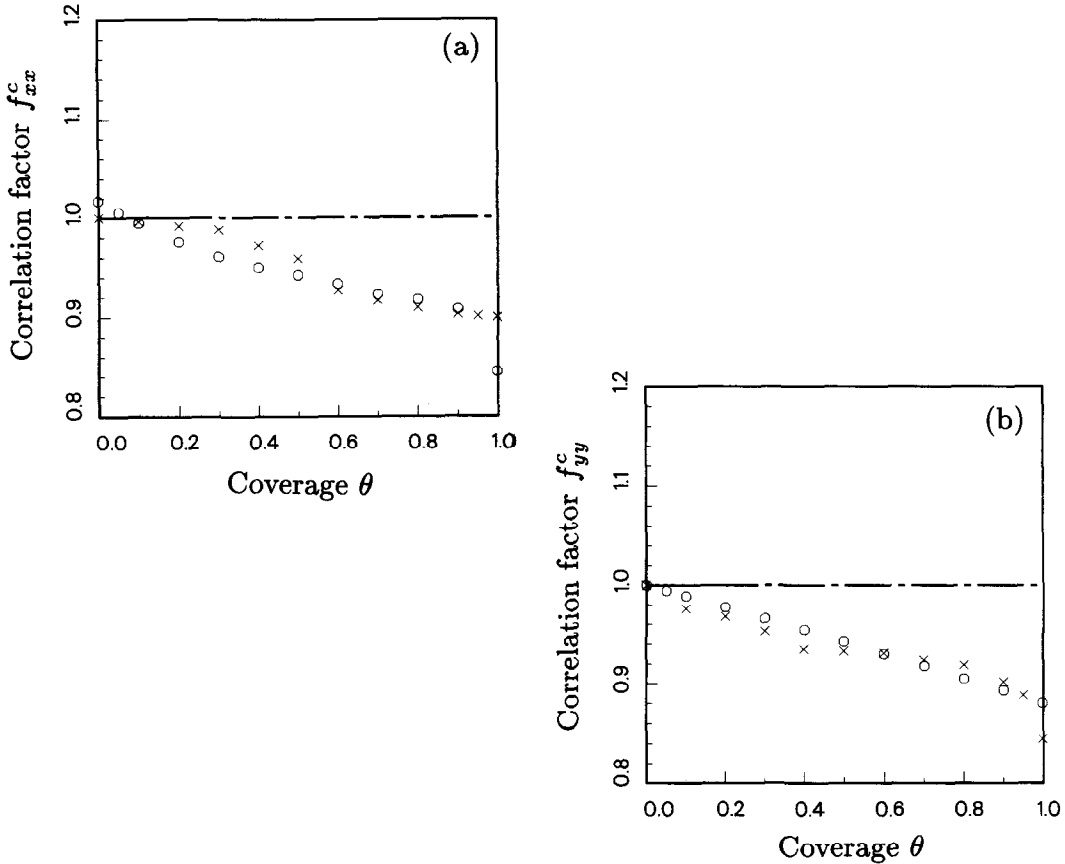


Fig. 20. Comparisons of results for the correlation factors  $f_{xx}^c$  and  $f_{yy}^c$  from the improved solution of Ala - Nissila *et al.* [13] with the simulations (crosses). In each case, the trivial mean field result  $f_{xx}^c = f_{yy}^c \equiv 1$  is shown by a horizontal chain - dashed line. (a)  $f_{xx}^c$  and (b)  $f_{yy}^c$  for branching ratio  $r = 3$ . Error bars in the Monte Carlo results are less than or about the size of the crosses.

diffusion separately. By definition,  $f_{\alpha\beta} \leq 1$  since the mean field results overestimate the true diffusion coefficients.

We start by discussing the collective diffusion case. In Fig. 19 we show results of our simulations for two branching ratios  $r = 1/10$  and  $r = 3$ , corresponding to the geometry of the  $W(110)$  surface of Fig. 2. First,  $D_{xx}^c$  which is shown in Fig. 19 (a) is a relatively slowly varying function of coverage for branching ratios  $r \gtrsim 1$ . For  $r = 3$ , it is already rather close

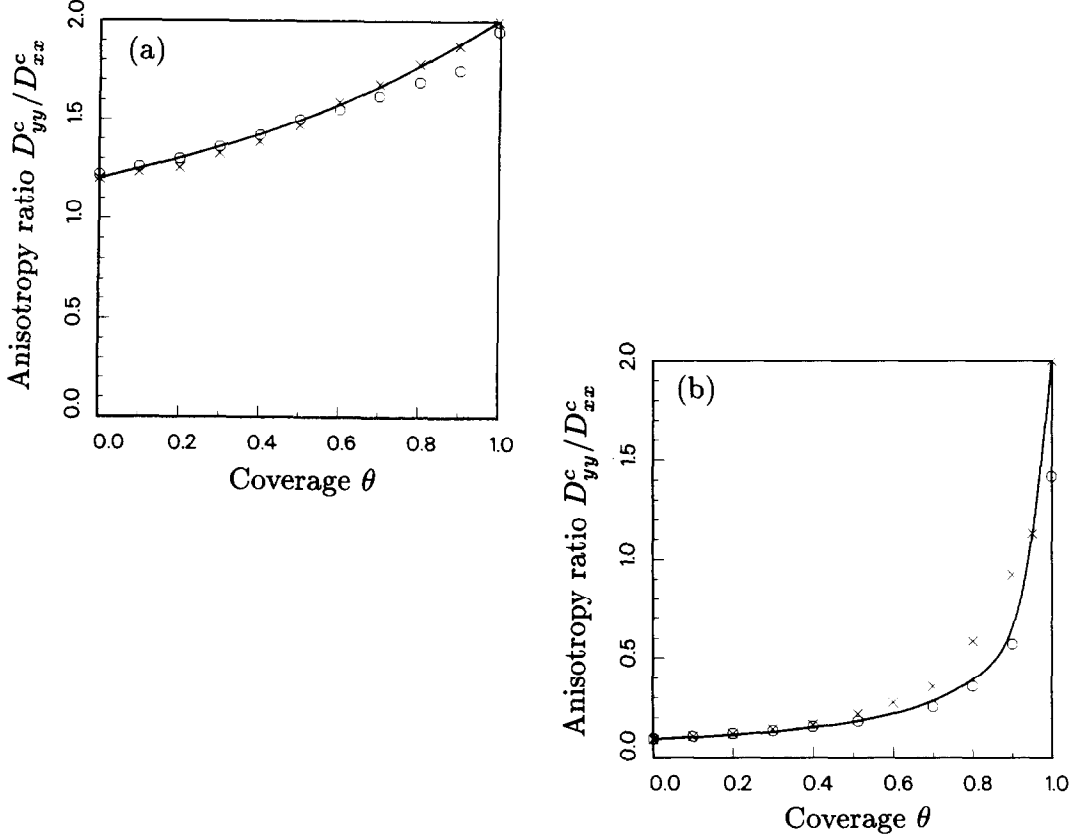


Fig. 21. Anisotropy ratio  $D_{yy}^c/D_{xx}^c$  for (a)  $r = 3$  and (b)  $r = 1/10$  corresponding to the geometry of the  $W(110)$  surface. Solid line is the mean field result of Eq (5.17), while crosses denote simulations and circles denote the improved analytic solution [13].

to the coverage independent limit of  $r \rightarrow \infty$ .  $D_{yy}^c$  shows stronger coverage dependence even for  $r = 3$  evident in Fig. 19 (b). However, for both quantities the correlation effects remain rather weak for  $\theta \lesssim 0.5$ , which indicates that Eq. (5.17) is a relatively good approximation of the anisotropy ratio for these branching ratios. In Fig. 20 we show results of comparisons of the analytic results for  $f_{zz}^c$  and  $f_{yy}^c$  with the simulations, for the physically most interesting case of  $r = 3$ . For reference, we also display the mean field results which are trivially given by  $f_{zz} \equiv f_{yy} \equiv 1$ . We can see that the improved solution is considerably more accurate than the mean field result for  $r = 3$ . However, it has been shown that it becomes quantitatively

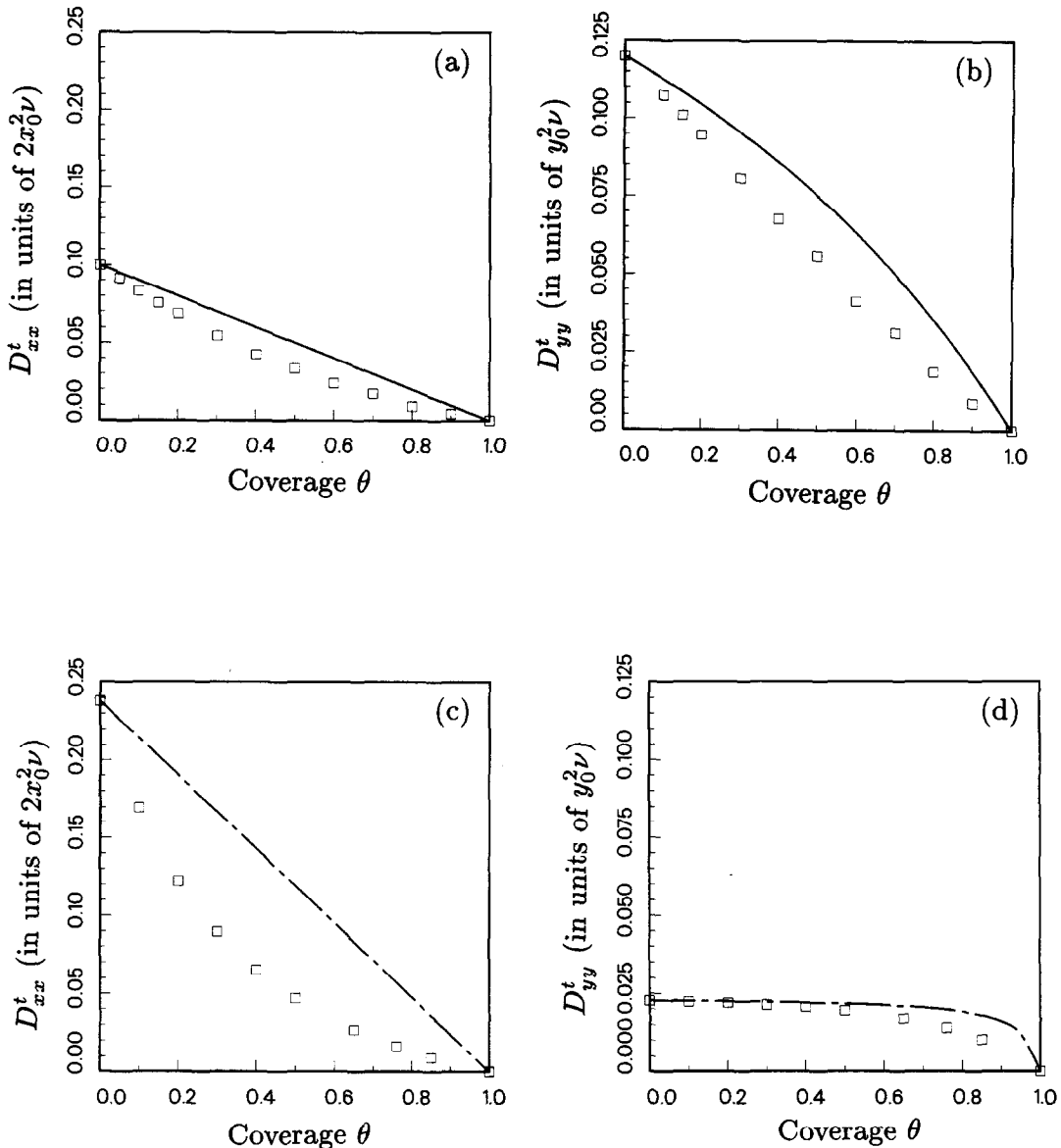


Fig. 22. Figure showing tracer diffusion simulations (open squares) for the geometry of Fig. 2. The magnitude of the overall rate constant  $\nu$  is arbitrary. For comparison, the mean field results of (5.15) - (5.16) are also shown by a solid line. (a)  $D_{xx}^t$  and (b)  $D_{yy}^t$  for  $r = 3$ ; (c)  $D_{xx}^t$  and (d)  $D_{yy}^t$  for  $r = 1/10$ . The error bars for the Monte Carlo results are smaller than the size of the points [14].

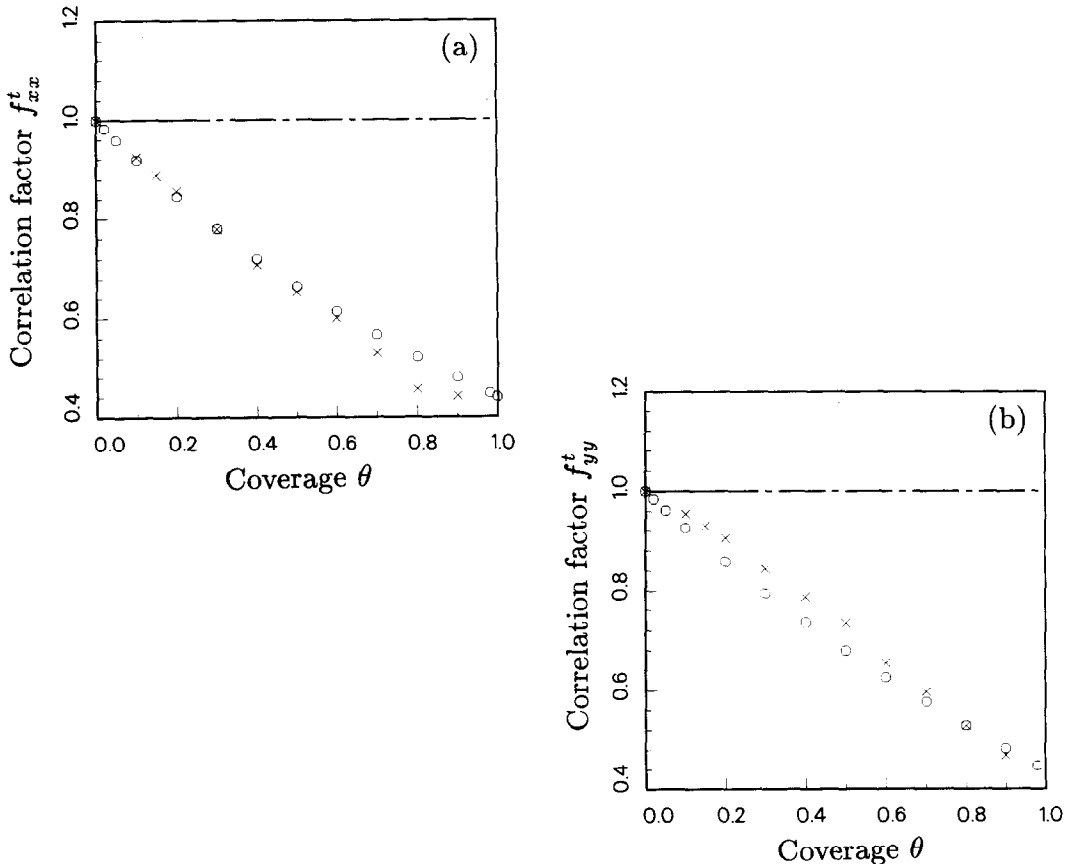


Fig. 23. Comparisons of results for the correlation factors  $f_{xx}^t$  and  $f_{yy}^t$  from the solution of Ala-Nissila *et al.* [14] (circles) with Monte Carlo simulations (crosses). In each case, the mean field result  $f_{xx}^t \equiv f_{yy}^t \equiv 1$  is shown for reference by a horizontal chain - dashed line. (a)  $f_{xx}^t$  and (b)  $f_{yy}^t$  for branching ratio  $r = 3$ . Error bars in the Monte Carlo results are smaller than or about the size of the crosses.

rather inaccurate for  $r = 1/10$ . This is due to the intercell jumps causing strong multiparticle correlations, which are not included in the solution. In Fig. 21 (a) we show results for the anisotropy ratio corresponding to  $r = 3$ , which gives  $D_{yy}^c/D_{xx}^c = 1.2$  at  $\theta = 0$ . For reference, we also show the corresponding result for  $r = 1/10$  in Fig. 21 (b). An important feature of our model is that in the regime  $\theta \lesssim 0.5$  where the  $W(110)$  surface remains unreconstructed, the diffusion anisotropy is a rather slowly varying function of coverage, and is well described

by Eq. (5.17).

Next, we discuss the case of tracer diffusion. In Fig. 22 we show results of comparisons of the mean field theory with the simulations. For the  $x$  direction, the coverage dependence of  $D_{zz}^t$  is given by a straight line and the Monte Carlo results lie below this line. For  $r = 1/10$ , the discrepancy between the two results becomes quite large. However, for  $D_{yy}^t$ , the unusual form of coverage dependence in (5.16) yields a better agreement for very small values of  $r$ , where diffusion in the  $y$  direction has a rather weak coverage dependence. This result may be explained as follows. Namely, for small  $r$  and low coverages the rate of motion of the tracer and the background particles within the cells becomes very small, while background particles can still move relatively fast in the  $x$  direction. This fast motion may cause the correlations of the tracer particle to the background density fluctuation field to weaken, which would improve the mean field approximation. A similar effect in the case of a square lattice with fast background particles has been originally pointed out by Tahir - Kheli [170]. We also note that  $f_{yy}^c$  for the case of collective diffusion exhibits similar behavior. In Fig. 23 we further present results of calculations for the correlation factors in the case  $r = 3$ . The mean field results are given for comparison by straight horizontal lines. For large values of  $r$ , the improved solution gives a much better agreement with the simulations than the mean field theory, as expected. However, as  $r \lesssim 1$ , for  $f_{zz}^t$  the theory starts to deviate from Monte Carlo results at large coverages. More dramatically, for  $f_{yy}^t$  the deviation becomes large already for small coverages where the second order solution shows an overall downward curvature, while the simulation results approach mean field like behavior for small coverages. In Fig. 24 we finally present results for the anisotropy ratio  $D_{yy}^t/D_{zz}^t$  for the two branching ratios studied here. Even for  $r = 3$ , the ratio is not described by the analytic theory as accurately as in the case of collective diffusion, and the discrepancy as compared to Monte Carlo results becomes quite large for  $r = 1/10$ .

(ii) Model with adatom - adatom interactions. To realistically study a model of  $H$  diffusion within the two - step model, we have to include the effects of adatom - adatom interactions, which leads to the appearance of ordered phases at low temperatures. To this end, we present extensive Monte Carlo simulation results for a set of adatom interaction parameters. This set defines the lattice gas model of Sahu *et al.* [168] which they used to study the adsorption system  $H/W(110)$  in various parts of its phase diagram. This simplified model excludes the surface reconstruction of the  $W(110)$  substrate at  $\theta \gtrsim 0.5$ ; however, the experimentally observed ordered phases formed by  $H$  are reproduced. Thus, these results may not be applicable to  $H/W(110)$  at higher coverages.

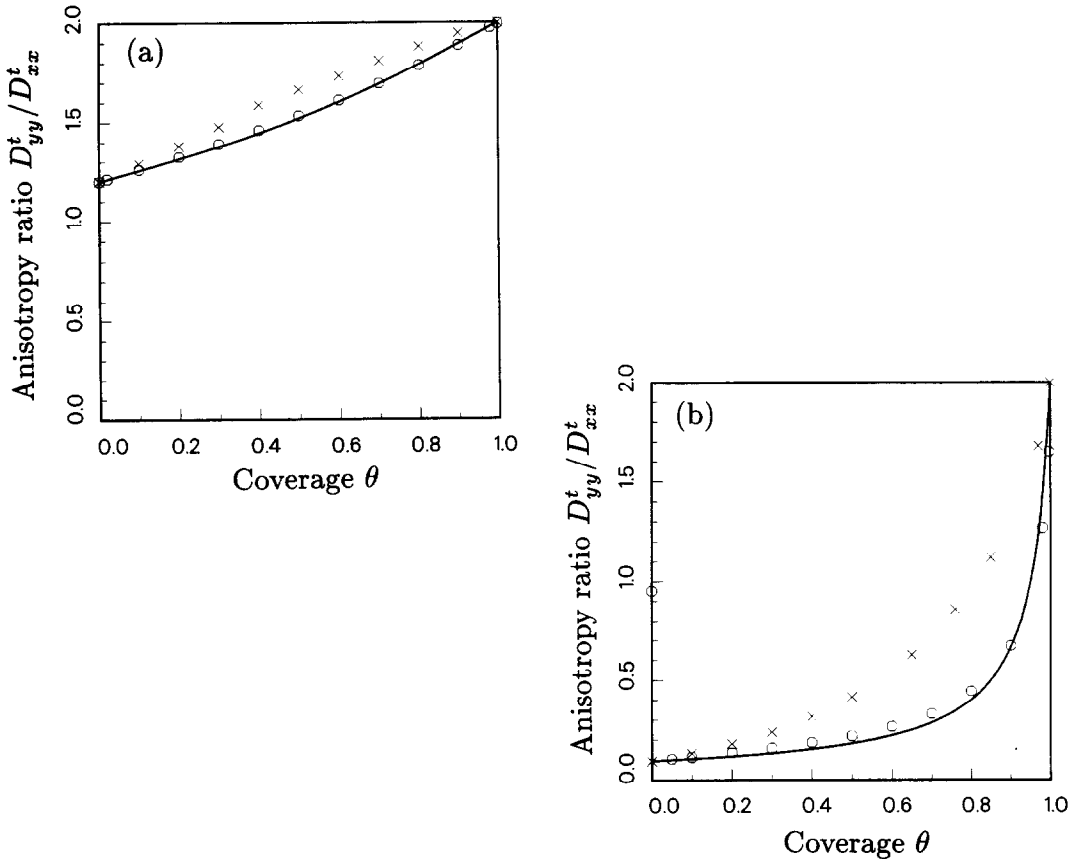


**Fig. 24.** Anisotropy ratio  $D_{yy}^t/D_{xx}^t$  for (a)  $r = 3$  and (b)  $r = 1/10$  corresponding to the geometry of the  $W(110)$  surface. Solid line denotes the mean field result, while crosses denote simulations and open circles the improved analytic solution [14].

When finite adatom - adatom interactions are introduced in the two - step model, the transition rates  $I$  and  $M$  become explicitly dependent both on interactions and local configurations. In particular, in the presence of symmetry breaking as caused by the appearance of low temperature ordered phases, we expect the diffusion coefficients and the anisotropy to be strongly affected. Before presenting the results of our simulations, we discuss below the role of the transition probabilities in determining the coverage and temperature dependence of diffusion coefficients in the model.

Aside from the usual problem of the interpretation of the dynamics in the Metropolis Monte

Carlo method [162,171,172] there is an additional ambiguity associated with the choice of the transition probabilities when time dependent phenomena such as diffusion are simulated [119,120,156,162,163,173-193]. Namely, the condition of microscopic reversibility

$$w_{i,f} p_i = w_{f,i} p_f, \quad (5.19)$$

where  $w_{i,f}$  is the transition rate from a state  $\{i\}$  to a state  $\{f\}$ , and  $p_i$  and  $p_f$  are corresponding probability densities, does not specify the transition rates uniquely. Two of the most commonly used functional forms for the rates are the Metropolis form [194]

$$w_{i,f} = \begin{cases} \nu e^{-\beta \Delta E}, & \text{if } \Delta E > 0 \\ \nu, & \text{if } \Delta E \leq 0 \end{cases} \quad (5.20)$$

and the symmetric Kawasaki form [195-197]

$$w_{i,f} = \frac{1}{2} \nu [1 - \tanh(\frac{\beta \Delta E}{2})], \quad (5.21)$$

where  $\Delta E \equiv E_f - E_i$  is the energy difference between the final and initial states,  $\nu$  is the attempt frequency and  $\beta \equiv 1/(k_B T)$  is the inverse temperature. Usually,  $\nu$  is set to unity and time is measured in units of transition attempts per particle.

In studying diffusion, either (5.20) or (5.21) can in principle be employed. Some studies have also been done using the exponential function in (5.20), but identifying  $\Delta E = E_i$  as the initial state energy instead of the energy difference [156]. An additional normalization factor including the maximum value of energy has to be included also. This choice is based on the activated nature of classical diffusion processes, and is sometimes called the "initial value dynamics". However, the barrier introduced with this choice of transition probability is somewhat artificial. Second and a more serious problem is that if the energy distribution is relatively wide, the initial value dynamics becomes very inefficient at low temperatures. We should also note already at this point that the coverage dependence of diffusion is clearly rather sensitive to the choice of  $w_{i,f}$ . For example, the choice of the Kawasaki form (5.21) preserves particle - hole symmetry whereas the initial value dynamics does not.

The fundamental problem with all these choices, including (5.20) and (5.21) is that they do not realistically describe the diffusion process in terms of an intermediate energy state, which for classical diffusion is the saddle point of the adiabatic surface potential. This becomes particularly serious for the two - step model. Namely, consider the intracell jumps, for which  $\Delta E$  is always zero. This means that not only the absolute diffusion rates but also the *diffusion anisotropy* depend on the particular choice of the transition probabilities. However, in reality

the intracell rate should be controlled by a saddle point within the cell, created by the local distortion, as shown by our microscopic calculations of single particle diffusion in Sec. B of this chapter.

Since the dynamics of diffusion will always depend on the choice of the transition probabilities, we can actually utilize this freedom to more realistically model the diffusion process within the two - step model. To this end we have chosen a new form of the transition probability in which the intracell and intercell diffusion jumps are decomposed into two steps, i.e.

$$w_{i,f} = w_{i,s} w_{s,f}. \quad (5.22)$$

The first transition rate  $w_{i,s}$  describes a transition from an initial energy state  $E_i$  to an intermediate energy state  $E_s$ , and it is given by

$$w_{i,s} = \frac{1}{2} \nu_1 \{1 - \tanh[\beta(E_s - E_i)/2]\}. \quad (5.23)$$

Similarly, the second transition rate describes a transition from the intermediate state to the final energy state  $E_f$  :

$$w_{s,f} = \frac{1}{2} \nu_2 \{1 - \tanh[\beta(E_f - E_s)/2]\}. \quad (5.24)$$

Thus, for both steps the transition probabilities have the familiar Kawasaki form, although Eq. (5.20) is also equally applicable. It is easy to verify that (5.22) - (5.24) satisfy the detailed balance condition, as required. Our choice of the transition probabilities describes explicitly the effect of an intermediate energy state in the diffusion process, which in the classical picture is the saddle point of the potential. We shall refer to this choice of probability of transition as *Transition Dynamics Algorithm*. Within the algorithm, there is still a freedom of choice for the intermediate barrier  $E_s$ , which will be discussed below.

When applied to the two - step model, neither the rates  $\nu_1$  and  $\nu_2$  nor the saddle point energies for the intercell and intracell jumps need to be identical. The definition of a "bare" one - particle branching ratio then becomes  $r = (\nu_1 \nu_2)^M / (\nu_1 \nu_2)^I$ , while the *effective* branching ratio  $r^{\text{eff}}$  is given by

$$r^{\text{eff}} \equiv \frac{w_{i,s}^M w_{s,f}^M}{w_{i,s}^I w_{s,f}^I}, \quad (5.25)$$

where  $I$  and  $M$  refer to intracell and intercell jumps, respectively. Note that only in the limit of an infinite temperature does Eq. (5.25) reduce to a constant. In general,  $r^{\text{eff}}$  is temperature

and coverage dependent and could even change with different configurations according to the choice of  $E_s$ .

We now describe the simulation results for the two step lattice gas model in which the interaction parameters are taken from a study of Sahu *et al.* [168] on the phase diagram of the  $H/W(110)$  adsorption system. This model makes no allowance for a local distortion or surface reconstruction but the direct  $H - H$  interactions are chosen such that the experimentally observed phase diagram of  $H/W(110)$  is correctly reproduced. Thus, it should provide a good description for  $H/W(110)$  at least for  $\theta \lesssim 0.5$  before the global surface reconstruction takes place. For the interaction between the adatoms, no distinction is being made between the "up" and "down" sites of the cells within the two - step model. The interaction Hamiltonian is given by

$$H = \sum_{\langle gg' \rangle, ss'} J(g, g') n_g^s n_{g'}^{s'}. \quad (5.26)$$

Here  $s, s' = A$  or  $B$ , and  $g, g'$  denote the cell indices. The interaction parameters are chosen such that  $J_1 = -1$ ,  $J_2 = J_3 = -\frac{1}{2}$ ,  $J_4 = -1$ , and  $J_{t1} = J_{t2} = 0.6$  in some arbitrary energy scale [168], and their meaning is illustrated in Fig. 25 (a). In Fig. 25 (b) we show the phase diagram of the model, as calculated by Sahu *et al.* [168].

Our simulations of both collective and tracer diffusion were carried out using the transition dynamics algorithm exclusively. The intermediate "barrier" energy parameter  $E_s$  was chosen to be

$$E_s = \frac{E_i + E_f}{2} + \Delta. \quad (5.27)$$

The first term in Eq. (5.27) is an approximate representation of the interaction energy with other adsorbates when the atom making the jump is at the "transition state". The quantity  $\Delta$  represents the intrinsic saddle point barrier, and in most runs we set  $\Delta = 0.5$  in the same units as the interaction parameters [198]. For the results presented below, the bare branching ratio  $r$  was set to three. Note that with this choice of  $E_s$ ,  $r^{\text{eff}}$  in Eq. (5.25) is not only temperature dependent but also a running variable in the simulations since  $E_s$  changes with configurations. The calculations for  $D^c$  and  $D^t$  were done essentially in the same way as in Sec. C.(i).

We shall first describe the results for the coverage dependence of the tracer diffusion tensor  $\mathbf{D}^t$ . At the temperature  $T = 1.5$ , according to the phase diagram in Fig. 25 (b), the adsorbate will form a  $(2 \times 1)$  (or  $(1 \times 2)$ ) ordered phase around  $\theta = 1/2$  and a  $(2 \times 2)$  phase around  $\theta = 3/4$ . In Figs. 26 (a) and (b) we present results for  $D_{zz}^t$ ,  $D_{yy}^t$  and  $D_{xy}^t$  as a function of

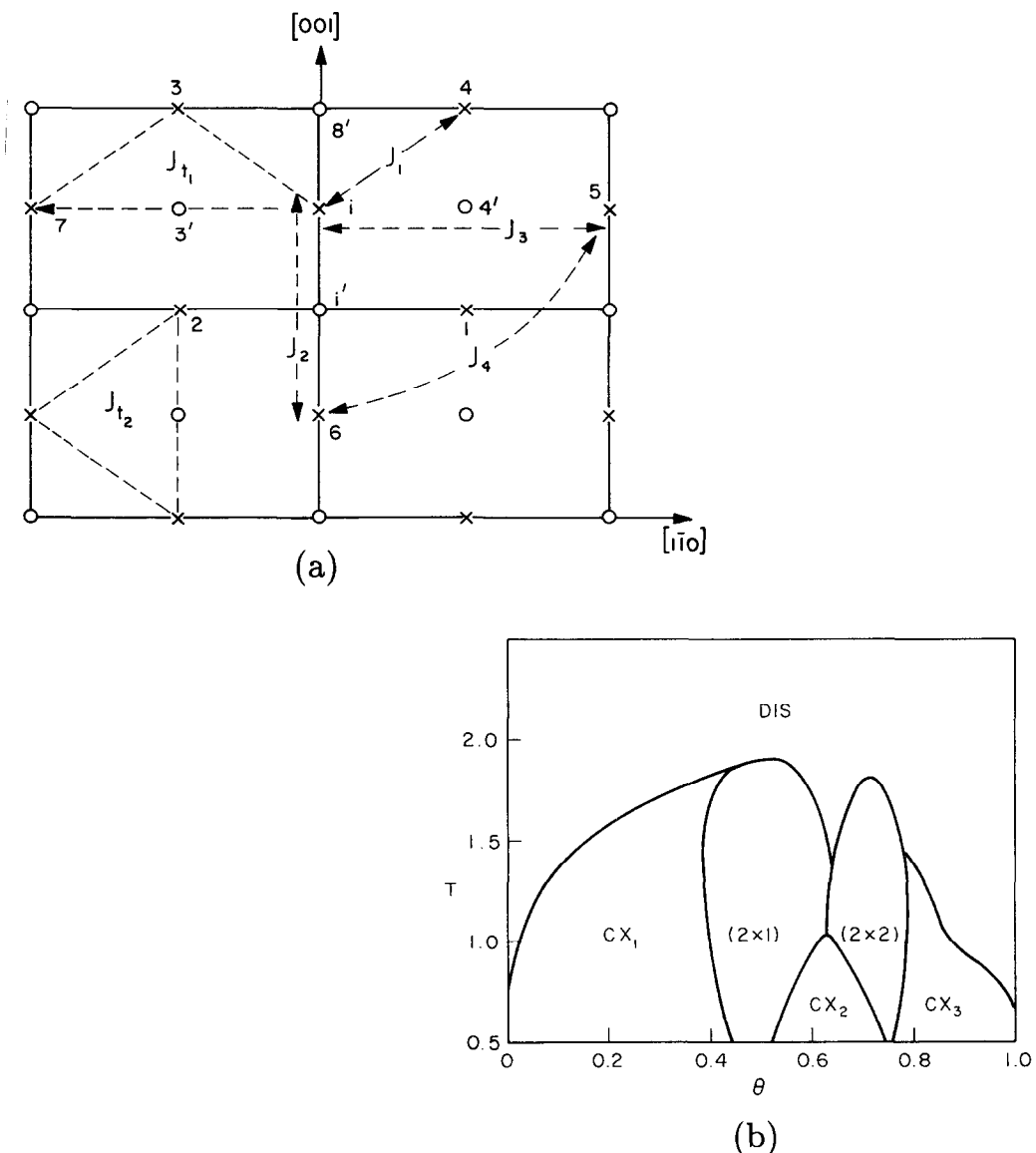


**Fig. 25.** (a) A Schematic figure of the interaction parameters used in the model of  $H/W(110)$ . Crosses denote the positions of the hourglass adsorption sites for  $H$ . (b) The corresponding model phase diagram for  $H/W(110)$ .  $CX_i$ 's denote coexistence regions between different phases [168].

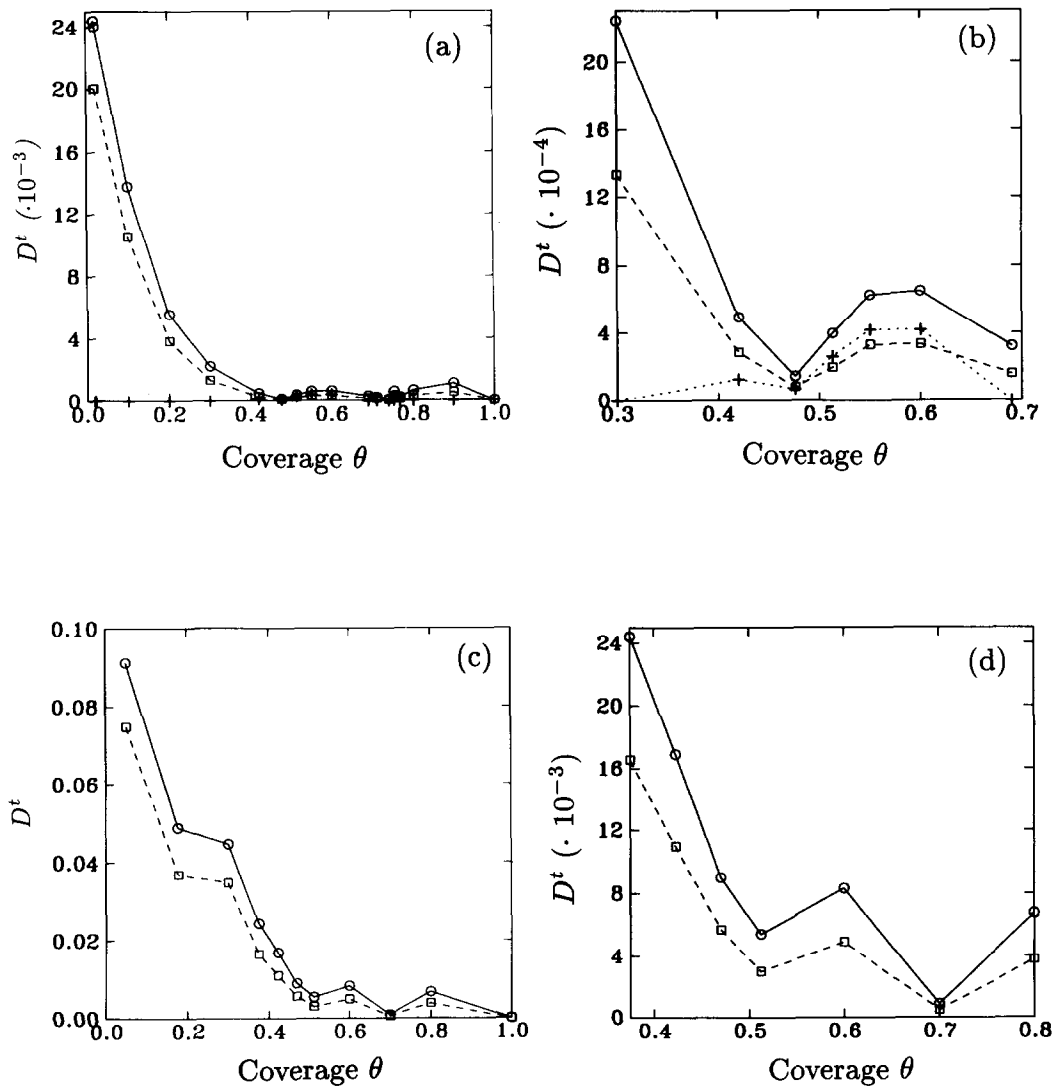


Fig. 26. (a) Coverage dependence of  $D_{zz}^t$  (squares),  $D_{yy}^t$  (circles), and  $D_{xy}^t$  (crosses) for the model of  $H/W(110)$  at  $T = 1.5$ , in units of  $2x_0^2\nu$ ,  $y_0^2\nu$  and  $y_0^2\nu$ , respectively, where  $2x_0^2 = y_0^2$  and  $\nu$  is an arbitrary rate constant. (b) shows details for intermediate coverages. Lines are only guides to the eye. (c) - (d) Coverage dependence of  $D_{zz}^t$  (squares) and  $D_{yy}^t$  (circles) for the model of  $H/W(110)$  at  $T = 2.2$ .  $D_{xy}^t$  is now virtually zero, as the global order is very weak.

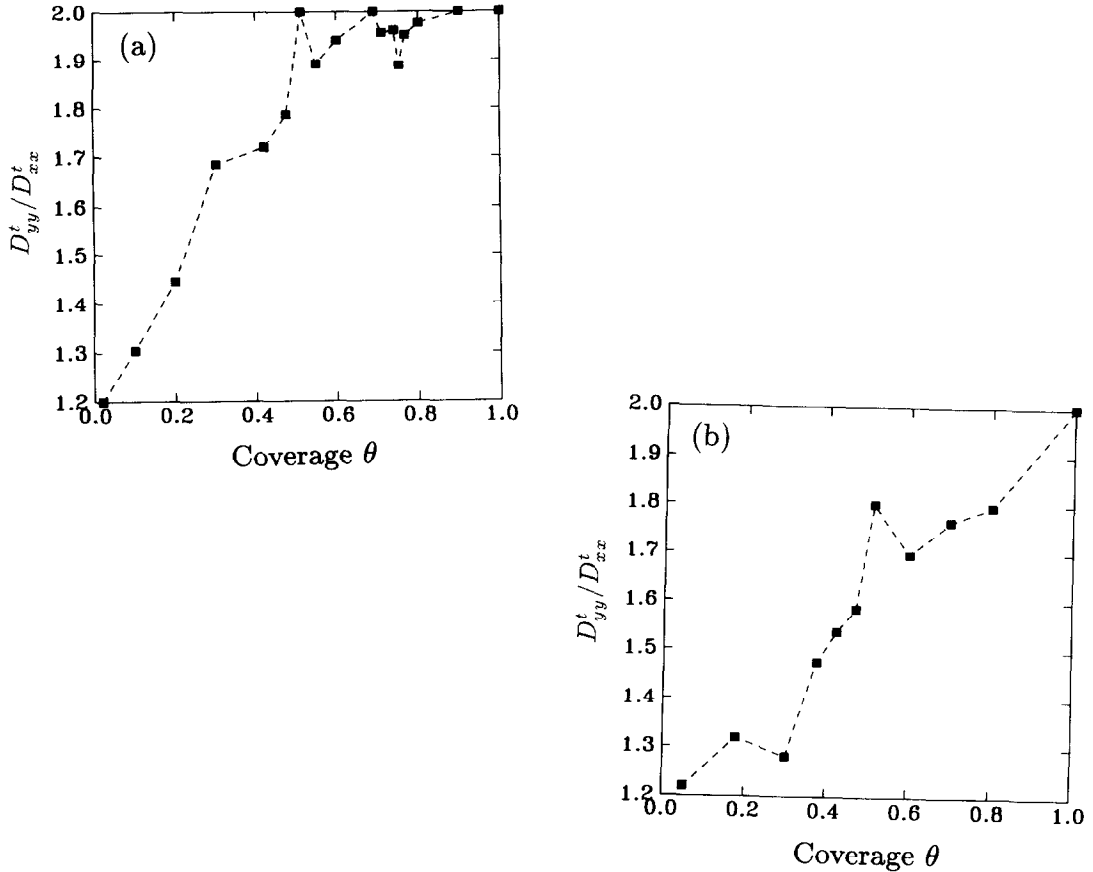


Fig. 27. (a) Tracer diffusion anisotropy corresponding to Fig. 26 (a), and (b) tracer diffusion anisotropy corresponding to Fig. 26 (c).

coverage at  $T = 1.5$ . The first feature to note is that the diffusion constants drop off much more rapidly as a function of coverage as compared with the hardcore interaction case. This is because of the fact that besides the blocking factor which increases as the coverage increases, a well ordered local environment for the diffusing adatom means that any jump leading to a different configuration will necessarily involve a large activation energy hence leading to a smaller diffusion constant. Using this simple argument, we also expect the diffusion constants  $D_{xx}^t$  and  $D_{yy}^t$  to show a local minimum at  $\theta = 1/2$  and  $3/4$  which correspond to the maximal ordering of the  $(2 \times 1)$  and  $(2 \times 2)$  phases, respectively. This is precisely the case as seen in Figs. 26 (a) - (b). The behaviour of the off - diagonal component of the diffusion tensor  $D_{xy}^t$

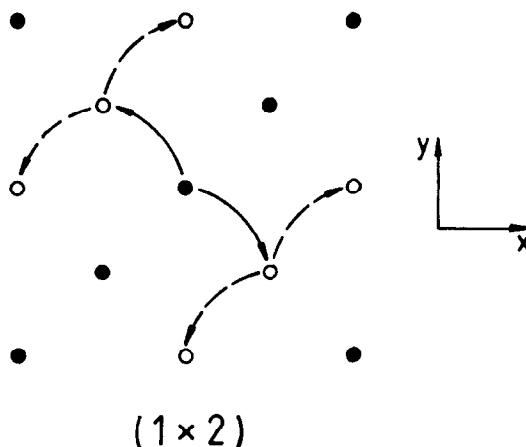


Fig. 28. Figure showing schematically, how in a fully ordered ( $1 \times 2$ ) ( $(2 \times 1)$ ) phase the particles (filled circles) can only move diagonally along the empty rows of adsorption sites (open circles). This leads to a rotation of the principal axes for diffusion and a finite  $D_{xy}$ , as discussed in the text.

on the other hand is rather different. It is zero at most values of the coverage but becomes finite around  $\theta = 1/2$  where it displays a local maximum. The reason for this is that  $D_{xy}^t$  is a measure of the symmetry of the diffusion behaviour. For the disordered phase and the  $(2 \times 2)$  phase, the principal axes of diffusion are just along the  $x$  and  $y$  axes of the lattice. However, in the  $(2 \times 1)$  or the  $(1 \times 2)$  phase, diffusion is obviously taking place mainly along the direction of the occupied rows, as shown schematically in Fig. 28. Thus the nonzero value of  $D_{xy}^t$  around  $\theta = 1/2$  simply indicates that the principal axes of diffusion at those coverages are rotated from their original direction.

At a higher temperature  $T = 2.2$ , the phase diagram in Fig. 25 (b) indicates that there are no more ordered phases at any coverages. However, this result is for the infinite size limit, as obtained from finite size scaling studies [168]. For the actual  $30 \times 30$  system studied here, the adsorbate layer is still in a weakly ordered  $(2 \times 1)$  (or  $(1 \times 2)$ ) phase around  $\theta = 1/2$ . Thus the diffusion constants  $D_{xx}^t$  and  $D_{yy}^t$  still have weak local maxima at  $\theta = 1/2$  as shown in Figs. 26 (c) and (d). The local maximum at  $\theta = 3/4$ , however, has almost completely disappeared because the  $(2 \times 2)$  phase is disordered at this temperature.

In Figs. 27 (a) and (b) we show the anisotropy ratios  $D_{yy}^t/D_{zz}^t$  for these two temperatures. As expected from the above discussions, the result for  $T = 2.2$  is very similar to the case of hardcore interactions only, except for the peak at  $\theta = 1/2$  arising from the weak remnant of the  $(2 \times 1)$  (or  $(1 \times 2)$ ) phase. For the lower temperature of  $T = 1.5$ , the ratio rises rapidly towards the asymptotic value of two for  $\theta > 0.5$ . This is due to the large activation energies in the ordered phases for the intercell jumps, as opposed to intracell jumps which are controlled only by the intrinsic saddle point barrier. The effective branching ratio  $r$  therefore rises rapidly. Since the anisotropy ratio becomes two in the limit where  $r$  approaches infinity, this gives rise to the observed behaviour of the rapid rise of the anisotropy ratio as a function of coverage at lower temperatures.

For the collective diffusion tensor  $\mathbf{D}^c$  we show results for the two temperatures  $T = 1.5$  and  $T = 2.2$  in Figs. 29 (a) - (b) and (c), respectively. There are two major qualitative differences when compared with the corresponding results for the tracer diffusion. First, the collective diffusion falls off much more slowly as a function of coverage. This is not unexpected because the success rate of single adatom jump event is not the sole factor in determining the rate of collective diffusion. In fact, the mean field results in Sec. C.(i) for the hardcore interaction model already indicate a weak dependence of the collective diffusion tensor on the coverage. The second major difference is that the collective diffusion rises to a local maximum instead of a minimum at  $\theta = 1/2$  and  $3/4$  where the adlayer is in the  $(2 \times 1)$  (or  $(1 \times 2)$ ) and  $(2 \times 2)$  phases, respectively. This can be seen clearly in the case where  $T = 1.5$ . For  $T = 2.2$ , the local maximum persists at  $\theta = 1/2$  but disappears at  $3/4$ . This is again due to the disordering of the  $(2 \times 2)$  phase at this higher temperature. The reason for this behaviour can be best understood from the phenomenological expression relating the collective diffusion to an effective jump frequency  $\nu(\theta)$  of single particles [5,180]:

$$D^c = \frac{1}{4} \nu(\theta) a^2 \frac{1}{k_B T \rho \kappa}, \quad (5.28)$$

where  $\rho$  is density, and  $\kappa$  is the adlayer compressibility. In this expression, the numerator is obviously minimized at  $\theta = 1/2$  and  $3/4$  because the single adatom jump success rate is lowest for the fully ordered  $(2 \times 1)$  (or  $(1 \times 2)$ ) and  $(2 \times 2)$  phases. However, the denominator contains the compressibility  $\kappa$ , which displays a minimum at the fully ordered phases of the adlayer. Thus, there is a competition between these two factors. For the model system studied here, the compressibility is the dominant factor and thus the diffusion constants acquire a maximum at  $\theta = 1/2$  and  $3/4$ . This kind of behaviour has indeed been observed experimentally in such systems as *Li/W(110)* and *Ba/Mo(011)* [6]. For other systems, the situation could be reversed

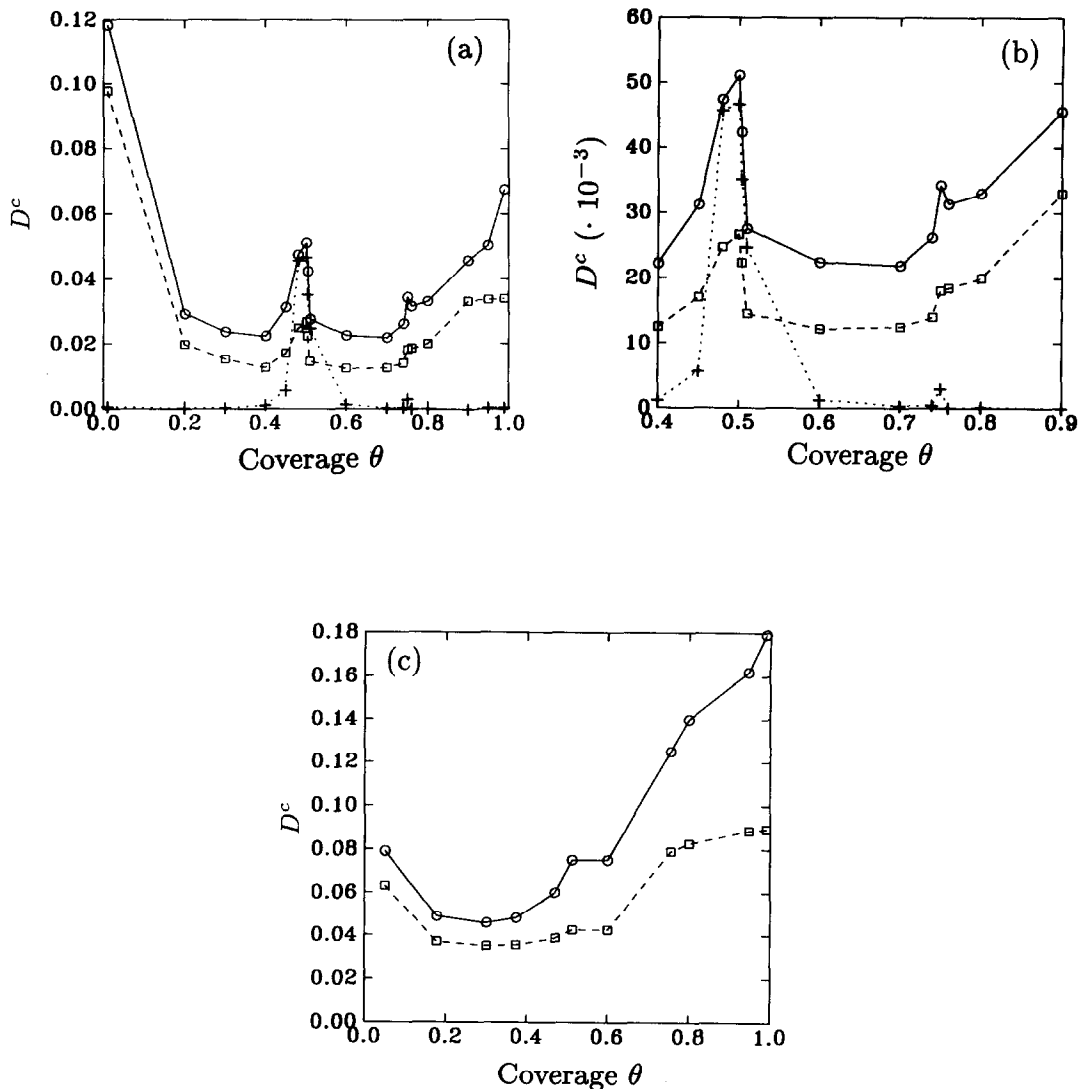


Fig. 29. (a) Coverage dependence of  $D_{xx}^c$  (squares),  $D_{yy}^c$  (circles), and  $D_{xy}^c$  (crosses) for the model of  $H/W(110)$  at  $T = 1.5$ . Units are as in Fig. 26, and (b) shows details for intermediate coverages. Lines are only guides to the eye. (c) Coverage dependence of  $D_{xx}^c$  (squares) and  $D_{yy}^c$  (circles) for the model of  $H/W(110)$  at  $T = 2.2$ .  $D_{xy}^c$  is again zero at this higher temperature.

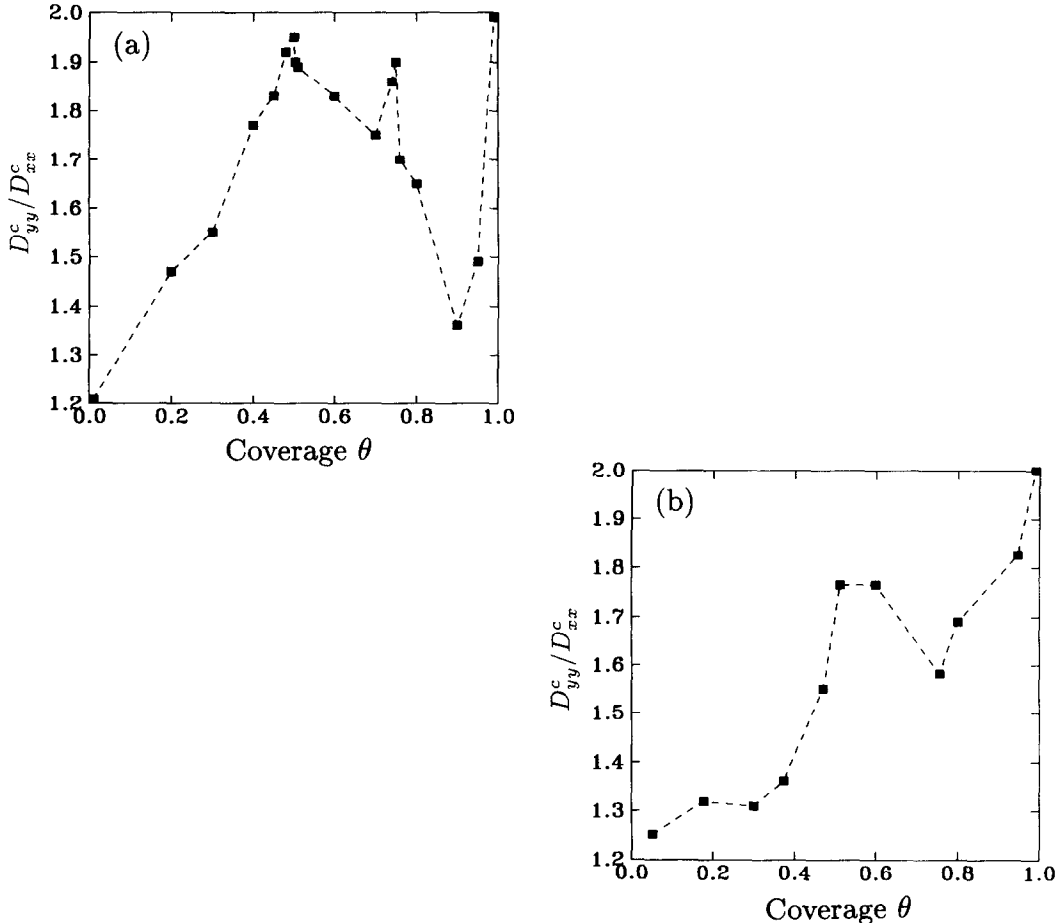


Fig. 30. (a) Collective diffusion anisotropy corresponding to Fig. 29 (a), and (b) collective diffusion anisotropy corresponding to Fig. 29 (c).

[135,136]. For example, in the simulation studies of Sadiq and Binder [183], they observe a minimum instead of a maximum for the collective diffusion at a fully ordered phase.

The off - diagonal element  $D_{xy}^c$  shows a behaviour similar to the tracer diffusion case. This is to be expected because the principal axes of the collective diffusion tensor should be identical to those of the tracer diffusion tensor. Finally, the anisotropy ratio  $D_{yy}^c / D_{zz}^c$  for low coverages is similar to that for tracer diffusion, as can be seen in Fig. 29 (d). In the higher temperature of  $T = 2.2$ , the ratio again displays a weak peak around  $\theta = 1/2$ , beyond which it drops off before rising to its eventual limit of  $D_{yy}^c / D_{zz}^c = 2$ .

Our results in this section demonstrate clearly the influence of ordered adlayer phases to

diffusion, and also delineate the fundamentally different nature of tracer and collective diffusion in interacting systems. Most strikingly, for our model tracer diffusion shows pronounced *minima* for maximal ordering as a function of coverage while the collective diffusion displays local *maxima* for the same values of coverage. This difference can be qualitatively explained by the difference between adatom mobilities and the compressibility of the adlayer. Despite the well known fact that Monte Carlo studies cannot be used to quantitatively estimate diffusion coefficients in real interacting systems, we believe that at least the *qualitative* features of the model should apply to  $H/W(110)$  for  $\theta \lesssim 0.5$ . Most importantly, the results demonstrate that the *diffusion anisotropy ratios*  $D_{yy}^t/D_{zz}^t$  and  $D_{yy}^c/D_{zz}^c$  behave in a very similar fashion, and are mostly determined by the *global symmetry* of the adlayer. The temperature dependence of the anisotropy is also sensitive to the ratio of the intracell barrier  $\Delta_i$  to the intercell barrier  $\Delta_e$ . In this work  $\Delta_i/\Delta_e = 1$  for lack of microscopic information [198]. Within the model, the diffusion anisotropies are always less than two, except at low temperatures where long range order in the adlayer emerges. These results are consistent with the current experiments [5,105] on the anisotropy of collective diffusion in  $H/W(110)$ . Finally, we would like to comment on the energy scale chosen here. Although there is no first principles knowledge of the interaction parameters, they are expected to have a magnitude corresponding to a temperature of about 300 - 400 K. This implies that our chosen values of  $\Delta_i$  and  $\Delta_e$  are on the low side as compared with the conventional estimates of  $\Delta_e$  in the range of a few thousand degrees [5]. Our choice of the barriers was done to facilitate the Monte Carlo computations. The main quantity of interest here is the diffusion anisotropy which should be sensitive only to the ratio  $\Delta_i/\Delta_e$  rather than their individual values.

## 6. Diffusion Anomaly Near Structural Phase Transitions

Anomalous behavior of diffusion has often been used to identify phase transitions on surfaces [5], and has implications for a variety of systems, including diffusion limited chemical reactions [199,200], and flux line motion in high  $T_c$  superconductors [201]. In this chapter, we consider an adatom diffusing on a surface which undergoes a structural phase transition at some critical temperature  $T_c$ . Near a structural transition, it is well established that the vibrational excitations of the medium display strong anomalies [202-205]. Besides the softening of a phonon branch, there is also a collective "central peak" excitation, which is apparent in the dynamical structure function  $S(\vec{q}, \omega)$ , near the critical wavevector  $\vec{q}_0$ . The coupling of these excitations to the adatom leads to anomalous temperature dependence of the friction exerted by the medium on the diffusion particle. In fact, we will show using the microscopic theory of chapter 3 that the diffusion coefficient is expected to *vanish anomalously* at  $T_c$ , due to the

divergence of  $S(\vec{q}_0, \omega = 0)$ . To demonstrate this anomaly, we study the diffusion of adatoms for a model of the  $W(100)$  surface, which undergoes a  $(1 \times 1) \rightarrow c(2 \times 2)$  reconstruction [12,206].

### A. Critical dynamics of the surface at the reconstruction

The  $(1 \times 1) \rightarrow c(2 \times 2)$  reconstruction of a clean  $W(100)$  surface is one of the most actively studied examples of structural phase transitions [202-233]. It has recently been shown that the critical dynamics near the structural phase transition of a clean  $W(100)$  surface displays a richness of behavior [202-204]. At the transition there are large critical fluctuations and strong anharmonic effects. In that region, the central peak at zero frequency which is due to the diffusive motion of domains contains the dominant vibrational excitations. Additionally, as one approaches the transition there is a soft phonon mode with decreasing frequency which becomes overdamped at the transition.

A two dimensional model Hamiltonian which successfully describes the surface critical dynamics near the reconstruction of the  $W(100)$  surface, is given by

$$H = \sum_i \left\{ \frac{p_i^2}{2} + \frac{A}{2} u_i^2 + \frac{B}{4} u_i^4 + 8H_4 u_{ix}^2 u_{iy}^2 \right\} + C_1 \sum_{n.n.} \vec{u}_i \cdot \vec{u}_j. \quad (6.1)$$

Here  $\vec{u}_i$  is the in - plane displacement of a  $W$  atom on the  $i^{\text{th}}$  site,  $\vec{R}_i^0 = a_0(l, m)$ , with integers  $l$  and  $m$  indicating the equilibrium position of  $W$  atoms in units of the lattice constant  $a_0 = 3.16 \text{ \AA}$ .  $C_1 (> 0)$  is the nearest neighbor interaction strength. For the on - site terms,  $A < 0$  and  $B > 0$ , and  $H_4 (< 0)$  determines the anisotropy of the system. In our model, the Hamiltonian parametrization in dimensionless unit system are such that  $A = -10$ ,  $B = 40$ ,  $H_4 = -1.85$ , and  $C_1 = 3.75$ . Length scale  $L_0$  and temperature scale  $T_0$  are chosen such that the transition temperature  $T_c$  and ground state displacement  $u_0$  agree with the experimentally observed values. The frequency scale factor  $\omega_0$  is then determined by fixing the coefficient of  $p_i^2$  to be  $1/2$ . This gives  $\omega_0 = \sqrt{k_B T_0 / M L_0^2}$ , with  $M$  as the mass of a  $W$  atom. Although not all the phonon modes are included in this two dimensional Hamiltonian the important central peak mode which determines the critical behavior of the diffusion constant near the structural transition of  $W(100)$  is properly included. For the study of the critical dynamics near the transition, the crucial quantity to calculate is the dynamic structure factor  $S(\vec{q}, \omega)$  which can also be written as

$$S(\vec{q}, \omega) = \frac{k_B T}{N} \chi(\vec{q}) \Phi(\vec{q}, \omega), \quad (6.2)$$

where  $\chi(\vec{q})$  is the static susceptibility and  $\Phi(\vec{q}, \omega)$  is the relaxation function. Using Mori's

projection operator formalism, the continued fraction expansion for the structure function can be developed as [204]

$$S(\vec{q}, \omega) = -2 \frac{k_B T}{N} \chi(\vec{q}) \lim_{\delta \rightarrow 0} \text{Im} \frac{1}{\omega + i\delta + \frac{\Delta^{(1)}}{\omega + i\delta + \frac{\Delta^{(2)}}{\omega + i\delta + \dots}}}, \quad (6.3)$$

where  $\Delta^{(i)}$ 's are associated with the various moments of the structure function.

The quantities  $\Delta^{(i)}$  appearing in Eq. (6.3) are *equilibrium* thermodynamic averages. We have evaluated them near the transition through Monte Carlo simulation of the model Hamiltonian (6.1) on  $L \times L$  periodic lattices, with  $L = 20, 30$  and  $40$ . We have identified the transition temperature as  $T_c = 2.42 \pm 0.02$  from the nontrivial fixed points of the block cumulants  $U_L$  and  $V_L$ , using the Monte Carlo renormalization group method. Comparison with the experimental value of  $T_c \approx 230$  K yields a temperature scale of  $T_0 = 95$  K leading to a frequency scale of  $\hbar\omega_0 = 2.05$  meV. We note that for  $T > T_c$ ,  $S_{zz} = S_{yy}$  and  $S_{xy} = S_{yz} = 0$  by the symmetry consideration of the model system. Thus the longitudinal and transverse phonons are identical for this model.

In Fig. 31 we show typical results for the relaxation function in the vicinity of the transition, which is continuous. The main features are the softening and overdamping of the soft phonon mode as  $T \rightarrow T_c$  and  $\vec{q} \rightarrow \vec{q}_0$ . This is accompanied by the emergence of a central peak mode. The main critical behavior in the relaxation function arises from  $\Delta^{(1)}(\vec{q}) = \chi^{-1}(\vec{q})$  [234]. Thus, the zero frequency limit of the dynamic structure function diverges as

$$S(\vec{q}, \omega = 0) \propto \chi^2(\vec{q}), \quad (6.4)$$

where the susceptibility near the transition obeys the scaling form [235,236]

$$\chi(T, L, \vec{q}) = L^{\gamma/\nu} F[(1 - T_c/T)L^{1/\nu}, \tilde{q}L]. \quad (6.5)$$

Here  $\tilde{q} = |q - q_0|$  is the magnitude of the wavevector measured from the critical value  $\vec{q} = \vec{q}_0$ ,  $\gamma$  and  $\nu$  are the susceptibility and correlation length exponents, respectively, and  $F$  is an unknown scaling function. In Fig. 32 we show  $\chi(T, \tilde{q}, L)L^{-\gamma/\nu}$  as a function of  $(1 - T_c/T)L^{1/\nu}$  for each value of  $\tilde{q}L$  from the simulations. The relatively small scatter in the data shows that scaling is well obeyed for the system up to  $\tilde{q}L = 2\pi\sqrt{32}$ , and thus a well defined  $F$  exists. Using our data to estimate the critical exponents for the transition, we obtain  $\gamma = 1.55 \pm 0.02$  and  $\gamma/\nu = 1.7 \pm 0.2$ . These numbers are consistent with the expectation from the Hamiltonian

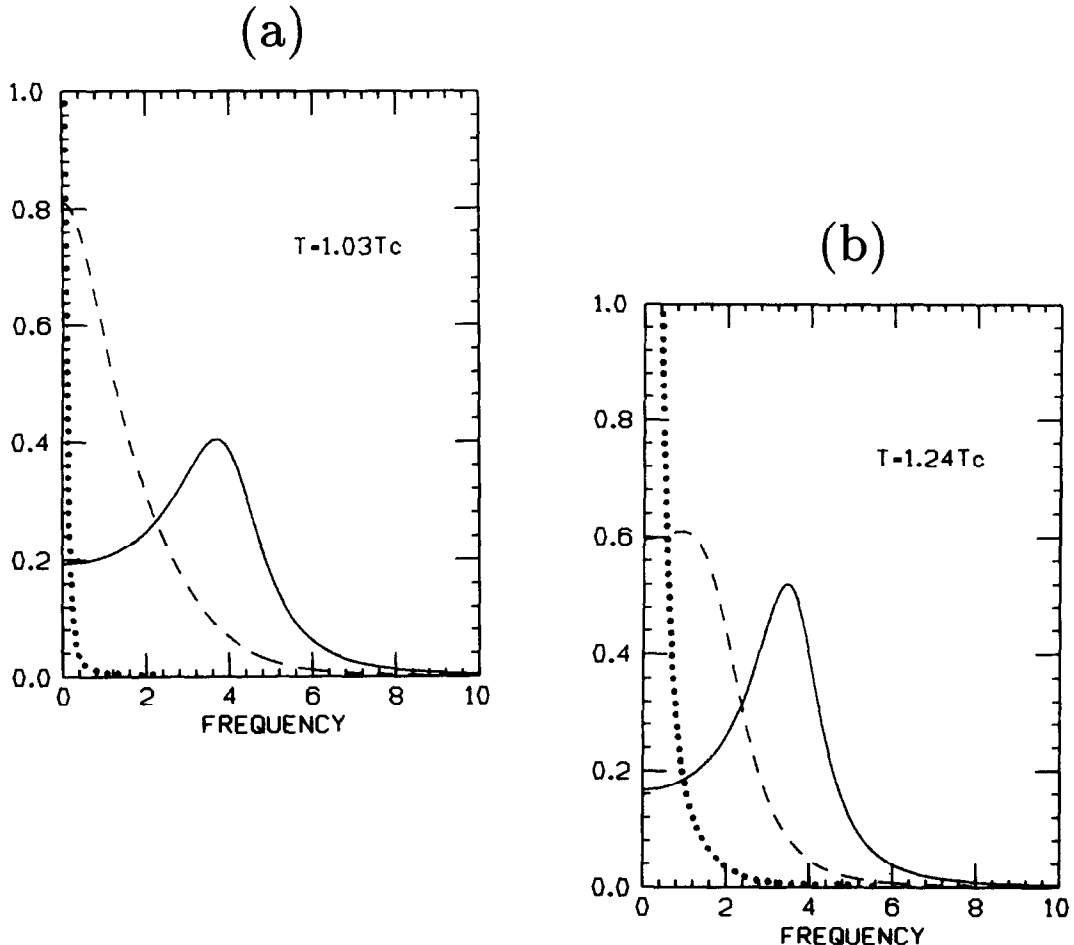


Fig. 31. The dynamical relaxation function  $\Phi(\vec{q}, \omega)$  at (a)  $T = 1.03T_c$  and (b)  $T = 1.24T_c$ , for  $\vec{q} = \vec{q}_0$  (dotted line),  $0.8\vec{q}_0$  (dashed line), and  $0.6\vec{q}_0$  (solid line). The diverging peak of  $\Phi$  at  $\vec{q}_0$  has a value of about 190 for (a), and 6 for (b) [12].

that the transition belongs to the universality class of an *xy* model with a cubic anisotropy term [229,237].

#### B. Evaluation of the diffusion coefficient

The key point for the evaluation of the diffusion coefficient at the transition point is to note from Eqs. (3.43) and (3.44) that the friction tensor  $\eta$  depends on the zero frequency limit of

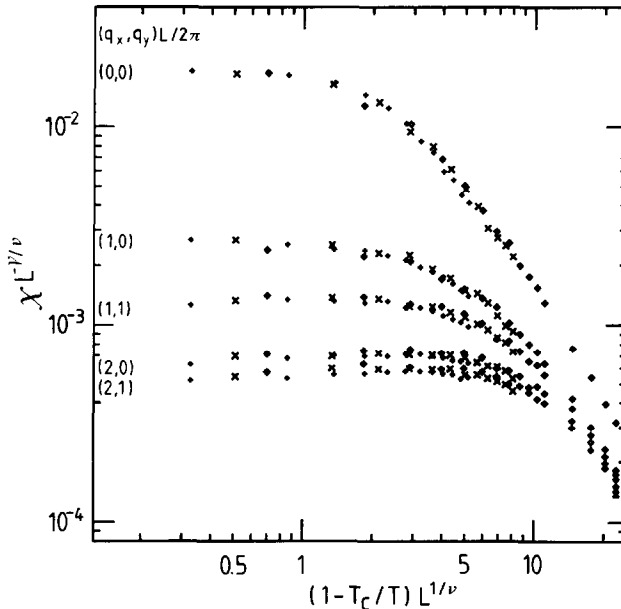


Fig. 32. Figure of the scaling behavior for the susceptibility of Eq. (6.5), for several values of  $\vec{q}$  vectors (in units of  $2\pi/L$ ). Different symbols are for the three different sizes. Good overlap between these points is evident in the data.

the dynamic structure factor  $S(\vec{q}, \omega = 0)$ . The explicit expression for the Fourier components of  $\eta$  is given by

$$\eta^{\alpha\beta}(\vec{G}, \vec{G}'; \omega = 0) = \frac{N}{k_B T} \int \frac{d\vec{q}}{(2\pi)^2} \sum_{\mu, \delta} S_{\mu\delta}(\vec{q}; \omega = 0) v^*(\vec{q} + \vec{G}) v(\vec{q} + \vec{G}') , \quad (6.6)$$

$$\times (\vec{q} + \vec{G})_\alpha (\vec{q} + \vec{G})_\mu (\vec{q} + \vec{G}')_\beta (\vec{q} + \vec{G}')_\delta ,$$

where  $v(\vec{q})$  denotes the Fourier components of the pair interaction potential between the adatom and the surface atoms, and  $v^*$  its complex conjugate.  $\vec{G}$  and  $\vec{G}'$  are reciprocal lattice vectors of the surface, and the integral in Eq. (6.6) is evaluated within the first Brillouin zone. As  $T \rightarrow T_c$ , the various Fourier components of the friction diverge due to the divergent behavior of  $S(\vec{q}; \omega = 0)$  for  $\vec{q} \rightarrow 0$ . To estimate this divergence, we evaluate the component  $\eta_{\alpha\beta}(\vec{G} = 0, \vec{G}' = 0; \omega = 0)$  in Eq. (6.6) neglecting all the  $q$ -dependence in the integral over the Brillouin zone, except for the dominant behavior of  $S(\vec{q}; \omega = 0)$  as given by Eq. (6.4). Using the scaling behavior of the susceptibility (cf. Sec. A), the integral in Eq. (6.6) gives a power law behavior for the friction as

$$\eta^{\alpha\beta}(\vec{G} = 0, \vec{G}' = 0; \omega = 0) \sim \epsilon^{2\nu(1-\eta)} , \quad (6.7)$$

where  $\epsilon \equiv |T - T_c|/T_c$ , and  $\hat{\eta}$  is the static correlation function exponent. Since  $D$  is inversely proportional to the friction tensor (cf. Chap. 3),  $D$  behaves in an anomalous fashion at the transition [238]. The scaling argument predicts that as  $T \rightarrow T_c$ ,  $D$  vanishes as a power law given by

$$D \sim \epsilon^{2\nu(\hat{\eta}-1)} \sim \epsilon^{1.6 \pm 0.2}. \quad (6.8)$$

We note that within this simple scaling picture, the divergence of the friction near  $T_c$  has exactly the same form as the divergence of the EPR linewidth at a structural transition in the fast motion regime [239]. The linewidth is also proportional to the integral of  $S(\vec{q}; \omega = 0)$  over the first Brillouin zone, albeit without the complicated noncritical weighting factors present in Eq. (6.6).

For a quantitative calculation of  $D$ , we must specify an explicit form for the adiabatic surface potential (cf. Chap. 3). To this end, we have neglected the vertical motion and discuss here results for two model potentials A and B of the form

$$v(\vec{q}) = w e^{-\alpha(q-q_0)^2} - r e^{-\alpha'(q-q_0)^2}, \quad (6.9)$$

where  $q_0 = (\pi/a, \pi/a)$ . For potential A,  $\alpha = (a_0/\pi)^2$ ,  $\alpha' = 2(a_0/\pi)^2$ ,  $w = 1$ , and  $r = 1.4$ , and for B,  $\alpha = (3/10)(a_0/\pi)^2$ ,  $w = 1$ , and  $r = 0$ . In the integration over the Brillouin zone in Eq. (6.6), the scaling form for  $\chi(\vec{q})$  is used for the small  $\vec{q}$  region up to  $\vec{q}L = 2\pi\sqrt{32}$ . It was also found that the large  $\vec{q}$  region contributes insignificantly to the total integral for the present choice of the interaction potentials and can be safely neglected [206]. The higher order parameters in the continued fraction expansion for  $S(\vec{q}; \omega)$  ( $\Delta^{(n)}$  for  $n \geq 2$ ) are not sensitive to the critical fluctuations and can be assumed to be size independent for  $L \geq 40$ . This then allows us to extend the study of friction and hence the diffusion tensor to systems of arbitrary large sizes using the numerical data for  $\chi(\vec{q})$ . In Figs. 33 and 34, we show results for the components of the friction tensor for the two different choices of the interaction potentials. In Figs. 35 (a) and (b) we show results for  $D$  obtained with the interaction potentials corresponding to Figs. 3 and 4. Compared with the simple Arrhenius form with a constant friction the actual value of  $D$  is reduced by several orders of magnitude near  $T_c$ , where  $D \approx \epsilon^x$  with the exponent being about  $0.9 - 1.8$  depending on the choice of the the scaling region. This is in complete accordance with the scaling prediction of Eq. (6.8). However, because of numerical uncertainties, the exact exponent cannot be determined with great accuracy. At this point we cannot exclude the possibility of the existence of corrections to the simple scaling prediction for the exponent [240]. In any case, the diffusion anomaly itself is very robust. With other choices of the coupling

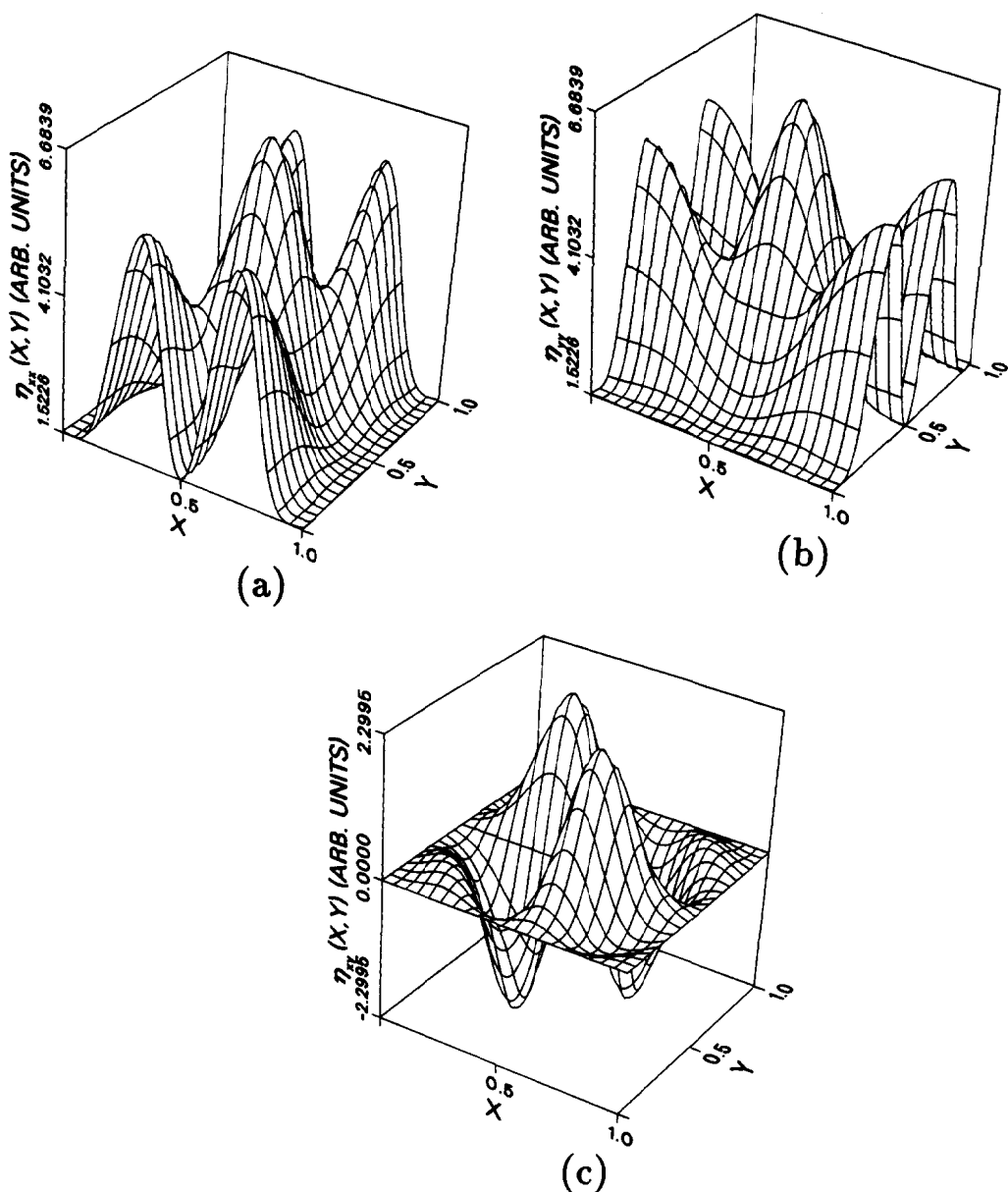


Fig. 33. Typical components of the friction tensor for model potential A: (a)  $\eta_{xx}$ , (b)  $\eta_{yy}$  and (c)  $\eta_{xy} = \eta_{yx}$ .

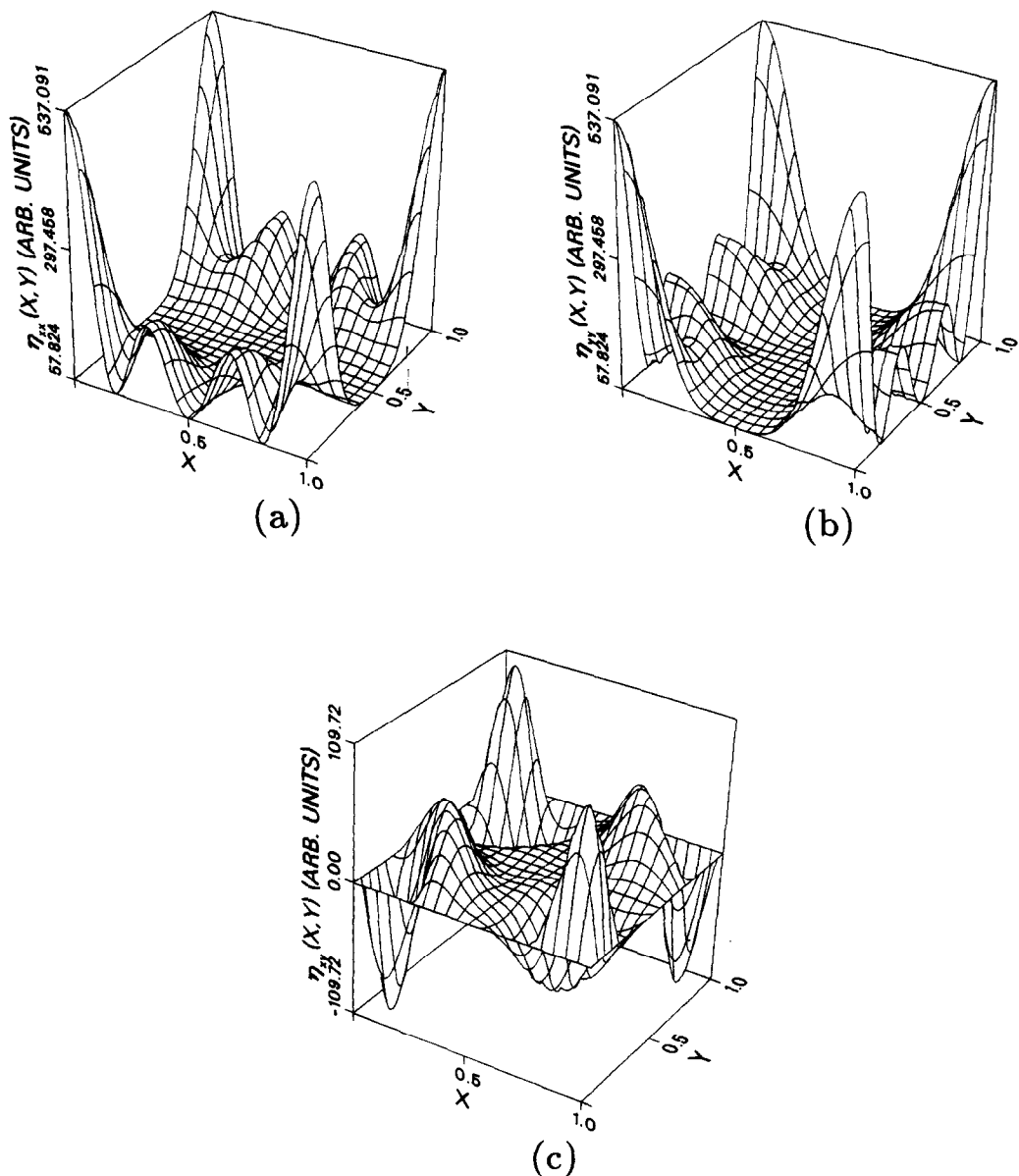


Fig. 34. Typical components of the friction tensor for model potential  $B$ : (a)  $\eta^{xx}$ , (b)  $\eta^{yy}$  and (c)  $\eta^{xy} = \eta^{yx}$ .

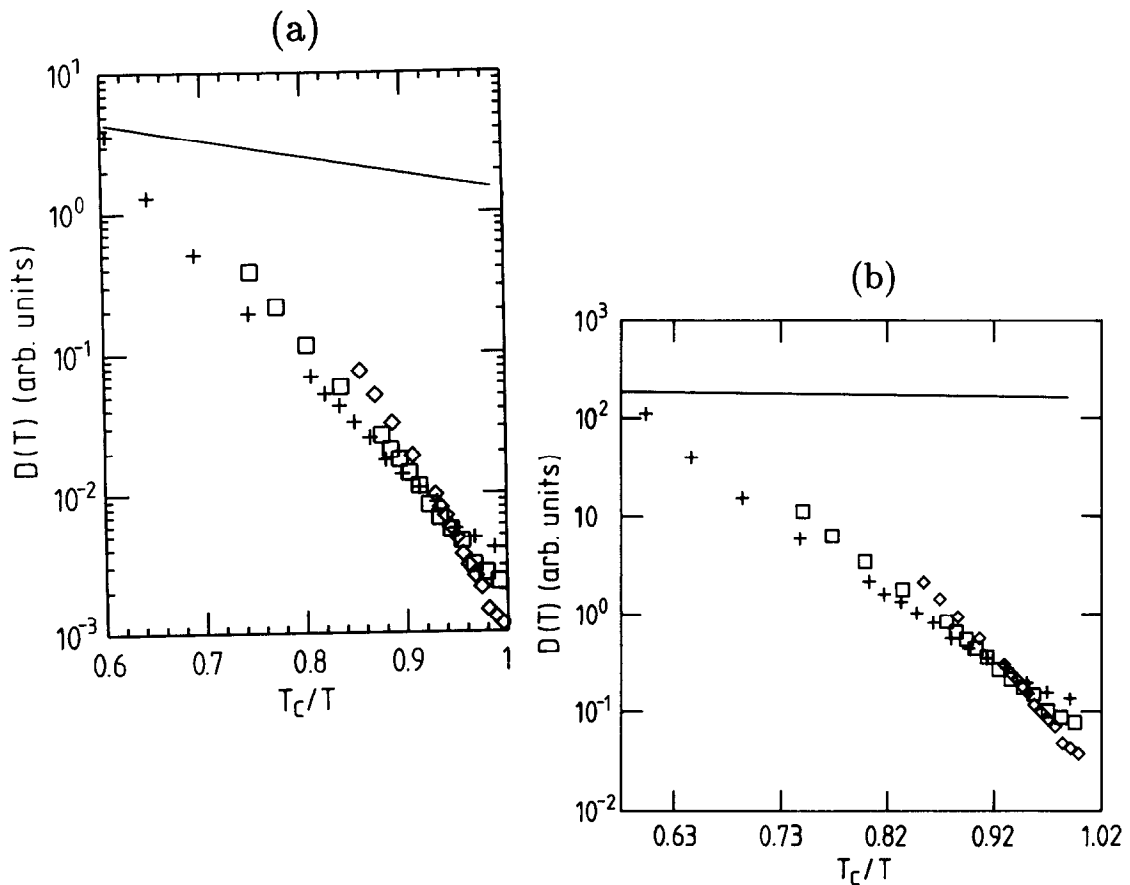


Fig. 35. The diffusion coefficient  $D(T)$  shown as a function of the inverse temperature. The crosses are for a  $40 \times 40$ , the squares for a  $60 \times 60$ , and the diamonds for a  $100 \times 100$  system. The solid line is the expected Arrhenius behavior in the absence of critical fluctuations of the substrate. (a) results for model A; (b) results for model B.

potential the results are very similar, except that the strength of the anomaly depends on the relative weighting of the critical region for different choice of  $v(\vec{q})$ 's. In Fig. 36 we finally show results for the saddle point value of the friction for three different system sizes, corresponding to Fig. 35 (a). As expected, on approaching  $T_c$  the value of the friction indeed diverges until a finite size rounding occurs just before  $T_c$ .

Experimentally, anomalous dips in the temperature dependence of surface diffusion have been observed, and qualitatively interpreted as indicating phase transitions on surfaces [5].

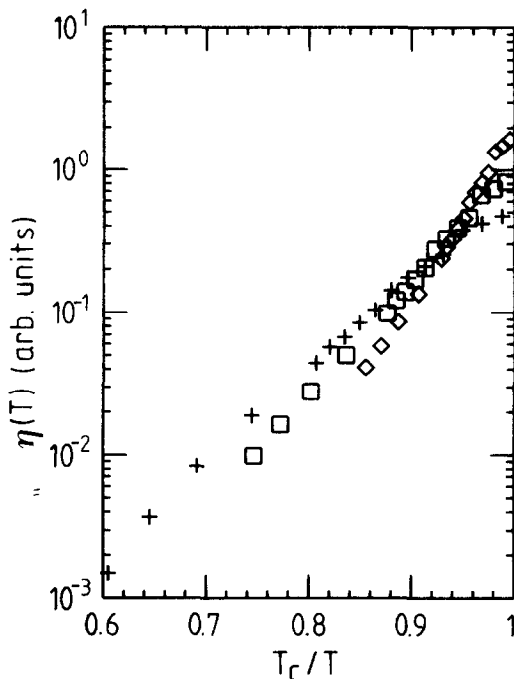


Fig. 36. The saddle point friction  $\eta^{zz}(T)$  as a function of the inverse temperature, corresponding to model A. Symbols are the same as in Fig. 35.

For example, data for  $H$  diffusion on the  $W(110)$  surface displays a distinct downward cusp around  $T = 74 - 91$  K, which was ascribed to a phase transition on the surface [159]. Unfortunately, the true nature of this transition is not known. At present, the  $(1 \times 1) \rightarrow c(2 \times 2)$  surface reconstruction on  $W(100)$  is best studied and understood. Measurements of adatom diffusion and other kinetic processes on this surface in the vicinity of  $T_c$  would be the best avenue to study the anomaly described here.

## 7. Summary and Discussion

In the chapters above, we have surveyed the existing experimental and theoretical studies of surface diffusion and then presented a new microscopic theory based on a Hamiltonian describing the motion of an adatom interacting with substrate vibrational excitations. This microscopic theory allows us to examine many qualitative features of surface diffusion from first principles and offers a rigorous theoretical basis for more phenomenological approaches based on random walk processes or a simple Arrhenius form assumption for the temperature

dependence. The theory provides a natural transition from the low temperature regime where the motion is predominantly hopping between neighboring sites to the high temperature limit in which the periodic nature of the substrate becomes negligible and the adatom motion reduces to that of a Brownian particle motion in a uniform viscous medium. In our discussion of the qualitative features, we have paid particular emphasis on the anisotropy of the diffusion tensor. We found that this is a property that is often insensitive to the details of the model and various theoretical approximations. It depends mainly on the fundamental symmetry of the adsorption sites both on a global and on a local level. Thus detailed studies of the surface diffusion tensor and comparisons between experimental results and theoretical predictions can yield valuable information about the adsorption system.

Beyond diffusion on a normal substrate with the surface adatoms executing small vibrational motions around the equilibrium positions, we have also examined surface diffusion on substrates with large local distortions induced by the adatoms. Quite often this can be the precursor to an adatom induced reconstruction, as in the case of  $H/W(110)$ . We have also examined the adatom diffusion in the vicinity of a surface structural phase transition. In the case of a substrate with a large local adatom induced distortion, the crucial point is that the local symmetry is altered. Internal barriers can arise in addition to the usual external barriers between adsorption sites. This leads to additional hopping paths for the adatom and changes the diffusion anisotropy. We have examined this issue using both the microscopic theory and a more phenomenological two - step lattice gas model. The latter has the advantage of easy generalizability to the case of finite coverages of fully interacting adatoms. This allows us to examine the correlation of diffusion with the various ordered phases in the phase diagram of the adsorption system. In the case of diffusion on a substrate with an intrinsic structural phase transition, the power of the microscopic theory is shown to full advantage. The reason is that in this theory, the frictional force acting on the adatom is not just assumed to be a parameter as in most phenomenological approaches, but actually expressed in terms of substrate atom displacement correlation functions. Near the surface structural phase transition, critical fluctuations lead to a strong divergence of the dynamical structure factor at zero frequency, which in turn leads to the divergence of the frictional force and the vanishing of the diffusion constant as the transition is approached. Since diffusion rate is one of the fundamental parameters that enter almost any kinetic processes on the surface such as chemical reactions, growth of overlayers and catalysis, this diffusion anomaly near the transition is expected to have broad consequences and implications.

Aside from the topics discussed in this review, there are many issues in surface diffusion

or related to surface diffusion which can be examined in the spirit of the microscopic theory discussed here. Work is in progress on a number of these topics but it is beyond the scope of this review to go into the details here. However, we will briefly discuss some of the ideas here to demonstrate that this is still a very fruitful field and many issues remain to be explored in detail, both experimentally and theoretically.

The diffusive motion of particles in random media is a problem, which has recently been extensively studied [241]. Besides having direct applications to diffusion in amorphous materials and inhomogeneous surfaces these problems are important theoretically, too. Most of the current theoretical work has concentrated on the application of the random walk formalism by using spatially dependent transition probabilities, which contain the randomness inherent in the background medium. In general, diffusive behavior in such cases may not even exist depending on dimensionality and the strength of randomness [241,242].

In the case of surface diffusion, we expect some randomness in the adiabatic potential to be present for any real system. On clean surfaces, this may be caused by the presence of steps or surface defects, or long - range strain fields generated by dislocations or grain boundaries within the material. On adsorption systems, randomness can be easily generated by adsorption of foreign molecules, which may either trap or repel the diffusing adatoms. Microscopically, this is obviously very difficult to describe in a realistic manner within the analytic theory of chapter 3. However, the case of small local variations which obey a well defined probability distribution can be used to illustrate the qualitative effects one expects randomness to cause for single adatom motion. To this end, we consider the analytic expression of Eq. (3.50) for a quasi one - dimensional case neglecting both the vertical motion and the spatial variation of the friction tensor. Thus, for example, if we assume that the potential  $V_A(\vec{r})$  obeys a Gaussian distribution around its mean maximum value  $\bar{V}_s(y)$  (for any direction  $y$ )

$$p(V_A) = \frac{1}{\sigma_s(y)\sqrt{2\pi}} e^{-(V_A - \bar{V}_s(y))^2/(2\sigma_s^2(y))}, \quad (7.1)$$

we can integrate for  $D_{zz}$  by extending the unit cell to be arbitrary large, and obtain

$$\langle \int dx e^{\beta V_A} \rangle = e^{\beta \bar{V}_s(y)} e^{\beta^2 \sigma_s^2(y)/2}. \quad (7.2)$$

Here the brackets  $\langle \rangle$  denote an average over the probability distribution. On the other hand, the configuration integral  $Z$  always gives the smallest minimum. For an independent Gaussian distribution of minima, it becomes

$$\langle Z \rangle = e^{-\beta \bar{V}_m} e^{\beta^2 \sigma_m^2/2}, \quad (7.3)$$

where the subscript  $m$  now refers to the minima. Combining these two results we can write  $D_{zz}$  as

$$D_{zz} = \frac{k_B T}{M\eta} e^{-\beta\bar{\Delta}} e^{-\beta^2(\sigma_m^2 + \sigma_s^2)/2}, \quad (7.4)$$

where  $\bar{\Delta} \equiv \bar{V}_s - \bar{V}_m$  is the average Arrhenius barrier of the potential along  $y = 0$ . The result for  $D_{yy}$  is completely analogous. However, since we are considering a quasi one-dimensional process, at very low temperatures  $D$  will be dominated by the largest saddle point barriers and it will approach zero. Obviously, in case variations become so large that lower energy barriers appear in other directions, the behavior of  $D$  is more complicated.

Finally, we note that in the special case of one dimension, Eq. (3.50) has a particularly simple form which has been derived earlier [59,243,244] and used to obtain exact analytic solutions of  $D$  for different model potentials in randomly modulated systems [17,245]. On the experimental side, we know of no systematic studies of well characterized surface randomness to single adatom motion. There exist, however, some works for the cases of adatom trapping and random site blocking by foreign adsorbates, where collective diffusion has been studied as a function of coverage [83,111,114-116,146].

One of the topics closely related to surface diffusion is the relaxation of an adatom vibrational excitation. When the diffusive motion of the adatom is neglected, it can be viewed as executing vibrational motion about the minimum of the potential well at the adsorption site. However, the anharmonic nature of the well can contribute significantly to the broadening of the observed vibrational frequency. Another source of broadening comes from relaxation of the vibrational energy through coupling with substrate vibrational excitations. When the diffusive motion is included, additional broadening can occur. These various mechanisms contributing to the broadening of the adatom vibrational frequency are usually treated one at a time within some perturbational scheme. This is highly unsatisfactory. It is well recognized that the anharmonic interaction is not easily amenable to perturbation treatment. Also, the very fact that diffusive motion of the adatom is observed implies that the adsorption well is highly anharmonic, so the contribution of anharmonicity and diffusive motion to vibrational broadening are intimately related and has to be treated on an equal footing. The microscopic theory discussed in chapter 3 provides exactly such a formalism. It is really a theory for the evaluation of various dynamic self-correlations associated with the adatom. The zero frequency limit of the velocity autocorrelation function yields exactly the diffusion constant which is the main focus of this review. However, the finite frequency correlation function can be easily evaluated using the same method. This function peaks at the adatom vibrational frequency while the width of the

peak contains the broadening contributions from the various mechanisms discussed above. It is worth pointing out here that since the adatom vibrational frequencies are usually comparable or higher than the substrate vibrational frequencies, the initial value approximation used to obtain the diffusion results discussed in this work is no longer appropriate. One needs to employ the full mode-mode coupling scheme as described briefly in Chap. 3 for a quantitative study of the adatom vibrational relaxations. We note also that while the inclusion of the vertical motion mostly just renormalizes the parameters and has little significance concerning the qualitative features of surface diffusion, it is of crucial importance in the discussion of the vibrational relaxation because this allows the inclusion of the vibrations normal to the surface. In fact, these are the only observable vibrational modes in many experimental studies.

Beyond these additional applications, there are two major directions for the generalizations of the microscopic theory as presented in this review. The first concerns finite coverage effects. This is of great practical importance. As we have discussed earlier, many additional issues in surface diffusion arises for the case of finite coverage of interacting adatoms. Without a microscopic theory, we are limited to the phenomenological lattice gas model in these type of studies. The other direction of generalization is to consider adatom motion in the quantum regime [149,246-266]. This is of particular importance in the experiments of hydrogen adatom diffusion [5,108]. Evidences concerning the quantum nature have been reported for both the diffusion and vibration of hydrogen adatoms on various metal and semiconductor substrates. This is one of the rare systems that by varying the temperature alone, one can observe the continuous crossover from classical to quantum mechanical behaviour. Work in both directions are in progress and we hope to report on the results in a future update of this review.

### Acknowledgements

This work has been supported by an ONR contract, and by the Academy of Finland. We want to acknowledge the Illinois National Center for Supercomputer Applications at Urbana-Champaign, and the Scientific Computer Centre of Finland for allocations of computer time. Ms. Heidi Koskela's expertise in preparing the figures is gratefully appreciated.

### References

1. L. Hamburger, Kolloid-Z., **23**, 12 (1918).
2. M. Volmer and I. Estermann, Z. Phys., **7**, 13 (1921).
3. I. Langmuir and J. B. Taylor, Phys. Rev., **40**, 463 (1932).
4. A. J. Ahearn and J. A. Becker, Phys. Rev., **54**, 448 (1938).

5. R. Gomer, Rep. Prog. Phys., **53**, 917 (1990).
6. A. G. Naumovets and Yu. S. Vedula, Surface Sci. Repts., **4**, 365 (1985).
7. J. Kjoll, T. Ala - Nissila, and S. C. Ying, Surface Sci., **218**, L476 (1989).
8. T. Ala - Nissila and S. C. Ying, Phys. Rev. Lett., **65**, 879 (1990).
9. T. Ala - Nissila and S. C. Ying, Phys. Rev. B, **42**, 10264 (1990).
10. T. Ala - Nissila and S. C. Ying, Surface Sci. Lett., **235**, L341 (1990).
11. T. Ala - Nissila and S. C. Ying, Modern Phys. Lett. B, **4**, 1005 (1990).
12. T. Ala - Nissila, W. K. Han, and S. C. Ying, Journal of Electron Spectroscopy and Related Phenomena, **54/55**, 245 (1990).
13. T. Ala - Nissila, J. Kjoll, S. C. Ying, and R. A. Tahir - Kheli, Phys. Rev. B, **44**, 2122 (1991).
14. T. Ala - Nissila, J. Kjoll, S. C. Ying, and R. A. Tahir - Kheli, Phys. Rev. B, **44**, 2133 (1991).
15. G. L. Kellogg and P. J. Feibelman, Phys. Rev. Lett., **64**, 3143 (1990).
16. P. J. Feibelman, Phys. Rev. Lett., **65**, 729 (1990).
17. T. Ala - Nissila and S. C. Ying, unpublished.
18. N. A. Gjostein, in Techniques of Metals Research, vol. 4, part 2, ed. R. F. Bunshah, Interscience Publications (1970).
19. G. Erlich and K. Stolt, Annu. Rev. Phys. Chem., **31**, 603 (1980).
20. H. P. Bonzel, in Surface Mobilities on Solid Materials, ed. V. T. Bihm, Plenum Press (1983).
21. S. Glasstone, K. J. Laidler, and H. Eyring, The Theory of Rate Processes, McGraw - Hill, New York (1941).
22. M. Kac, Am. J. Math., **65**, 609 (1943).
23. G. Vineyard, J. Phys. Chem. Solids, **3**, 121 (1957).
24. S. O. Rice, J. Phys. Chem. Solids, **3**, 133 (1954).
25. N. B. Slater, Theory of Unimolecular Reactions, Cornell Univ. Press, Ithaca (1959), p. 230.
26. J. D. Doll, J. Chem. Phys., **73**, 2760 (1980).
27. A. F. Voter and J. D. Doll, J. Chem. Phys., **80**, 5832 (1984).
28. A. F. Voter, J. Chem. Phys., **82**, 1890 (1985).
29. J. C. Tully, G. H. Gilmer, and M. Shugard, J. Chem. Phys., **71**, 1630 (1979).
30. M. R. Mruzik and G. M. Pound, J. Phys. F, **11**, 1403 (1981).
31. G. DeLorenzi, G. Jacucci, and V. Pontikis, Surface Sci., **116**, 391 (1982).
32. J. D. Doll and H. K. McDowell, J. Chem. Phys., **77**, 479 (1982).
33. J. D. Doll and H. K. McDowell, Surface Sci., **123**, 99 (1982).
34. H. K. McDowell and J. D. Doll, J. Chem. Phys., **78**, 3219 (1983).
35. I. NoorBatcha, L. M. Raff, and D. L. Thompson, J. Chem. Phys., **81**, 3715 (1984).

36. S. M. Levine and S. H. Garofallini, Surface Sci., **167** 198 (1986).
37. J. D. Doll and D. L. Freeman, Annu. Rev. Phys. Chem., **38**, 413 (1987).
38. J. C. Keck, Discuss. Faraday Soc., **33**, 173 (1962).
39. J. C. Keck, Adv. Chem. Phys., **13**, 85 (1967).
40. R. L. Jaffe and J. B. Anderson, J. Chem. Phys., **54**, 2224 (1971).
41. R. L. Jaffe, J. M. Henry, and J. B. Anderson, J. Chem. Phys., **59**, 1128 (1973).
42. R. N. Porter, D. L. Thompson, L. M. Raff, and J. M. White, J. Chem. Phys., **62**, 2429 (1975).
43. C. H. Bennett, in Diffusion in Solids, A. S. Nowick and J. J. Burton, eds., Academic, New York (1975), pp. 73-113.
44. C. H. Bennett, in Algorithms for Chemical Computation, ed. R. E. Christofferson, Am. Chem. Soc., Washington D.C. (1977).
45. D. Chandler, J. Chem. Phys., **68**, 2959 (1978).
46. J. L. Skinner and P. G. Wolynes, J. Chem. Phys., **69**, 2143 (1978).
47. J. A. Montgomery, D. Chandler, and B. J. Berne, J. Chem. Phys., **70**, 4056 (1979).
48. J. L. Skinner and P. G. Wolynes, J. Chem. Phys., **72**, 4913 (1980).
49. A. F. Voter and J. D. Doll, J. Chem. Phys., **82**, 80 (1985).
50. A. F. Voter and J. D. Doll, to be published.
51. C. P. Flynn and G. Jacucci, Phys. Rev. B, **25**, 6225 (1982).
52. G. Jacucci, M. Troller, G. DeLorenzi, and C. P. Flynn, Mater. Sci. Forum, **1**, 187 (1984).
53. G. Jacucci, M. Troller, G. DeLorenzi, and C. P. Flynn, Phys. Rev. Lett., **52**, 295 (1984).
54. D. G. Truhlar and B. C. Garrett, Ann. Rev. Phys. Chem., **35**, 159 (1984).
55. M. Troller, G. Jacucci, G. DeLorenzi, and C. P. Flynn, Phys. Rev. B, **32**, 2082 (1985).
56. G. Mazenko, T. R. Banavar, and R. Gomer, Surface Sci., **107**, 459 (1981).
57. P. J. Estrup, in Chemistry and Physics of Solid Surfaces V, R. Vanselow and R. Howe, eds., Springer - Verlag (1984).
58. D. Forster, Hydrodynamic Fluctuations, Broken Symmetry and Correlation Functions, Benjamin, New York (1975).
59. H. Risken, The Fokker - Planck Equation, Springer - Verlag, Berlin (1984).
60. W. G. Kleppmann and R. Zayher, Phys. Rev. B, **22**, 6044 (1985).
61. G. Wahnnström, Surface Sci., **159**, 311 (1985).
62. S. C. Ying, Phys. Rev. B, **41**, 7068 (1990).
63. G. A. Baraff, M. Schluter, and G. Allan, Phys. Rev. Lett., **50**, 739 (1983).
64. R. Car, P. J. Kelly, A. Oshiyama, and S. T. Pantelides, Phys. Rev. Lett., **52**, 1814 (1984).

65. R. Car, P. J. Kelly, A. Oshiyama, and S. T. Pantelides, *Phys. Rev. Lett.*, **54**, 360 (1985).
66. Y. Bar - Yam and J. Joannopoulos, in Proceedings of the Thirteenth International Conference on Defects in Semiconductors, L. C. Kimerling and J. M. Parsey, Jr., eds., The Metallurgical Society of AIME, New York (1985), p. 261.
67. K. C. Pandey, *Phys. Rev. Lett.*, **57**, 2287 (1986).
68. J. Bernholc, A. Antonelli, T. M. Del Sole, Y. Bar - Yam, and S. T. Pantelides, *Phys. Rev. Lett.*, **61**, 2689 (1988).
69. J. Wrigley and G. Ehrlich, *Phys. Rev. Lett.*, **44**, 661 (1980).
70. C. Chen and T. T. Tsong, *Phys. Rev. Lett.*, **64**, 3147 (1990).
71. T. T. Tsong and C.-L. Chen, *Surface Sci.*, **246**, 13 (1991).
72. G. L. Kellogg, *Surface Sci.*, **246**, 31 (1991).
73. E. W. Müller, CRC Crit. Rev. Solid State Sci., **4**, 85 (1974).
74. G. Erlich, CRC Crit. Rev. Solid State Sci., **4**, 205 (1974).
75. R. Gomer, Field Emission and Field Ionization, Harvard University Press, Cambridge (1961).
76. H. P. Bonzel, CRC Crit. Rev. Solid State Sci., **5**, 171 (1975).
77. M. S. Isaacson, J. Langmore, N. W. Parker, D. Kopf, and M. Utlaut, Ultramicroscopy, **1**, 359 (1976).
78. G. Kellogg, T. T. Tsong, and P. Cowan, *Surface Sci.*, **70**, 485 (1978).
79. T. T. Tsong and P. L. Cowan, CRC Crit. Rev. Solid State Sci., **7**, 289 (1978).
80. D. W. Bassett, in Surface Mobilities on Solid Materials, ed. V. T. Bihm, Plenum Press (1983).
81. R. Gomer, in Surface Mobilities on Solid Materials, ed. V. T. Bihm, Plenum Press (1983), p. 127.
82. T. T. Tsong, in Surface Mobilities on Solid Materials, ed. V. T. Bihm, Plenum Press (1983).
83. S. M. George, in Diffusion at Interfaces: Microscopic Concepts, M. Grunze, H. J. Kreuzer, and J. J. Weimer, eds., Springer - Verlag (1988).
84. H.-W. Fink, in Diffusion at Interfaces: Microscopic Concepts, M. Grunze, H. J. Kreuzer, and J. J. Weimer, eds., Springer - Verlag (1988).
85. J. A. Venables, T. Doust, J. S. Drucker, and M. Krishnamurty, in Kinetics of Ordering and Growth on Surfaces, ed. M. G. Lagally, Plenum Press, New York (1990).
86. G. Erlich, *Surface Sci.*, **246**, 1 (1991).
87. G. Erlich and F. G. Hudda, *J. Chem. Phys.*, **44**, 1039 (1966).
88. D. W. Bassett and M. J. Parsley, *J. Phys. D*, **3**, 707 (1970).
89. G. Ayraut and G. Erlich, *J. Chem. Phys.*, **60**, 281 (1974).

90. G. Erlich, *Surface Sci.*, **63**, 422 (1977).
91. M. Utlaut, *Phys. Rev. B*, **22**, 4650 (1980).
92. G. Binning, H. Fuchs, and E. Stoll, *Surface Sci.*, **169**, L295 (1986).
93. E. Gauz, K. Sattler, and J. Clarke, *Surface Sci.*, **219**, 33 (1989).
94. R. M. Feenstra, A. J. Slavin, G. A. Held, and M. A. Lutz, *Phys. Rev. Lett.*, **66**, 3257 (1991).
95. M. Lagally, Y.-W. Mo, R. Kariotis, B. S. Swartzentruber, and M. B. Webb, in *Kinetics of Ordering and Growth on Surfaces*, ed. M. G. Lagally, Plenum Press, New York (1990).
96. W. W. Mullins, *J. Appl. Phys.*, **28**, 333 (1957).
97. W. W. Mullins, *J. Appl. Phys.*, **28**, 77 (1959).
98. H. P. Bonzel, A. M. Franken, and W. Schwarting, *Surface Sci.*, **87**, 13 (1979).
99. G. Rhead, *Surface Sci.*, **192**, 597 (1987).
100. M. Drechsler, in *Surface Mobilities on Solid Materials*, ed. V. T. Bihm, Plenum Press (1983), p. 405.
101. H. P. Bonzel and E. E. Latta, *Surface Sci.*, **76**, 275 (1978).
102. R. Butz and H. Wagner, *Surface Sci.*, **87**, 69 (1979).
103. R. Butz and H. Wagner, *Surface Sci.*, **87**, 85 (1979).
104. R. Gomer, *Appl. Phys. A*, **39**, 1 (1986).
105. M. Tringides and R. Gomer, *Surface Sci.*, **155**, 254 (1985).
106. M. Tringides and R. Gomer, *Surface Sci.*, **166**, 419 (1986).
107. M. Tringides and R. Gomer, *J. Chem. Phys.*, **84**, 4049 (1986).
108. R. D. DiFoggio and R. Gomer, *Phys. Rev. B*, **25**, 3490 (1982).
109. R. Viswanathan, D. R. Burgess, P. C. Stair, and E. Weitz, *J. Vacuum Sci. Technol.*, **20**, 605 (1982).
110. S. M. George, A. M. De Santolo, and R. B. Hall, *Surface Sci.*, **159**, L425 (1985).
111. C. H. Mak, J. L. Brand, A. A. Deckert, and S. M. George, *J. Chem. Phys.*, **85**, 1676 (1986).
112. C. H. Mak, J. L. Brand, B. G. Koehler, and S. M. George, *Surface Sci.*, **188**, 312 (1987).
113. E. G. Seebauer, A. C. F. Kong, and L. D. Schmidt, *J. Chem. Phys.*, **88**, 6597 (1988).
114. C. H. Mak, J. L. Brand, B. G. Koehler, and S. M. George, *Surface Sci.*, **191**, 108 (1987).
115. J. L. Brand, A. A. Deckert, and S. M. George, *Surface Sci.*, **194**, 457 (1988).
116. C. H. Mak, H. C. Andersen, and S. M. George, *J. Chem. Phys.*, **88**, 4052 (1988).
117. A. A. Deckert, J. L. Brand, M. V. Arena, and S. M. George, *Surface Sci.*, **208**, 441 (1989).
118. M. V. Arena, A. A. Deckert, and S. M. George, *Surface Sci.*, **241**, 369 (1991).
119. M. C. Tringides, *Surface Sci.*, **204**, 345 (1988).
120. M. C. Tringides, *J. Chem. Phys.*, **92**, 2077 (1990).

121. L. A. Ray, R. C. Baetzold, and J. Simon, Surface Sci., **235**, 47 (1990).
122. J. W. M. Frenken, B. J. Hinch, and J. P. Toennies, Surface Sci., **211/212**, 21 (1989).
123. H.-J. Ernst, F. Fabre, and J. Lapujoulade, to be published.
124. B. J. Hinch, J. W. M. Frenken, G. Zhang, and J. P. Toennies, Surface Sci., **259**, 288 (1991).
125. P. S. Riseborough and P. Hanggi, Surface Sci., **122**, 459 (1982).
126. J. E. Reutt - Robey, D. J. Doren, Y. J. Chabal, and S. B. Christman, Surface Sci., **208**, 441 (1989).
127. M. Riehl-Chudoba, U. Memmert, and D. Fich, Surface Sci., **245**, 180 (1991).
128. G. A. Reider, U. Höfer, and T. F. Heinz, Phys. Rev. Lett., **66**, 1994 (1991).
129. X.-D. Xiao, X. D. Zhu, W. Daum, and Y. R. Shen, Phys. Rev. Lett., **66**, 2352 (1991).
130. R. Butz and H. Wagner, Surface Sci., **63**, 448 (1977).
131. Yu. S. Vedula, A. T. Loburets, and A. G. Naumovets, JETP Lett., **28**, 239 (1978).
132. Yu. S. Vedula, A. T. Loburets, and A. G. Naumovets, Sov. Phys. JETP, **50**, 391 (1979).
133. A. T. Loburets, A. G. Naumovets, and Yu. S. Vedula, Surface Sci., **120**, 347 (1982).
134. R. Morin, Surface Sci., **155**, 187 (1985).
135. A. G. Naumovets, V. V. Poplovsky, and Yu. S. Vedula, Surface Sci., **200**, 321 (1988).
136. T. S. Lin, H.-J. Lu, and R. Gomer, Surface Sci., **234**, 251 (1990).
137. B. Bayat and H.-W. Wassmuth, Surface Sci., **133**, 1 (1983).
138. N. Freger and H. P. Bonzel, Surface Sci., **160**, L501 (1985).
139. D. Ghaleb and B. Perrailon, Surface Sci., **162**, 103 (1985).
140. E. A. Daniels, J. C. Lin, and R. Gomer, Surface Sci., **204**, 129 (1988).
141. S. C. Wang and G. Erlich, Surface Sci., **206**, 451 (1988).
142. D.-S. Choi and R. Gomer, Surface Sci., **230**, 277 (1990).
143. C.-L. Chen and T. T. Tsong, Phys. Rev. Lett., **66**, 1610 (1991).
144. G. Brocks, P. J. Kelly, and R. Car, Phys. Rev. Lett., **66**, 1729 (1991).
145. R. Morin, Surface Sci., **162**, 109 (1985).
146. C. H. Mak, B. G. Koehler, J. L. Brand, and S. M. George, J. Chem. Phys., **87**, 2340 (1987).
147. D. Kashchiev, Surface Sci., **86**, 14 (1979).
148. Diffusion in Crystalline Solids, G. E. Murch and A. S. Norwick, eds., Academic Press, New York (1984).
149. K. Haug, G. Wahnström, and H. Metiu, J. Chem. Phys., **90**, 540 (1989).
150. Z. Zhang and H. Metiu, to be published.
151. H. Mori, Prog. Theor. Phys., **34**, 399 (1965).
152. V. P. Zhdanov, Surface Sci. Repts., **12**, 183 (1991).

153. V. Ambegaokar and B. I. Halperin, *Phys. Rev. Lett.*, **22**, 1364 (1969).
154. G. Wahnström, *Surface Sci.*, **164**, 437 (1985).
155. W. Jones and N. H. March, *Theoretical Solid State Physics*, Volume I, Wiley, New York (1973).
156. M. Tringides and R. Gomer, *Surface Sci.*, **145**, 121 (1984).
157. M. S. Altman, P. J. Estrup, and I. K. Robinson, *Phys. Rev. B*, **38**, 5211 (1988).
158. J. R. Chen and R. Gomer, *Surface Sci.*, **79**, 413 (1979).
159. S. C. Wang and R. Gomer, *J. Chem. Phys.*, **83**, 4193 (1985).
160. P. Norlander, S. Holloway, and J. K. Norskov, *Surface Sci.*, **136**, 59 (1984).
161. G. B. Blanchet, N. T. Dinardo, and E. W. Plummer, *Surface Sci.*, **118**, 496 (1982).
162. Yu. K. Tovbin, *Prog. Surface Sci.*, **34**, 1 (1990).
163. K. W. Kehr and K. Binder, in *Applications of the Monte Carlo Method in Statistical Physics*, ed. K. Binder, Springer - Verlag, New York (1987).
164. R. Kutner, *Phys. Lett. A*, **81**, 239 (1981).
165. H. J. Kreuzer, in *Diffusion at Interfaces: Microscopic Concepts*, M. Grunze, H. J. Kreuzer, and J. J. Weimer, eds., Springer - Verlag (1988).
166. J. W. Chung, S. C. Ying, and P. J. Estrup, *Phys. Rev. Lett.*, **56**, 749 (1986).
167. A. D. Bruce, *Advances in Physics*, **29**, 111 (1980).
168. D. Sahu, J. M. Kosterlitz, and S. C. Ying, in *The Structure of Surfaces II*, J. F. Van der Veer and M. A. Van Hove, eds., Springer - Verlag, New York (1988).
169. R. A. Tahir - Kheli and R. J. Elliot, *Phys. Rev. B*, **27**, 844 (1983).
170. R. A. Tahir - Kheli, *Phys. Rev. B*, **27**, 6072 (1983).
171. K. Binder, in *Monte Carlo Methods in Statistical Physics*, ed. K. Binder, Springer - Verlag, New York (1979).
172. K. Binder, in *Applications of the Monte Carlo Method in Statistical Physics*, ed. K. Binder, Springer - Verlag, New York (1987).
173. J. P. Van der Eerden, D. Kaschiev, and P. Bennema, *J. Cryst. Growth*, **42**, 31 (1977).
174. G. E. Murch and R. J. Thorn, *Phil. Mag.*, **35**, 493 (1977).
175. G. E. Murch and R. J. Thorn, *Phil. Mag.*, **36**, 517 (1977).
176. G. E. Murch and R. J. Thorn, *Phil. Mag.*, **36**, 529 (1977).
177. M. Bowker and D. King, *Surface Sci.*, **71**, 583 (1978).
178. M. Bowker and D. King, *Surface Sci.*, **72**, 208 (1978).
179. H. Aasada and M. Masuda, *Surface Sci.*, **99**, L429 (1980).
180. D. A. Reed and G. Erlich, *Surface Sci.*, **102**, 588 (1981).

181. D. A. Reed and G. Erlich, Surface Sci., 105, 603 (1981).
182. T. T. Tsong, Surface Sci., 122, 99 (1982).
183. A. Sadiq and K. Binder, Surface Sci., 128, 350 (1983).
184. A. Natori and H. Ohtsubo, Surface Sci., 171, 13 (1986).
185. M. Tringides and R. Gomer, Surface Sci., 166, 440 (1986).
186. A. Natori and H. Ohtsubo, Surface Sci., 184, 289 (1987).
187. X.-P. Jiang and H. Methiu, J. Chem. Phys., 88, 1891 (1988).
188. H. C. Kang and W. H. Weinberg, J. Chem. Phys., 90, 2824 (1989).
189. A. M. Bowler and E. S. Hood, J. Chem. Phys., 94, 5162 (1991).
190. C. Uebing and R. Gomer, J. Chem. Phys., 95, 7626 (1991).
191. C. Uebing and R. Gomer, J. Chem. Phys., 95, 7636 (1991).
192. C. Uebing and R. Gomer, J. Chem. Phys., 95, 7641 (1991).
193. C. Uebing and R. Gomer, J. Chem. Phys., 95, 7648 (1991).
194. M. Metropolis, A. W. Rosenbluth, M. N. Rosenbluth, A. N. Teller, and E. Teller, J. Chem. Phys., 21, 1087 (1953).
195. K. Kawasaki, Phys. Rev. B, 145, 224 (1966).
196. K. Kawasaki, Phys. Rev. B, 148, 375 (1966).
197. K. Kawasaki, Phys. Rev. B, 150, 285 (1966).
198. Note that since the experimental estimate for the intercell barrier  $\Delta_e$  is about 2000 K and the interaction parameters are about 300 K, the barriers chosen in this work are probably lower than in reality. However, for the purpose of studying the anisotropy, only the barrier ratios are relevant. In either circumstance, the quantum tunneling effects of H atoms are totally negligible at room temperature.
199. J. D. Doll and D. L. Freeman, Surface Sci., 134, 769 (1983).
200. U. Seifert and S. Dietrich, Europhys. Lett., 3, 593 (1987).
201. T. Ala - Nissila, E. Granato and S. C. Ying, J. Phys. Cond. Matter, 2, 8537 (1990) 8537.
202. H.-J. Ernst, E. Hulpke, and P. J. Toennies, Phys. Rev. Lett., 58, 1941 (1987).
203. J. P. Wood and J. L. Erskine, J. Vac. Sci. Technol. A, 4, 1414 (1986).
204. W. K. Han, S. C. Ying, and D. Sahu, Phys. Rev. B, 41, 4403 (1990).
205. W. K. Han and S. C. Ying, Phys. Rev. B, 41, 9163 (1990).
206. T. Ala - Nissila, W. K. Han, and S. C. Ying, unpublished.
207. T. E. Felter, R. A. Barker, and P. J. Estrup, Phys. Rev. Lett., 38, 1128 (1977).
208. M. K. Debe and D. A. King, Phys. Rev. Lett., 39, 708 (1977).
209. M. K. Debe and D. A. King, Surface Sci., 81, 193 (1979).

210. P. Heilmann, K. Heintz, and K. Müller, *Surface Sci.*, **89**, 84 (1979).
211. I. Stensgaard, L. C. Feldman, and P. J. Silverman, *Phys. Rev. Lett.*, **42**, 247 (1979).
212. R. A. Barker and P. J. Estrup, *J. Chem. Phys.*, **74**, 1442 (1981).
213. D. A. King, *Phys. Scr.*, **T4**, 34 (1981).
214. J. C. Campuzano, J. E. Inglesfield, D. A. King, and C. Somerton, *J. Phys. C*, **14**, 3099 (1981).
215. M. K. Debe and D. A. King, *J. Phys. C*, **15**, 2257 (1982).
216. J. F. Wendelken and G. C. Wang, *Phys. Rev. B*, **32**, 7542 (1985).
217. B. Salanon and J. Lapujoulade, *Surface Sci.*, **173**, L613 (1986).
218. I. K. Robinson, M. S. Altman, and P. J. Estrup, in *Structure of Surfaces II*, J. F. van der Veen and M. A. van Hove, eds., Springer - Verlag, Berlin (1987).
219. J. B. Pendry, K. Heinz, W. Oed, H. Landskron, K. Müller, and G. Schmidlein, *Surface Sci.*, **193**, L1 (1988).
220. I. Stensgaard, K. G. Purcell, and D. A. King, *Phys. Rev. B*, **39**, 897 (1989).
221. J. Jupille, K. G. Purcell, and D. A. King, *Phys. Rev. B*, **39**, 6871 (1989).
222. I. K. Robinson, A. A. MacDowell, M. S. Altman, P. J. Estrup, K. Evans - Lutterodt, J. D. Block, and R. J. Birgenau, *Phys. Rev. Lett.*, **62**, 1294 (1989).
223. A. Fasolino, G. Santoro, and E. Tosatti, *Phys. Rev. Lett.*, **44**, 1684 (1980).
224. S. C. Ying and L. D. Roelofs, *Surface Sci.*, **125**, 218 (1983).
225. G. Y. Hu and S. C. Ying, *Surface Sci.*, **150**, 47 (1985).
226. S. C. Ying, in *Dynamical Phenomena in Surfaces, Interfaces and Superlattices*, F. Nizzoli, K. Rieder, and R. F. Willis, eds., Springer - Verlag, Berlin (1986).
227. L. D. Roelofs, *Surface Sci.*, **178**, 306 (1986).
228. L. D. Roelofs and J. F. Wendelken, *Phys. Rev. B*, **34**, 3319 (1986).
229. G. Y. Hu and S. C. Ying, *Physica*, **140A**, 585 (1987).
230. C. Z. Wang, A. Fasolino, and E. Tosatti, *Phys. Rev. Lett.*, **59**, 1845 (1987).
231. C. Z. Wang, A. Fasolino, and E. Tosatti, *Europhys. Lett.*, **6**, 43 (1988).
232. D. Singh and H. Krakauer, *Phys. Rev. B*, **37**, 3999 (1988).
233. C. L. Lu and A. J. Freeman, *Phys. Rev. B*, **37**, 2685 (1988).
234. T. Schneider, *Phys. Rev. B*, **7**, 201 (1973).
235. P. Nightingale, *Physica*, **83A**, 561 (1976).
236. D. P. Landau, *Phys. Rev. B*, **13**, 2997 (1976).
237. J. V. Jose, L. P. Kadanoff, S. Kirkpatrick, and D. R. Nelson, *Phys. Rev. B*, **16**, 1217 (1977).

238. A similar anomaly near the critical point of a gas - liquid or binary fluid system has been discussed in detail in P. C. Hohenberg and B. I. Halperin, *Rev. Mod. Phys.*, **49**, 435 (1977).
239. Th. von Waldkirch, K. A. Müller, and W. Berligner, *Phys. Rev. B*, **7**, 1052 (1973).
240. G. Meissner and K. Binder, *Phys. Rev. B*, **12**, 3948 (1975).
241. J. P. Bouchaud and A. Georges, *Phys. Rep.*, **195**, 127 (1990).
242. J. Bricmont and A. Kupiainen, *Phys. Rev. Lett.*, **66**, 1689 (1991).
243. R. Festa and E. G. d'Agliano, *Physica*, **90A**, 299 (1978).
244. P. A. Ferrari, S. Goldstein, and J. J. Lebowitz, in *Statistical Physics and Dynamical Systems*, J. Fritz, A. Jaffe, and D. Szasz, eds., Birkhauser, Boston (1985).
245. K. Golden, S. Goldstein, and J. L. Lebowitz, *Phys. Rev. Lett.*, **55**, 2629 (1985).
246. C. P. Flynn and A. M. Stoneham, *Phys. Rev. B*, **1**, 3966 (1970).
247. M. D. Miller, *Surface Sci.*, **127**, 383 (1983).
248. C. Aslangul, N. Pottier, and D. Saint James, *Phys. Lett.*, **111A**, 175 (1985).
249. R. Jacquet and W. H. Miller, *J. Phys. Chem.*, **89**, 2193 (1985).
250. K. F. Freed, *J. Chem. Phys.*, **82**, 5264 (1985).
251. S. M. Valone, A. F. Voter, and J. D. Doll, *Surface Sci.*, **155**, 687 (1985).
252. J. G. Lauderdale and D. G. Truhlar, *Surface Sci.*, **164**, 558 (1985).
253. K. A. Muttalib and J. Sethna, *Phys. Rev. B*, **32**, 3462 (1985).
254. J. G. Lauderdale and D. G. Truhlar, *J. Chem. Phys.*, **84**, 1843 (1986).
255. K. B. Whaley, A. Nitzan, and R. B. Gerber, *J. Chem. Phys.*, **84**, 5181 (1986).
256. S. M. Valone, A. F. Voter, and J. D. Doll, *J. Chem. Phys.*, **85**, 7480 (1986).
257. A. Auerbach, K. F. Freed, and R. Gomer, *J. Chem. Phys.*, **86**, 2356 (1987).
258. M. J. Gillan, *Phys. Rev. Lett.*, **58**, 563 (1987).
259. T. N. Truong and D. G. Truhlar, *J. Phys. Chem.*, **91**, 6229 (1987).
260. G. Wahnström, B. Carmeli, and H. Metiu, *J. Chem. Phys.*, **88**, 2478 (1988).
261. T. N. Truong and D. G. Truhlar, *J. Chem. Phys.*, **88**, 6611 (1988).
262. B. M. Rice, L. M. Raff, and D. L. Thompson, *J. Chem. Phys.*, **88**, 7221 (1988).
263. G. Wahnström, *J. Chem. Phys.*, **89**, 6996 (1988).
264. B. M. Rice, B. C. Garrett, M. L. Koszykowski, S. M. Foiles, and M. S. Daw, *J. Chem. Phys.*, **92**, 775 (1990).
265. I. C. da Cunha Lima, A. Troper and S. C. Ying, *Phys. Rev. B*, **41**, 11798 (1990).
266. K. Haug and H. Metiu, *J. Chem. Phys.*, **94**, 3251 (1991).